The global transcription factor reservoir in TLR9 activated pDCs and the role of BATF for development and function of pDCs

Inaugural-Dissertation

zur Erlangung des Doktorgrades
der Mathematisch-Naturwissenschaftlichen Fakultät

der Heinrich-Heine-Universität Düsseldorf

vorgelegt von

Ritu Mann-Nüttel

aus Essen

Essen, Juli 2021

aus dem Institut für Medizinische Mikrobiologie und Krankenhaushygiene

der Heinrich-Heine-Universität Düsseldorf

Gedruckt mit der Genehmigung

der Mathematisch-Naturwissenschaftlichen Fakultät

der Heinrich-Heine-Universität Düsseldorf

Berichterstatter:

1. Prof. Dr. Stefanie Scheu
2. Prof. Dr. Michael Feldbrügge

Tag der mündlichen Prüfung:

(bitte bei der Abgabe Ihrer Dissertation noch offenlassen)

Table of Contents

List of Abbreviations

AP-1	Activator protein 1
APC	Antigen presenting cell
AICE	AP-1-IRF composite element
ANOVA	Analysis of variance
ATAC-Seq	Assay for transposase-accessible chromatin with high-throughput sequencing
BACH2	BTB domain and CNC homolog 2
BATF	Basic leucine zipper transcription factor
BLAST	Basic local alignment search tool
BM-d	Bone marrow derived
BST2	Bone marrow stromal cell antigen 2
BZIP	Basic leucine zipper domain
CD	Cluster of differentiation
cDC	Conventional dendritic cell
CDP	Common dendritic cell progenitor
ChIP-Seq	Chromatin immunoprecipitation sequencing
CLP	Common lymphoid progenitor
CMP	Common myeloid progenitor
CpG	CpG containing oligonucleotide
Cpm	Counts per million
CRE	Cyclic AMP response element
Cy	Cyanin
DAVID	Database for annotation, visualization and integrated discovery
Db	Database
DBD	DNA-binding domain
DC	Dendritic cell

DNA	Desoxyribonucleic acid
DOTAP	N-[1-(2,3-Dioleoyloxy)propyl]-N,N,N trimethylammoniummethylsulfate
E2-2	E-protein 2-2
EAE	Experimental autoimmune encephalomyelitis
EDTA	Ethylenediaminetetraacetic acid
ELISA	Enzyme-linked immunosorbent assay
FACS	Fluorescence activated cell sorting
FCS	Fetal calf serum
FDR	False discovery rate
FITC	Fluorescein isothiocyanate
Flt3	FMS-like tyrosine kinase 3
Flt3-L	FMS-like tyrosine kinase 3 ligand
GEO	Gene expression omnibus
GSEA	Gene set enrichment analysis
HOMER	Hypergeometric optimization of motif enrichment
H	Hours
Id2	Inhibitor of DNA-binding 2
IFN	Interferon
IFNAR	Type I interferon receptor
IGV	Integrative genomics viewer
IL	Interleukin
IRF	Interferon regulatory factor
ISG	Interferon stimulated gene
LCMV	Lymphocytic choriomeningitis virus
Lin	Lineage
LMPP	Lymphoid-primed multi-potential progenitor
MACS	Magnetic cell separation

MACS	Model-based analysis of ChIP-Seq
MDP	Macrophage dendritic cell progenitor
MEF	Mouse embryonic fibroblast
MHC	Major histocompatibility complex
MyD88	Myeloid differentiation primary response gene 88
NFIL3	Nuclear factor, interleukin 3 regulated
NFκB	Nuclear factor kappa-light-chain enhancer of activated B cells
NGS	Next generation sequencing
NK cell	Natural killer cell
ODN	Oligodeoxynucleotide
PBMC	Peripheral blood mononuclear cell
PBS	Phosphate buffered saline
PCR	Polymerase chain reaction
pDC	Plasmacytoid dendritic cell
PLP	Periodate-lysine-paraformaldehyde
qRT-PCR	Quantitative real time polymerase chain reaction
RELA	Nuclear factor NFκB p65 subunit
RNA	Ribonucleic acid
RNA-Seq	RNA sequencing
Rpm	Revolutions per minute
RT	Room temperature
RUNX2	Runt-related transcription factor 2
SiglecH	Sialic acid binding Ig-like lectin H
Spi1	Spleen focus forming virus (SFFV) proviral integration oncogene 1, encodes PU.1
STAT	Signal transducer and activator of transcription

TF	Transcription factor
TLR	Toll like receptor
TRE	TPA response element
TNF	Tumor necrosis factor
TRRUST2	Transcriptional regulatory relationships unravelled by sentence-based text mining version 2
TSS	Transcriptional start site
WT	Wild-type
YFP	Yellow fluorescent protein
ZFP366	Zinc finger protein 366

List of Figures

Summary

This doctoral thesis is composed of two parts, one dealing with the transcription factor (TF) reservoir and chromatin landscape in activated plasmacytoid dendritic cells (pDCs), and the second one with the role of the TF BATF in pDC development and cell effector function. TFs control gene expression by direct binding to regulatory regions of target genes but also by impacting chromatin landscapes and thereby modulating DNA accessibility for other TFs. To date, the global TF reservoir in pDCs, a cell type with the unique capacity to produce unmatched amounts of type I interferons, has not been fully characterized. To fill this gap, we have performed a comprehensive analysis in naïve and TLR9-activated pDCs in a time course study covering early time points after stimulation (2h, 6h, 12h) integrating gene expression (RNA-Seq), chromatin landscape (ATAC-Seq) and Gene Ontology studies. We found that 70% of all described TFs are expressed in pDCs for at least one stimulation time point and that activation predominantly "turned on" the chromatin regions associated with TF genes. We hereby define the complete set of TLR9-regulated TFs in pDCs. Further, this study identifies the AP-1 family of TFs as potentially important but so far less well characterized regulators of pDC function.

In the second part of this doctoral thesis, we have evaluated the role of the TF BATF (basic leucine zipper ATF-like transcription factor) on pDC development and cell effector function. We found that BATF is highly expressed in type I IFN-producing pDCs (Bauer et al., 2016). Type I interferons are essential initiators of subsequent protective innate and adaptive immune responses to viruses, bacteria and other pathogens. Furthermore, these cytokines can play an ambivalent role in auto-immune diseases, which are often characterized by an excessive production of type I IFN in the body. While the necessity of BATF expression in lymphocytes such as T helper and T regulatory cell differentiation and B cell class switching has been well described, no biological role of BATF in pDCs has been shown so far. In analyzing *Batf*$^{-/-}$ vs WT mice we found increased type I IFN levels and numbers and frequencies of pDCs in Flt3-L treated *in vitro* bone marrow cultures in *Batf* deficiency. To unravel the underlying mechanism, we characterized the role of BATF (1) in regulating global gene expression using next generation sequencing,

and (2) in modulating the chromatin landscape using ATAC-Seq in sorted *Batf*$^{-/-}$ and WT pDCs, and (3) regarding its genome wide direct DNA binding in pDCs using BATF ChIP-Seq. We found that BATF regulates type I IFN expression in pDCs indirectly via regulating the expression of the TF Zfp366, also known as DC-SCRIPT. Strikingly, BATF reduced pDC mediated LCMV infection control in an *in vitro* plaque assay. RNA-Seq and ChIP-Seq comparison revealed that expression of pDC lineage specific TFs such as E2-2 and Irf8 is significantly increased in naïve *Batf*$^{-/-}$ vs WT pDCs, and that BATF binds to promoter and enhancer regions of these genes, respectively. This suggests that BATF regulates pDC differentiation by controlling expression levels of pDC-lineage driving TFs. This impact of BATF on pDC development was found to be independent of signalling through the IFNAR. Lastly, global ATAC-Seq analysis showed that BATF acts as a pioneering TF which regulates chromatin accessibility of ~8,500 DNA regions, including around one third of all known TFs in pDCs.

In summary, TLR9 activation of pDCs with CpG significantly altered the global TF reservoir and chromatin landscape of the cell. Further, we found that BATF is a dual negative regulator of type I IFN production and development of pDCs. Both CpG and BATF may be exploited for immunotherapeutic treatment to control infection and autoimmune disease.

1. Introduction

Plasmacytoid dendritic cells (pDCs) are known as one of the major producers of type I interferon (IFN) during various infections (Ali et al., 2019; Bauer et al., 2016). Regulation of pDC differentiation and produced type I IFN levels by pDCs is essential to protect us from a plethora of parasites, bacteria and viruses, while limiting autoimmunity. Transcription factors (TF) are key modulators of global gene expression and chromatin accessibility. This thesis will firstly focus on the impact of TLR9 activation in pDCs on the global TF reservoir, and secondly on the role of a specific TF called BATF for pDC development and type I IFN production. The following chapters will introduce the importance of pDCs and type I IFN, the global TF reservoir in mouse pDCs and the known functions of BATF in innate and adaptive immunity.

1.1 Plasmacytoid dendritic cells

Dendritic cells (DCs) provide the first line of innate immune defense against pathogens which have breached epithelial barriers. They are the major antigen presenting cells (APCs) and act as important sensor and effector cells at the interface of the innate and adaptive immune system (Gaudino and Kumar, 2019). Among the cells classified as DCs there are different subtypes which appear to have distinct functions during immune responses, despite sharing common features. In general, four cell types have been typically classified as members of the DC family – conventional DCs (cDCs) and pDCs, Langerhans cells and monocyte-derived DCs. In this thesis we focused on pDCs. These cells were first described in humans as natural interferon producing cells (IPCs) that activate NK cells after virus recognition more than 40 years ago (Trinchieri and Santoli, 1978). The murine equivalent was reported with plasmacytoid morphology in 2001 (Asselin-Paturel et al., 2001; Bjorck, 2001; Nakano et al., 2001). pDCs are present in blood and lymphoid tissues like the spleen, and are able to enter the lymph nodes through the blood circulation where they migrate to the T cell areas in a CCR7 dependent manner (Seth et al., 2011). They are characterized by intermediate expression of the canonical DC marker CD11c and a high expression of surface molecules like Ly6C, B220, mPDCA-1 and SiglecH. CD11b is not expressed on their surface, and CD4 and CD8 show variable expression (Blasius

et al., 2006a; Blasius et al., 2006b). Co-stimulatory molecules such as CD80 and CD86 as well as major histocompatibility complex (MHC) molecules such as MHC class II are highly upregulated on pDCs upon external stimulation. In contrast to other DC subsets pDCs express only a limited repertoire of TLRs, namely predominantly TLR7 and TLR9 (Hornung et al., 2002), which recognize guanosine- and uridine-rich ssRNA and DNA containing CpG motifs (Diebold et al., 2004; Ishii and Akira, 2006; Wu et al., 2019). After TLR7 and TLR9 activation pDCs acquire the ability to more efficiently present antigen and stimulate T cells of the adaptive immune system (Salio et al., 2004). CpG can be considered as an optimal and specific microbial stimulus for pDCs which induces TLR9 mediated signaling that leads to the activation of the JAK-STAT and NF-κB signaling pathways (Volpi et al., 2013). Unremitting production of type I IFN by pDCs has been reported in auto-immune diseases like systemic lupus erythematosus (Elkon and Wiedeman, 2012). Moreover, when recruited to the tumor microenvironment pDCs may induce immune tolerance in humans (Le Mercier et al., 2013; Li et al., 2017).

1.1.1 Development of plasmacytoid dendritic cells

Different DC subsets can be discriminated by surface marker expression and classified based on their ontology which takes into account the cell origin and the expression of specific TFs. Hematopoietic stem cells have the potential to differentiate into common myeloid progenitors (CMP) or common lymphoid progenitors (CLP) that subsequently can give rise to pDCs in a Flt3-L-dependent manner (Karsunky et al., 2003; Manz et al., 2001). Flt3-L itself was found to be under the control of PU.1 (Carotta et al., 2010). The differentiation of pDCs from a common DC progenitor (CDP) occurs in the myeloid branch (Naik et al., 2006). Recently, pDCs have been reported to develop predominantly from IL-7R^{+} lymphoid progenitors rather than from CDPs (Dress et al., 2019; Rodrigues et al., 2018). Within the IL-7R^{+} lymphoid branch expression of SiglecH and Ly6D defines pDC lineage commitment, with Ly6D^{+} SiglecH^{+} double positive precursors being only few divisions away from pDC maturity (Rodrigues et al., 2018). Further, specific TFs have been identified to positively drive pDC development. In particular, absence of the interferon regulatory factor 8 (*Irf8*) in conventional *Irf8*$^{-/-}$

mice resulted in pDC deficiency (Tamura et al., 2005; Tsujimura et al., 2002). Yet, in mixed bone marrow chimeras from wild-type (WT) and *Irf8*$^{-/-}$ mice and in late IRF8 deletion no effect on pDC development or survival was observed, but rather an increased T cell stimulatory function and decreased type I IFN production in pDCs (Sichien et al., 2016). Bornstein et al. further identified IRF8 as an inducer of cell-specific chromatin changes in thousands of pDC enhancers (Bornstein et al., 2014). Further, *Spi-B* deficient mice showed decreased and increased pDC numbers in the bone marrow (BM) and periphery, respectively, indicating involvement of *Spi-B* in pDC development (Sasaki et al., 2012). In contrast to the phenotype in *Spi-B*-deficient mice, *Runx2*-deficient animals exhibited normal pDC development in the BM but significantly reduced pDC numbers in the periphery (Sawai et al., 2013). Also, the TF *Tcf4* is an essential requirement for pDC development as either its constitutive or inducible deletion blocked pDC differentiation (Cisse et al., 2008). Yet, the detailed mechanisms of control of pDC development, and in particular whether they are of myeloid versus lymphoid origin, remains poorly understood.

1.1.2 Type I IFN in host defense

Type I IFNs comprise different IFNα subtypes (11 in mice and 13 in humans), IFNβ, IFNκ, IFNω and IFNε. They are crucial for host protection against viruses but have also important functions in the immune response to other classes of pathogens, namely bacteria, parasites, and fungi. Moreover, type I IFNs play a functional role in the pathogenesis of inflammatory autoimmune diseases (Kretschmer and Lee-Kirsch, 2017). pDCs are well known for their capacity to produce copious amounts of type I IFN upon stimulation. They detect single-stranded RNA and unmethylated DNA through the endosomal TLR7 and 9, respectively, which activates a diverse set of pathogen sensing pattern recognition receptor (PRR) pathways. The expression of type I IFNs is induced by binding of IRFs and NFκB to acute response elements in the respective gene promoters. IRF7 and 8 are constitutively expressed in pDCs and their expression is indispensable to induce type I IFN production in pDCs (Honda et al., 2005; Tailor et al., 2007). The type I IFNs themselves bind to the heterodimeric IFNα receptor (IFNAR), consisting of IFNAR1 and IFNAR2 subunits, which induces a cascade of signalling leading to the

expression of interferon stimulated genes (ISGs) along with production of more type IFN (Ivashkiv and Donlin, 2014; Platanias, 2005). What remains poorly understood is the regulation of type I IFN production in pDCs, as both an excessive overproduction and an underproduction of type I IFN may be detrimental to human health.

Of note, while pDCs are known as specialized type I IFN producing cells early in virus infections new studies suggest that their *in vivo* contribution in immune responses to viruses, bacteria, fungus and parasites exhibits restricted patterns in time of induction and duration. Particularly, cell sources other than pDCs have been determined as dominant producers of type I IFN at later time points of infection. Even though pDCs prove to often be an important source of type I IFN in systemic infections, antiviral immune responses on local tissues are more often characterized by a cell source other than pDCs that produces type I IFN, unless other lines of defense are broken. Important *in vivo* producers of type I IFN beside pDCs are mainly macrophages, inflammatory monocytes and cDCs. Hence, a protective anti-infectious immune response mediated by type I IFN is ensured by the production of type I IFN by multiple cellular sources (Ali et al., 2019).

1.2 Global transcription factor reservoir in pDCs

TFs are known to bind to regulatory sequences of DNA to either enhance or inhibit gene transcription during cell differentiation, at steady state, and for exertion of cell effector functions after pDC activation by pathogens or in autoimmune diseases (Reizis, 2019). Also, TFs show unique expression patterns for different cell types and cellular states. Efforts have been made to list and integrate all known mouse TFs in dedicated databases (db), such as Riken mouse TFdb (Kanamori et al., 2004) and TFCat (Fulton et al., 2009), amongst others. However, most of these were built before 2010 and have not been updated. We chose to base our TF analyses on the AnimalTFDB, which was first built in 2011 (Zhang et al., 2012) and has been most recently updated in 2019 (Hu et al., 2019). Another advantage of the AnimalTFDB is that it classifies the mouse TF reservoir based on the structure of the DNA binding domains, allowing a detailed analysis of different TF classes and families to uncover how TFs recognize and bind DNA, and also providing insight into their evolutionary histories.

Not only do TFs regulate cell development and effector functions by binding to cis-regulatory elements but they also impact the accessibility of chromatin in different cell states. These latter TFs are called pioneering TFs and have the ability to remodel chromatin and thus modify the epigenome (Drouin, 2014). Chromatin is dynamically modified during cell differentiation leading to a cell type specific landscape (Deaton and Bird, 2011), which may be altered after cell activation, making the DNA more or less accessible to a particular set of TFs, that in turn modulate the expression of other genes important for cell identity and function.
TFs regulate the development of pDCs from the stem cell reservoir and the expression of cytokines such as type I IFNs in the anti-infectious immune response. While the importance of a few key TFs for pDC differentiation and type I IFN signaling have been described no global analysis of the global TF reservoir in naïve or activated pDCs has been performed.

1.3 The Basic Leucin Zipper AP-1 like transcription factor (BATF)

pDCs are known to produce large amounts of type I IFN during viral infections. Contradicting the previous dogma, we found that only a small subpopulation of pDCs produces type I IFN after TLR9 activation (Bauer et al., 2016). Microarray experiments revealed that the TF BATF (basic leucine zipper ATF-like transcription factor) is highly expressed in these type I IFN-producing pDCs.
BATF belongs to the group of AP (activator protein)-1 factors and is part of the larger BATF family that is comprised of the three different members BATF, BATF2 and BATF3. AP-1 TFs are known to affect proliferation, differentiation and cell survival (Murphy et al., 2013; Sopel et al., 2016; Wagner and Eferl, 2005). BATF is predominantly expressed in cells of hematopoietic origin and some transformed myeloid and lymphoid cells (Echlin et al., 2000; Glasmacher et al., 2012; Liao et al., 2011; Senga et al., 2002; Sopel et al., 2016; Wang et al., 2012; Williams et al., 2001). Studies using a *Batf*-deficient mouse lines revealed its essential role for normal development of several T cell subtypes (Tfh, Th17, Th1, Th2) (Sopel et al., 2016). Furthermore loss of BATF led to defective class switch recombination in B cells (Ellyard and Vinuesa, 2011; Logan et al., 2012; Sahoo et al., 2015; Schraml et al., 2009). In addition BATF directly regulates cytokine expression by T cells and surface marker expression (e.g. CD117) on mast cells (Sahoo et al., 2015; Ubel et

al., 2014), and is involved in NKT cell development and function (Jordan-Williams et al., 2013; Williams et al., 2003; Zullo et al., 2007).

Loss of BATF3 caused defects in the development of $CD8\alpha^+$ and $CD103^+$ DCs, leading to an almost complete loss of this DC population and strikingly to protection from *Listeria monocytogenes* infection in *Batf3*$^{-/-}$ mice (Edelson et al., 2010; Ise et al., 2011; Schraml et al., 2009)). Interestingly, it has been shown that BATF can compensate for BATF3 in $CD8^+$ cDC development (Tussiwand et al., 2012). Nonetheless, mice deficient for *Batf3* show that the lack of $CD8\alpha^+$ cDCs and normal IL-12 production are significant as they are highly susceptible to infection by the protozoan parasite *Toxoplasma gondii* (Mashayekhi et al., 2011).

Not only has the role of BATF been investigated in naïve mice but also in infection, inflammatory and autoimmunity models. It has been established that BATF is required for sustained CD8 T cell effector function in LCMV infection, while virus specific $CD8^+$ T cells initially proliferated normally in BATF absence. Yet the lack of BATF resulted in an inability to sustain cytotoxic T cell responses and consequently caused LCMV persistence in various tissues as indicated by higher viral titres in *Batf*$^{-/-}$ mice (Grusdat et al., 2014). Moreover, BATF has been described to influence Th2 and Th9 responses in models of murine experimental asthma (Jabeen et al., 2013; Sopel et al., 2016; Ubel et al., 2014). T cells from *Batf*$^{-/-}$ mice that were stimulated to differentiate into Th17 cells *in vitro* produced normal levels of IL-2, IFNγ and IL10, but significantly reduced levels of IL-17. Strikingly, a mouse model for experimental autoimmune encephalomyelitis (EAE) revealed resistance to EAE in *Batf*$^{-/-}$ mice. The mechanism driving EAE pathogenesis is based on action of Th17 cells, which show developmental defects in *Batf*$^{-/-}$ mice, possibly explaining one major mechanism for the protective effect from EAE in *Batf* absence. Also, it could be shown that the adoptive transfer of WT CD4+ T cells into *Batf*$^{-/-}$ mice prior to induction of EAE abolished resistance to EAE, suggesting a BATF-dependent signalling in EAE development (Schraml et al., 2009)

While the importance of BATF for T helper cell subset and B cell differentiation and function has been well described, no biological role of BATF in pDCs has been shown so far. Therefore, the impact of BATF on pDC development and cell effector function was investigated at the heart of this thesis.

1.3.1 Molecular mechanisms for BATF function

AP-1 factors are generally characterized by a DNA-binding domain (DBD) and a leucine zipper motif (bZIP) and are active in the form of homo- or heterodimers. However, unlike other AP-1 family members like FOS and JUN all BATF TFs are unable to form homodimers and lack a trans-activation domain (Lee et al., 1987; Murphy et al., 2013; O'Shea et al., 1992; O'Shea et al., 1989).

The bZIP domain of BATF facilitates dimerization with other factors to form “composite TFs” which recognize palindromic RPA response elements (TREs) and cyclic AMP response elements (CRE). BATF is known to cooperate with JUN, IRFs and Bach2 (Dorsey et al., 1995; Kuwahara et al., 2016; Murphy et al., 2013). The BATF-JUN dimer preferentially binds to TREs rather than CRE motifs. Of note, phosphorylation of the DBD of BATF has been suggested to reduce AP-1 activity by sequestering JUN and making the TF complex transcriptionally inert (Deppmann et al., 2003). Initially, BATF family members were considered to inhibit gene transcription as they lack a transactivation domain. However, more recent studies have shown BATF can exert unique, non-redundant, and positive transcriptional activities through cooperative binding with IRF family members as well (Echlin et al., 2000; Kurachi et al., 2014; Li et al., 2012; Murphy et al., 2013; Williams et al., 2001). BATF multimer complexes containing IRF4 and IRF8 bind AP-1 IRF composite elements (AICEs) initiating gene transcription (Murphy et al., 2013; Tussiwand et al., 2012). AICE motifs are located in proximal or distal promoter sites as well as in intronic enhancer elements of genes (Murphy et al., 2013).

BATF can therefore both inhibit and initiate gene transcription. Schraml et al. showed that BATF in cooperation with JunB binds to the IL-17, IL-21 and IL-22 promoter in Th17 cells inducing gene transcription (Schraml et al., 2009). Further, ChIP assays from T cells indicate that BATF directly binds to promoter- and intergenic regions of TFs, activation markers, cytokines, chemokine receptors, and genes involved in cell proliferation and metabolism in T cells (Glasmacher et al., 2012; Kurachi et al., 2014; Li et al., 2012).

This thesis shows for the first time different classes of genes that BATF binds to in pDCs, and how it affects their expression and chromatin landscape, revealing cell-specific effects of BATF when comparing our data with current literature that discusses BATF action in immune cells other than pDCs.

1.4 Global ‘omics approach to investigate role of TLR9 activation and BATF in pDCs

A global ‘omics approach was used in this work to unravel the role pDC activation on the global TF reservoir and the role of BATF for pDC development and effector function. To this end we performed next generation RNA sequencing (RNA-Seq) of sorted BM-derived Flt3-L *in vitro* cultured pDCs from wild-type (WT) and *Batf*-deficient *(Batf*$^{-/-}$) mice that were stimulated with the TLR9 ligand CpG for 2h, 6h and 12h or left untreated. We used the data to (1) characterize how the global TF reservoir in pDCs is affected by TLR9 activation in a time dependent manner (2h, 6h 12h) in WT pDCs, and (2) determined how *Batf*-dependent gene expression affects different gene classes and pathways in a longitudinal study that represents early events after virus infection in pDCs.

To investigate direct vs indirect regulation of gene expression by BATF, we performed BATF ChIP-Seq (Chromatin immunoprecipitation sequencing) on sorted BM-derived Flt3-L cultured pDCs from WT mice stimulated with CpG for 2h or left untreated. ChIP-Seq is a method to analyze protein interactions with DNA. Chromatin immunoprecipitation is combined with parallel DNA sequencing to identify DNA binding sites of the protein in the whole genome. We assessed the binding of BATF to genes in naïve as well as CpG stimulated pDCs. The binding was correlated with changes in expression from the RNA-Seq data to evaluate whether BATF binding has any effect on gene expression levels. Additionally, the exact binding location of BATF was analyzed globally (distal vs proximal promoter, intron regions, 5’UTRs etc.).

In addition to TFs having direct impact on transcriptional activity by binding to free DNA TFs can also act as pioneering factors which modulate the chromatin landscape of a cell to regulate DNA accessibility and gene expression. The role of pDC activation on the chromatin landscape in WT cells and the role of BATF for

the chromatin structure in pDCs was investigated by ATAC-Seq (Assay for transposase-accessible chromatin with high-throughput sequencing) on sorted BM-derived Flt3-L cultured pDCs from WT and *Batf*$^{-/-}$ background. The method makes use of the hyperactive transposase Tn5 which inserts sequencing adapters into open regions of the genome. Regions with open chromatin and accessible DNA can thereby be identified with next generation sequencing (NGS).

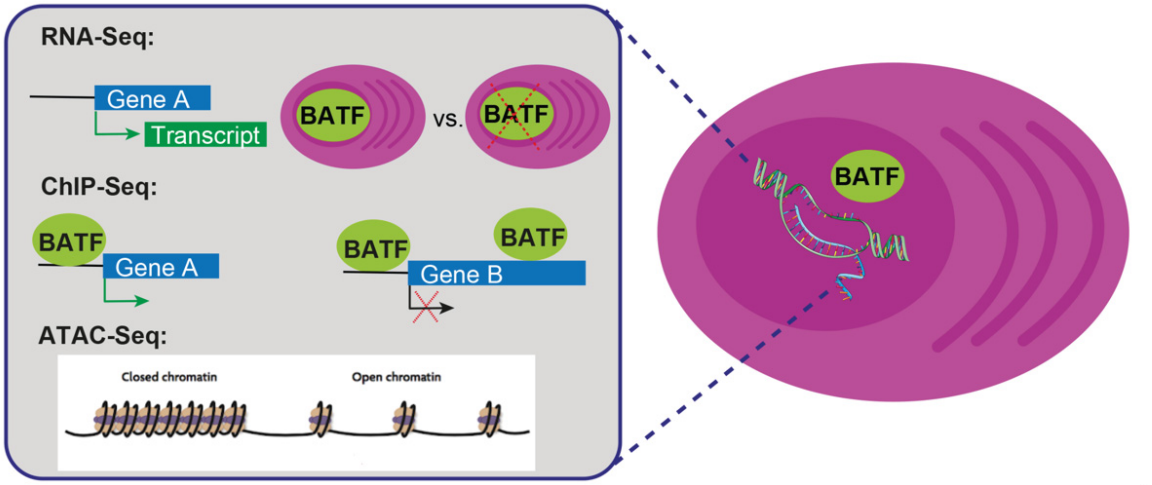

Figure 1 Overview of the global `omics approach.

1.5 Aims of the study

Functional and mature pDCs play a crucial role in various pathogenic infections as well as cancer and autoimmune disease. We used CpG as an optimal and specific microbial stimulus for pDCs which induces TLR9 mediated signaling that leads to activation of IRF7 and NFκB signaling pathways (Swiecki and Colonna, 2015). Using early time points after stimulation (2h, 6h, 12h) we modelled a situation which represents early events after virus infection.

The first aim of this thesis was to perform a longitudinal study to *in silico* evaluate the impact of the TLR9 activation in pDCs (CpG 0h, 2h, 6h, 12h) on the transcriptional and epigenetic landscape of the global TF reservoir in pDCs, which has not been published as such to this date. To this end the definition of all mouse TFs was used from the AnimalTFDB (Hu et al., 2019). Gene Ontology was applied to identify TLR9-induced TFs involved in various biological processes. In addition, a differential motif analysis on more or less accessible chromatin regions after pDC activation was performed to possibly discover new TF families with so far little or

no known role in pDC biology. The results of these analyses are briefly summarized in this thesis. A detailed analysis and interpretation has been posted on the bioRxiv preprint server (DOI: https://doi.org/10.1101/2021.04.14.439791) already and is attached in the appendix of this thesis.

The second aim of this thesis was to elucidate the role of the AP-1 TF BATF on pDC development and effector function at steady state and after TLR9 activation. We previously found in microarray experiments that *Batf* is highly expressed in type I IFN-producing pDCs (Bauer et al., 2016). While the role of BATF has been analyzed in detail for various T cell subtypes and B cells, among others, no possible impact of BATF on pDC biology has been described to date. To achieve our goal we used WT and *Batf*$^{-/-}$ mice (Schraml et al., 2009) to combine a global 'omics approach with wet lab experiments involving e.g. the characterization of secondary lymphoid organs via FACS and immunohistology. The global 'omics approach was helpful to analyze (1) the impact of *Batf* on global gene expression, (2) whether BATF directly binds to gene elements, and (3) the modulatory capacity of BATF to affect chromatin structure in pDCs. The wet lab experiments were useful to confirm data from the global 'omics analyses and to evaluate the role of BATF in pDC biology *in vivo* involving a complex interplay of different organs and cell types.

The knowledge taken from the longitudinal pDC activation study in WT pDCs together with the newly discovered functions of BATF in pDCs from the mouse experiments of this thesis could be used to develop novel opportunities of therapeutic intervention in viral infections or autoimmune disease in humans. This might involve the exploitation of the TLR9 ligand CpG or the manipulation of the BATF protein for immunotherapeutic treatment to both enhance and repress immune responses.

2. Materials and Methods

2.1 Materials

2.1.1 Chemicals

Chemicals	Manufacturer
Acetone	Merck, Darmstadt
Aqua ad injectabilia	Braun, Melsungen
Avidin/Biotin blocking solution	Vector Laboratories, Burlingame, USA
β-Mercaptoethanol (β-ME)	Invitrogen, Karlsruhe
Bovine Serum Albumin (BSA)	Sigma-Aldrich, Taufkirchen
Chloroform	Roth, Karlsruhe
DEPC	Sigma-Aldrich, Taufkirchen
Deoxynucleotides	Roche, Mannheim
Dexamethasone	Sigma-Aldrich, Taufkirchen
Doxycycline	Sigma-Aldrich, Taufkirchen
Distilled water, sterile	Invitrogen, Karlsruhe
DMEM medium VLE	Biochrom, Berlin
Diemethylsulfoxide (DMSO)	Sigma-Aldrich, Taufkirchen
Donkey normal serum	Jackson Laboratories, Suffolk, UK
DOTAP	Roche, Mannheim
EDTA	Sigma-Aldrich, Taufkirchen
Ef780	Thermofisher, Wesel
Erythrocyte lysis buffer	Morphisto, Frankfurt am Main
Ethanol	Merck, Darmstadt
FACS Clean solution	BD Biosciences, Heidelberg
FACS Flow solution	BD Biosciences, Heidelberg
FACS Rinse solution	BD Biosciences, Heidelberg

Fetal Calf Serum (FCS)	PAN, Aidenbach
Flt3-L	*In vitro* generated in NIH3T3 cells in our lab
Goat normal serum	DakoCytomation, Hamburg
HBSS	Gibco, Paisley, UK
Hydrochloric acid	Roth, Karlsruhe
Hydrogen peroxide, 30 %	Merck, Darmstadt
IMDM	Lonza, Verviers, Belgium
L-glutamine	Biochrom, Berlin
Methanol	Merck, Darmstadt
Mouse normal serum	Jackson Immuno Research, Suffolk, UK
Oligo-(dT)-Primer	Fermentas, St. Leon-Rot
Paraformaldehyde	Merck, Darmstadt
PBS chemical powder	Biochrom, Berlin
PBS, 0.5 l, sterile	Invitrogen, Karlsruhe
PBS, 10x	Gibco, Paisley, UK
PCR Nucleotide-Mix (dNTPs)	Fermentas, St. Leon-Rot
Penicillin/Streptomycin	Biochrom, Berlin
Phenylenediamine hydrochloride	Sigma-Aldrich, Taufkirchen
Potassium chloride	Sigma-Aldrich, Taufkirchen
Rat normal serum	Jackson Immuno Research, Suffolk, UK
RNase Zap	Applied Biosystems/Ambion, Darmstadt
RPMI 1640 VLE	Biochrom, Berlin
Saline solution, physiological	DeltaSelect, Dreireich
Sodium azide	Merck, Darmstadt
Sodium hydroxide	Merck, Darmstadt
Sucrose	Serva, Heidelberg
TissueTek™ O.C.T. Compound™	Sakura, Staufen
Triton X-100	Biochrom, Berlin

Trypan blue	Sigma-Aldrich, Taufkirchen
Trypsin/EDTA	Biochrom, Berlin
Tyramide kit	Perkin Elmer, Rodgau
Vectashield mounting medium with DAPI	Vector Laboratories, Burlingame, USA

2.1.2 Enzymes

Enzyme	Manufacturer
Collagenase type VIII	Sigma-Aldrich, Taufkirchen
DNAse I	Roche, Mannheim
SuperScript III	Roche, Mannheim
Trypsin/EDTA, 0.25 %	Gibco, Paisley, UK

2.1.3 Kits and other reagents

Kits/Reagents	Manufacturer
BD Compensation beads	BD Biosciences, Heidelberg
DakoCytomation pen	DakoCytomation, Hamburg
FastStart universal master mix	Roche, Basel
Hemacolor staining kit	Merck, Darmstadt
IFNα ELISA	eBioscience, San Diego, USA
IFNβ ELISA	Biolegend, Uithoorn, Netherlands
LS MACS columns and magnets	Miltenyi, Bergisch-Gladbach
MESA GREEN master mix	Eurogentec, Liège, Belgium
Miltenyi anti-biotin microbeads	Miltenyi, Bergisch-Gladbach
NucleoSpin RNA kit	Macherey-Nagel, Düren
Pappenheim staining kit	Morphisto, Frankfurt
Reverse transcription kit	Invitrogen, Karlsruhe
TissueTek	Sakura Finetek, Staufen

TSA FITC/Biotin system	Perkin Elmer, Rodgau

2.1.4 TLR agonists

TLR agonist	Manufacturer
CpG ODN 2216	TIB MolBiol, Berlin
LCMV	Kind gift of Prof. Philipp Lang (Institute of Molecular Medicine II, University of Düsseldorf)

2.1.5 Antibodies

The antibodies listed in the following table were purchased from the manufacturers BD Biosciences (Heidelberg), BioLegend (Uithoorn, Netherlands), BioXCell (Lebanon, New Hampshire, USA), eBiosience (San Diego, USA), Invitrogen (Karlsruhe), Jackson Immuno Research (Suffolk, UK), Jackson Laboratories (Bar Harbor, Maine, USA), and Miltenyi Biotec (Bergisch-Gladbach).

Antigen	Clone	Fluorochrome	Manufacturer
Donkey anti rabbit	polyclonal	Biotinylated	Jackson Immuno Research
B220	Ra3-6B2	APC, FITC, PerCP	BD Biosciences
CD3ε	145-2C11	PerCP	BD Biosciences
CD4	RM4-5	PerCP	
CD8α	53-6.7	APC, APC-Cy7, BV711	BD Biosciences
CD11b	M1/70	APC, APC-Cy7, PE, AF700	BD Biosciences
CD11c	HL3	APC, APC-Cy7	BD Biosciences
CD16/CD32	2.4G2	Unconjugated	BioLegend
CD19	1D3	PerCP, BV421, BV785	BD Biosciences
CD86	GL1	PerCP, PE-Cy7	eBioscience
HRP	/	/	Jackson Laboratories

MHCII (I-a/I-b)	M5/114	APC, FITC, PE, BV510	BD Biosciences
mPDCA-1 (CD317)	927	BV650, PE	Miltenyi Biotec
NK1.1	PK136	APC, FITC, BV421	BD Biosciences
NK1.1	PK136	Unconjugated	BioXCell
SA-Cy3	-	Cy3	Invitrogen
SA-FITC	-	FTC	Biolegend
SiglecH	55.3D3	APC	Miltenyi Biotec
TNFα	MP6-XT22	PE	eBioscience
VL-4 rat anti LCMV	/	Unconjugated	VL-4 hybridoma supernatant, kind gift of Prof. Lang (Institute of Molecular Medicine II, University of Düsseldorf)

2.1.7 Cell lines, media and buffers

2.1.7.1 Media

Cells	Concentration	Components
Flt3-L DCs		RPMI 1640 VLE
	10 %	FCS
	0.1 %	β-ME
	5 %	Flt3-L
MC57		Alpha-MEM
	5 %	FCS
	1 %	Penicillin/Streptomycin
MEF		DMEM
	10 %	FCS
	1 %	Penicillin/Streptomycin

2.1.7.2 Buffers and Solutions

Buffer	Components	
Collagenase VIII	100 mg/ml	in PBS
DNase I	3000 U/ml	in PBS
FACS buffer	1x	PBS
	2 %	FCS
	2 mM	EDTA
MACS buffer	1x	PBS
	0.5 %	BSA
	2 mM	EDTA
PFA fixation buffer, pH 7.4	1x	PBS
	4 %	Paraformaldehyde
	2 mM	$MgCl_2$
	1,25 mM	EGTA
PBS/BSA buffer		PBS
	1 %	BSA
PLP solution	1 %	PFA
	0,075 M	L-Lysin
	0,01 M	Natrium-M-Periodat
		Distilled water, pH 7.0-7.2
Stop buffer	1x	PBS
	10 mM	EDTA
Tissue digest buffer	93 %	PBS
	6 %	Collagenase type VIII solution
	1 %	DNase I solution
TNB	0.1 mM	Tris-HCl, pH 7.5
	0.15 mM	NaCl
	0.5 %	blocking reagent from TSA kit

2.1.8 Equipment

Device	Manufacturer
Axioskop 40 Microscope	Zeiss, Jena
Biofuge A (centrifuge)	Heraeus, Hanau
Biological safety cabinet	Kendro, Vienna, Austria
CFX96 RealTime C100 Thermal Cycler	Bio-Rad, Lunteren, Netherlands
Confocal microscope (LSM510Meta)	Zeiss, Jena
Cryotom (HM 650)	Thermo Fisher Scientific, Bonn
Digital camera: Axiocam 105	Zeiss, Jena
Digital camera: Axiocam MRc	Zeiss, Jena
FACS Aria II	BD Biosciences, Heidelberg
FACS Canto II	BD Biosciences, Heidelberg
FACS Fortessa	BD Biosciences, Heidelberg
Heat block Techne DB3	Biostep, Jahnsdof
Heidolph Polymax 1040 (shaker)	Heidolph Instruments, Schwabach
iCycler iQ5 (qRT-PCR)	Bio-Rad, Lunteren, Netherlands
Millipore Elix advantage 3	Millipore, Schwalbach
Multistep-Dispenser Handystep	Brand, Wertheim
NanoDrop 1000 (photometer)	Peqlab, Erlangen
Neubauer chamber	LO-Laboroptik, Friedrichsdorf
pH Meter MP 225	Mettler-Toledo, Giessen
Photometer: TECAN Sunrise	Tecan, Männedorf, Switzerland
Single- and multichannel pipette	Thermo Fisher Scientific, Bonn
Surgery tools	Fine Science Tools, Heidelberg
TE2000 (microscope)	Nikon, Düsseldorf
Thermocycler T1	Biometra, Göttingen
Tissue culture incubator (Heracell 20)	Heraeus, Hanau

Ultra Turrax T25	IKA, Staufen
Vortex shaker VVR	VWR, Darmstadt
Water bath	Köttermann Labortechnik, Uetze/Hänigsen

2.1.9 Animal experiments

Mice were kept under pathogen-free conditions in the animal research facility of the University of Düsseldorf. All experiments in this thesis were performed in strict accordance with the German Animal Welfare Act § 8 and approved by the government of North-Rhine Westphalia. All efforts were made to minimize suffering of laboratory animals.

2.1.10.1 Mice

Mouse strain	Description
WT	Wildtype mouse on C57BL/6 background
Batf$^{-/-}$	*Batf* deficient mouse (Schraml et al., 2009)
Ifnar$^{-/-}$	*Ifnar* deficient mouse (Muller et al., 1994)
Ifnar$^{-/-}$ x *Batf*$^{-/-}$	*Batf* and *Ifnar1*-double knockout mouse, intercross from respective single knockout mouse lines

2.1.6 Oligonucleotides

Gene	Primer sequence (5'-3')	Probe
β-Actin	TGA CAG GAT GCA GAA GGA GA CGC TCA GGA GGA GCA ATG	106
BATF	AGA AAG CCG ACA CCC TTC A CGG AGA GCT GCG TTC TGT	85
ID2	GAC AGA ACC AGG CGT CCA GG AGC TCA GAA GGG AAT TCA GAT G	89
IFNα	TCA AGC CAT CCT TGT GCT AA GTC TTT TGA TGT GAA GAG GTT CAA	3
IFNβ	CAG GCA ACC TTT AAG CAT CAG CCT TTG ACC TTT CAA ATG CAG	95

IRF8	GAG CCA GAT CCT CCC TGA CT GGC ATA TCC GGT CAC CAG T	26
NFIL3	CAT AGC CAC ACA ACC GAT CTC TCC TCC TCC ATG CAT AGC TC	46
RUNX2	AGG GAC TAT GGC GTC AAA CA GGC TCA CGT CGC TCA TCT T	/
SPI1	ATG TTA CAG GCG TGC AAA ATG G TGA TCG CTA TGG CTT TCT CCA	/
SPIB	GGT CCT AAC CCC TCC ACC TA TAC GGA GCA TAA GCC AAG GA	20
TCF4	TGG GCT CAG GGT ACG GAA CT CAG AGC CAC GCC ATC TTC AC	102

2.2 Experimental methods

2.2.1 Cell culture

Cell lines were cultured in tissue-culture-treated flasks. Primary cells were cultured in untreated petri dishes. All cell lines and primary cells were cultured at 37 °C and 10 % CO_2 in a humidified incubator.

Cell lines were passaged once a week or when necessary. Therefore, adherent cells were rinsed with PBS and incubated with Trypsin/EDTA for 1-5 min at 37 °C. Single cell solutions were diluted in a 1:2 or 1:5 ratio and cells were seeded into new tissue culture flasks.

2.2.2 Isolation of murine bone marrow

Mice with an age range of 10-24 weeks were sacrificed by cervical dislocation, hind legs removed and femurs and tibias were dissected. Bones were next disinfected in 70 % EtOH and washed in cold PBS. Subsequently bones were cut open on both sides and bone marrow was flushed out with RPMI containing FCS using a 20 ml syringe with a 23 G needle. The bone marrow was carefully resuspended to make a single cell suspension. The cells were transferred into a 50 ml tube and centrifuged for 5 min at 1200 rpm at RT. Supernatant was aspirated and the cell pellet was lysed in 3 ml erythrocyte lysis buffer for 3 min at RT. The reaction was stopped by adding 10 ml RPMI media, followed by a second centrifugation step for 5 min at 1200 rpm at RT. Afterwards cells were counted and used for *ex vivo* experiments and cell culture, respectively.

2.2.2.1 Differentiation of BM-derived Flt3-L-derived DCs

To differentiate BM cells into pDCs or cDCs $20x10^6$ cells/10 ml or $8x10^6$ cells/4 ml were seeded into 10cm or 5cm petri dishes containing RPMI media with Flt3-L, respectively. After 5 days half of the media were removed and replaced by fresh Flt3-L-containing media and after 7 days cells were fully differentiated. Fully differentiated cells were either left untreated or stimulated as indicated in 2.2.2.2.

2.2.2.2 CpG stimulation of *in vitro* differentiated cells

Stimulation of BM-derived Flt3-L cultures with CpG 2216 was done with complexation to DOTAP as follows:

6 µg CpG 2216 *ad* 100 µl with HBSS or PBS

- 20 µl DOTAP ad 100 µl with HBSS or PBS
- both solutions were mixed and incubated for 15 min at RT
- 200 µl were added into the cell culture supernatant.

Stimuli were pipetted directly into the cell supernatant, gently mixed and left on for 6 h, 12 h or 24 h, as indicated in the single experiments.

2.2.2.3 MACS depletion of lineage negative cells in *ex vivo* bone marrow

For depletion of T, B and NK cells *ex vivo* bone marrow was prepared as described in 2.2.2. Cells were taken up in MACS buffer, counted, stained for MACS depletion following the manufacturer's description (NK cell isolation kit II, Miltenyi Biotec) and purified using LS columns. An aliquot of purified cells was used for FACS analysis to evaluate success of depletion and the rest was used for RNA isolation as described under 2.2.4.1.

2.2.3 Harvesting of mouse tissues

After cervical dislocation spleen and mesenteric, brachial, axillary, inguinal and cervical lymph nodes were harvested. For histology samples were embedded in TissueTek-containing cryomolds, frozen on dry ice and stored at -80 °C till further processing as described in 2.2.3.4. For FACS analysis organs were transferred into 6-well plates containing tissue digest buffer (containing DNase and collagenase VIII), carefully disrupted using tweezers and digested at 37 °C for 30

min. Afterwards the digest was stopped by adding 3-5 ml of Stop buffer. Cells were resuspended and transferred into a 50 ml tube over a 40 or 100 µm cell strainer. Next cells were centrifuged at 1200 rpm for 5 min at 4 °C, supernatant aspirated and cells lysed by adding 3 ml of erythrocyte lysis buffer to each sample for 3 min at RT. Lysis was stopped by adding 10 ml of FACS buffer and samples were centrifuged at 1200 rpm for 5 min at 4 °C. Supernatant was discarded and the cell pellet was resuspended in 1 ml or 10 ml FACS buffer for lymph nodes and spleen, respectively, and cells were counted using Neubauer chambers. Samples were aliquoted into FACS tubes and stained as described in 2.2.3.1.

2.2.4 Immunological methods

2.2.4.1 Extracellular FACS staining

2.2.4.1.1 FACS BD Canto II

Cells from *in vitro* culture were cooled at 4°C for half an hour and scraped off the plate. *Ex vivo* cells were prepared as described in 2.2.2.3. Cell suspensions were centrifuged at 1200 rpm for 5 min at 4 °C and supernatant was removed. 25 µl of FC block solution containing a 1:100 dilution of the αCD16/CD32 antibody was added to each sample to block unspecific binding sites, mixed and incubated for 10 min at 4 °C. A primary antibody cocktail was prepared with antibodies diluted 1:100 for FACS analysis on the BD Canto II, or at a dilution of 1:25 for cell sorting on the BD Aria II. 25 µl of primary antibody cocktail was added to the samples, mixed well and incubated for another 30 min at 4 °C. After this samples were washed by adding 2-3 ml of FACS buffer and centrifuged at 1200 rpm for 5 min at 4 °C. Supernatant was aspirated and samples were resuspended in 100 µL of FACS buffer containing the live/dead marker 7-AAD or DAPI (dilution 1:200), respectively, and analysed on a BD Aria II or BD Canto II.

2.2.4.1.2 FACS BD Fortessa

Cells from *in vitro* cultures were cooled at 4 °C for half an hour and scraped off the plate. *Ex vivo* cells were prepared as described in 2.2.2.3. Cell suspensions were centrifuged at 1200 rpm for 5 min at 4 °C and supernatant was discarded. Cells were washed with PBS once to remove protein interfering with the following intracellular live/dead staining. After centrifugation at 1200 rpm for 5 min at 4 °C

the supernatant was discarded and cells were stained in 100µL ef780 solution diluted at 1:5000 in PBS. Next cells were incubated at room temperature for 15 min. after which 2 mL FACS buffer was added. Cells were washed and the supernatant discarded. 25 µl of FC block solution containing a 1:50 dilution of the αCD16/CD32 antibody was added to each sample to block unspecific binding sites, mixed well and incubated for 10 min at 4 °C. A primary antibody cocktail was prepared with antibodies diluted accordingly for each experimental setting. 50 µl of primary antibody cocktail was added to the samples, mixed and incubated for another 30 min at 4 °C. After this samples were washed by adding 2-3 ml of FACS buffer and centrifuged at 1200 rpm for 5 min at 4 °C. Supernatant was aspirated and samples were resuspended in 100 µL of FACS buffer for analysis on the BD Fortessa.

2.2.4.2 FACS cell sorting

For cell sorting *ex vivo* bone marrow or fully differentiated BM-derived Flt3-L cultured cells were prepared as described in 2.2.2. The MACS depletion system was used to enrich non B and T cells prior to RNA isolation for PCR. pDCs and BM progenitors were identified by labelling with fluorochrome- or biotin-conjugated monoclonal antibodies to mouse antigens. 7-AAD and DAPI staining, respectively, was used to allow identification of cell doublets and dead cells, after which pDCs were identified as $CD3^-$ $CD19^-CD11c^+$ $CD11b^{low}$ $B220^+$ $SiglecH^+$ $CD317^+$ cells. Cells were stained as described in 2.2.3.1, resuspended in 1 ml of FACS buffer per $2x10^6$ cells and populations were separated on a BD ARIA II. For further analysis or processing separated cells were collected in FCS coated tubes and stored on ice.

2.2.4.3 Histology and Immunohistochemistry

Spleens and lymph nodes from naïve WT and *Batf*$^{-/-}$ mice were used for immunohistochemical staining to evaluate the impact of Batf on organ structure, number and localization of pDCs. Half of the respective organ(s) was placed into cryomolds containing TissueTrek directly and frozen on dry ice. The other half of the organ(s) was fixed in PLP solution at 4°C overnight. After this, organs were immersed sequentially in 10 %, 20 % and 30 % sucrose at RT for 2h. Finally organs were placed into cryomolds containing TissueTek and frozen on dry ice. Organs

were stored at -80 °C till further processing. Frozen organs were cut into 8 µm thick sections using a cryotome (ThermoFisher Scientific), fixed to a microscope slide and stored at -20 °C.

For B220/mPDCA-1 staining non-PLP fixed slides were thawed, rehydrated in PBS and fixed in acetone for 10 min. The cut tissue sections were surrounded with a DAKOPen (wax/fat pen). Staining was performed in a humid chamber and slides were carefully rinsed with PBS three times in-between every staining step. Unspecific binding sites were blocked by incubating the slides in a solution containing different sera (goat, donkey, rat and mouse normal serum) and FC block (αCD16/CD32) diluted in PBS/BSA solution for 25 min at RT. After this, endogenous biotin was blocked using avidin followed by biotin blocking for 20 min each at RT. Following this, slides were stained with the primary antibody solution (B220-FITC 1:100 and mPDCA1-bio 1:50 in PBS/BSA solution) for 1 h at RT. The biotin-conjugated mPDCA1 signal was enhanced by incubating the slides with SA-Cy3 (in PBS/BSA, 1:200) for 45 min at RT. Finally, slides were embedded in Vectashield and slides were frozen at -20 °C.

The PLP-fixed organs were used for B220/SiglecH staining. Cut tissue slices on the slides were surrounded with a DAKOPen (wax/fat pen). Staining was performed in a humid chamber and slides were carefully rinsed with PBS three times in-between every staining step. First slides were incubated in a H_2O_2 (1 %) - NaN_3 (0.1%) -PBS solution for 1 h at RT under constant shaking. Subsequently, unspecific binding sites were blocked by incubating the slides in a blocking solution containing different sera (n-goat, n-donkey, n-rat, n-mouse) and FC block (αCD16/CD32) in TNB, for 25 min at RT. After this endogenous biotin was blocked using avidin followed by biotin blocking for 20 min each at RT. Next slides were stained with the primary antibody solution (SiglecH-bio 1:100 in TNB) for 1 h at RT. Next the SiglecH biotin-conjugated signal was intensified by incubating the slides with SA-HRP (in TNB, 1:200) for 25 min at RT followed by incubation with a FITC conjugated tyramide solution (in amplification buffer, 1:100) for 8 min. After this, slides were incubated in a H_2O_2 (1 %) -NaN_3 (0.1%) -PBS solution for a second time. After avidin/biotin blocking slides were incubated with the B220-biotin (in TNB, 1:500). The signal was intensified with SA-HRP (in TNB, 1:200) incubation for 25 min at RT, followed by applying bio-tyramide solution (in amplification buffer,

1:100) for 7 min. at RT. Finally, slides were incubated with SA-Cy3 (in TNB, 1:500) for 30 min at RT and embedded in Vectashield before freezing at -20 °C.

2.2.5 Molecular-biological methods

2.2.5.1 Isolation of RNA

RNA from *ex vivo* bone marrow and purified FACS sorted cells was isolated using the NucleoSpin RNA isolation kit according to the manufacturer's instructions (Macherey-Nagel). Purity and RNA concentration of each sample was measured at 260 nm using a NanoDrop 1000 photometer and RNA samples were stored at -80 °C.

2.2.5.2 Preparation of cDNA from RNA samples

cDNA was prepared using 0.1-5 µg RNA of sorted or *ex vivo* bone marrow cells. RNA was digested by adding DNase I to the samples for 30 min at 37 °C. DNase I then was heat-inactivated at 70 °C for 10 min. Subsequently RNA was added into a tube containing a mix of:

- 1 µl Oligo(dT) (50µM)
- 1 µl 10 mM dNTP Mix
- 6 µl RNase free H_2O.

This mixture was incubated at 65 °C for 5 min, followed by rest on ice for 1 min and centrifugation for a few seconds. Next the mixture was transferred into a PCR-reaction tube containing:

- 1 µl 0,1M DTT
- 4 µl 1 x First Strand Buffer
- 1 µl SuperscriptTM RTase (200U/µl)
- 1 µl RNAse Out

Reverse transcription PCR was run at 50 °C for 1 h, followed by an inactivation step at 70 °C for 15 min and a cooling down step to 4 °C. cDNA was diluted by adding 80 µL H_2O and stored at -20 °C.

2.2.5.3 Quantitative real time PCR

For analysing gene expression quantitative real time PCR was performed using MESA GREEN Mastermix or FastStart Universal Mastermix for the hydrolysis probe detection format.

MESA GREEN Mastermix per sample was prepared as follows:

- 12.5 µl MESA GREEN Mastermix (Eurogentec)
- 10 µl H_2O
- 0.075 µl primer forward
- 0.075 µl primer reverse

2.5 µL cDNA was pipetted into each well of a 96-well plate containing 22.5 µL of the Mastermix.

FastStart Universal Mastermix per sample was prepared as follows:

- 12.5 µl FastStart Mastermix (Roche)
- 6.4 µl H_2O
- 0.3 µl primer forward
- 0.3 µl primer reverse
- 0.,5 µl probe

5.0 µL cDNA was pipetted into each well of a 96-well plate containing 20.0 µL of the Mastermix.

The qRT-PCR reactions were performed on a CFX96 RealTime C100 Thermal Cycler (Bio-Rad) for MESA GREEN reactions without probe. PCRs with Roche probe were done on an Iq5 iCycler (Bio-Rad). PCR conditions were as follows:

1. DNA denaturation at 95 °C for 7 min
2. DNA denaturation at 95 °C for 20 s
3. hybridisation and elongation of at 60 °C for 1 min
4. hold at 4 °C
5. steps 2 - 3 were periodically repeated for 45 times

Relative gene expression was calculated using the Pfaffl method (Pfaffl, 2001). For every new primer pair there was a cDNA free control as a negative control included

for the qRT-PCR reaction. β-Actin was used as a reference gene for normalization and quantification. Every sample was run as a triplicate.

2.3 Global ‘omics and bioinformatics

2.3.1 RNA-Seq

Quantity of total RNA samples used for transcriptome analysis were analysed by Qubit RNA HS Assay (Thermo Fisher Scientific). Quality of RNA was determined by capillary electrophoresis using the Fragment Analyzer and the Total RNA Standard Sensitivity Assay (Agilent Technologies, Santa Clara, CA, USA). All samples in this study showed high quality RNA Quality Numbers (RQN; mean = 9.8). Library preparation was performed using the ‘TruSeq Stranded mRNA Library Prep Kit’ from Illumina® according to the manufacturer’s instructions. Briefly, 250 ng total RNA were used for mRNA capturing, fragmentation, the synthesis of cDNA, adapter ligation and library amplification. Bead purified libraries were normalized and finally sequenced on the HiSeq 3000/4000 system (Illumina, San Diego, CA, USA) with a read setup of 1x150 bp. The bcl2fastq tool was used to convert the bcl files to fastq files as well for adapter trimming and demultiplexing.
First data analyses on fastq files were conducted with CLC Genomics Workbench (version 10.1.1, QIAGEN, Venlo, Netherlands). The reads of all probes were adapter trimmed (Illumina TruSeq) and quality trimmed (using the default parameters: bases below Q13 were trimmed from the end of the reads, ambiguous nucleotides maximal 2). Mapping was done against the Mus musculus (mm38) genome sequence.
Samples were grouped (three biological replicates each) according to their respective experimental condition. Raw counts were next re-uploaded to the Galaxy web platform. The public server at usegalaxy.org was used to perform multi-group comparisons (Afgan et al., 2016). Differential expression of genes between any two conditions was calculated using the edgeR quasi-likelihood pipeline which uses negative binomial generalized linear models with F-test (Liu et al., 2015; Robinson et al., 2010). Low expressing genes were filtered with a count-per-million (CPM) value cut-off that was calculated based on the average library

size of our NGS run (Chen et al., 2016). The resulting P values were corrected for multiple testing by FDR correction. A P value of ≤0.05 was considered significant.

2.3.2 ChIP-Seq

Cells were fixed with 1% formaldehyde for 15 min and quenched with 0.125 M glycine, and sent to Active Motif Services (Carlsbad, CA) to be processed for ChIP-Seq. In brief, chromatin was isolated by the addition of lysis buffer, followed by disruption with a Dounce homogenizer. Lysates were sonicated and the DNA sheared to an average length of 300-500 bp. Genomic DNA (Input) was prepared by treating aliquots of chromatin with RNase, proteinase K and heat for de-crosslinking, followed by ethanol precipitation. Pellets were resuspended and the resulting DNA was quantified on a NanoDrop spectrophotometer. Extrapolation to the original chromatin volume allowed quantitation of the total chromatin yield. An aliquot of chromatin (20 µg, spiked-in with 200 ng of Drosophila chromatin) was precleared with protein A agarose beads (Invitrogen). Genomic DNA regions of interest were isolated using 4 ug of antibody against BATF (CST, 8638BF). Antibody against H2Av (0.4 µg) was also present in the reaction to ensure efficient pull-down of the spike-in chromatin (Egan et al., 2016). Complexes were washed, eluted from the beads with SDS buffer, and subjected to RNase and proteinase K treatment. Crosslinks were reversed by incubation overnight at 65 °C, and ChIP DNA was purified by phenol-chloroform extraction and ethanol precipitation. Quantitative PCR (QPCR) reactions were carried out in triplicate on specific genomic regions using SYBR Green Supermix (Bio-Rad). The resulting signals were normalized for primer efficiency by carrying out QPCR for each primer pair using Input DNA.

For ChIP Sequencing Illumina sequencing libraries were prepared from the ChIP and Input DNAs by the standard consecutive enzymatic steps of end-polishing, dA-addition, and adaptor ligation. Steps were performed on an automated system (Apollo 342, Wafergen Biosystems/Takara). After a final PCR amplification step, the resulting DNA libraries were quantified and sequenced on Illumina's NextSeq 500 (75 nt reads, single end). Reads were aligned consecutively to the mouse genome (mm10) and to the Drosophila genome (dm3) using the BWA algorithm (default settings). Duplicate reads were removed and only uniquely mapped reads

(mapping quality ≥ 25) were used for further analysis. The number of mouse alignments used in the analysis was adjusted according to the number of Drosophila alignments that were counted in the samples that were compared. Mouse alignments were extended *in silico* at their 3'-ends to a length of 200 bp, which is the average genomic fragment length in the size-selected library and assigned to 32-nt bins along the genome. The resulting histograms (genomic "signal maps") were stored in bigWig files. Peak locations were determined using the MACS algorithm (v2.1.0) with a cut-off of p-value = 1e-7. Peaks that were on the ENCODE blacklist of known false ChIP-Seq peaks were removed. Signal maps and peak locations were used as input data to Active Motifs proprietary analysis program, which creates Excel tables containing detailed information on sample comparison, peak metrics, peak locations and gene annotations. The results were further visualized using Integrative Genomics Viewer (IGV) (Robinson et al., 2011) and modified with Inkscape.

2.3.3 ATAC-Seq

Cells were harvested and frozen in culture media containing FBS and 5% DMSO. Cryopreserved cells were sent to Active Motif to perform the ATAC-Seq assay. The cells were then thawed in a 37°C water bath, pelleted, washed with cold PBS, and tagmented as previously described (Buenrostro et al., 2013), with some modifications based on (Corces et al., 2017). Briefly, cell pellets were resuspended in lysis buffer, pelleted, and tagmented using the enzyme and buffer provided in the Nextera Library Prep Kit (Illumina). Tagmented DNA was then purified using the MinElute PCR purification kit (Qiagen), amplified with 10 cycles of PCR, and purified using Agencourt AMPure SPRI beads (Beckman Coulter). Resulting material was quantified using the KAPA Library Quantification Kit for Illumina platforms (KAPA Biosystems), and sequenced with PE42 sequencing on the NextSeq 500 sequencer (Illumina).

Analysis of ATAC-Seq data was very similar to the analysis of ChIP-Seq data. Reads were aligned using the BWA algorithm (mem mode; default settings). Duplicate reads were removed, only reads mapping as matched pairs and only uniquely mapped reads (mapping quality ≥ 1) were used for further analysis. Alignments were extended *in silico* at their 3'-ends to a length of 200 bp and

assigned to 32-nt bins along the genome. The resulting histograms (genomic "signal maps") were stored in bigWig files. Peaks were identified using the MACS 2.1.0 algorithm at a cut-off of p-value $1e^{-7}$, without control file, and with the –no model option. Peaks that were on the ENCODE blacklist of known false ChIP-Seq peaks were removed. Signal maps and peak locations were used as input data to Active Motifs proprietary analysis program, which creates Excel tables containing detailed information on sample comparison, peak metrics, peak locations and gene annotations. For differential analysis, reads were counted in all merged peak regions (using Subread), and the replicates for each condition were compared using DESeq2.

2.4 Software and online tools

2.4.1 Analysis of data obtained from wet lab experiments

Immunofluorescent images of the organs used for immunohistochemical stainings were taken on a confocal microscope (LSM510Meta, Zeiss) and primarily analyzed using the Zen2012 software (Zeiss). Single pictures were exported as jpegs and edited using Adobe Photoshop CS1.

Raw data from RT-PCR was processed in Microsoft Excel for calculation of gene expression and then plotted in Graphpad Prism (Prism 8.4.3).

FACS data were analysed using the FlowJo Software (Tree Star, Ashland, USA). For *in vitro* experiments cells were pre-gated on living cells using various markers ($DAPI^-$, $7\text{-}AAD^-$, $ef780^-$) as indicated in the specific experiments.

2.4.2 Re-analysis of publicly available gene expression data

Human data (GEO68849, GEO70278, GEO93679) were analysed using Biobase, GEOquery and limma R packages (Davis and Meltzer, 2007); (Smyth, 2004).

2.4.3 Pathway and other downstream analyses

Data from RNA-Seq, BATF ChIP-Seq and ATAC-Seq was further processed and filtered in RStudio using a number of packages, namely xlsxjars (Dragulescu, 2014), xlsx (Arendt, 2020), readr (Hadley Wickham, 2018), and Rcpp (Balamuta, 2017).

Reactome pathway analyses on the Reactome website (https://reactome.org/) were performed using a list of differentially expressed genes (|FC|>2, FDR<0.05) between WT and *Batf*$^{-/-}$ pDCs for various conditions (naïve, CpG 2h, 6h, 12h). The same lists were used for Gene Ontology analyses using DAVID (**D**atabase for **A**nnotation, **V**isualization and **I**ntegrated **D**iscovery, https://david.ncifcrf.gov/) and ClueGO application (Bindea et al., 2009) installed on the Cytoscape software using ver 3.7.1 (Shannon et al., 2003).

Pearson correlation matrices were calculated in RStudio (Team, 2020) and plotted as a heatmap using gplots (Gregory R. Warnes, 2020) and RColorBrewer (Neuwirth, 2014). Other heatmaps in this work have been created using the Morpheus online tool (https://software.broadinstitute.org/morpheus) and pheatmap (Kolde, 2019) in RStudio. Volcano plots have been created using packages ggplot2 (Wickham, 2016), ggrepel (Slowikowski, 2020) and dplyr (Hadley Wickham, 2020) in RStudio. Further, Venn diagrams have been created using the R package eulerr (Larsson, 2018). The microarray data in **Fig. 3** was visualized using Gradphpad Prism version 8.4.3 on Windows (GraphPad Software, La Jolla California USA, www.graphpad.com). The circlized diagrams in **Fig. 10** were created using the Cytoscape software ver 3.7.1 (Shannon et al., 2003).

2.5 Statistical analyses

The extreme studentized deviate (ESD) method was used to identify significant outliers within a list of values for FACS and RT-PCR data. Data in this thesis are shown as mean ± SEM. Statistical significance was determined by t tests (unpaired, two-tailed) for two groups or two-way ANOVA (with Tukey's multiple comparison post test) for three or more groups performed in Graphpad Prism (Prism 8.4.3). Wilcoxon matched-pairs signed rank test was used to compare the relative expression of cluster-associated genes between WT and *Batf*$^{-/-}$ pDCs from RNA-Seq data (Prism 8.4.3). * indicates $p< 0.05$; ** indicates $p< 0.01$; *** indicates $p< 0.001$.

3. Results

The first part of the thesis deals with the impact of TLR9 activation on the expression and activity of the TF reservoir and chromatin landscape in pDCs. Even though the functions of selected cell fate TFs have been well described in pDCs, to our knowledge no global TF expression analysis after pDC activation has been performed for this cell type in mouse. The results of these detailed analyses have been published on bioRxiv, (https://doi.org/10.1101/2021.04.14.439791) and a revised version is under review with the Journal BMC Genomic Data. Therefore, the results on this work will be discussed only shortly in this thesis.

In the second part of this doctoral work we evaluated the role of the TF BATF on type I IFN production and development of pDCs. We will discuss in detail the results we obtained from using a global 'omics approach in combination with *in vitro* and *ex vivo* lab experiments on secondary lymphoid organs from WT and *Batf*$^{-/-}$ mice.

3.1 Global 'omics approach

We used a global 'omics approach for both parts of this thesis. In the work described here, we performed a comprehensive analysis on the (1) murine TF reservoir and chromatin landscape in WT pDCs, and (2) the role of the TF BATF on global gene expression, DNA binding and chromatin modulation in a time course early upon TLR9 activation of pDCs. To this end we sorted BM-derived Flt3-L *in vitro* cultured pDCs from WT and *Batf*-deficient *(Batf*$^{-/-}$*)* mice that were left either untreated or stimulated with CpG (2h, 6h, 12h). The cells were used

(1) to assess the impact of TLR9 activation with CpG (2h, 6h, 12h) on the murine TF reservoir expression WT pDCs and the impact *Batf* absence on global gene expression in pDCs by next generation sequencing (RNA-Seq),

(2) to investigate direct vs indirect regulation of gene expression by BATF ChIP-Seq (Chromatin immunoprecipitation sequencing) in naïve and 2h CpG stimulated pDCs, and

(3) to evaluate how TLR9 activation with CpG (2h) modulates the chromatin landscape and DNA accessibility for different TF families in WT pDCs, and

whether BATF regulates chromatin accessibility as a pioneering factor in pDCs by ATAC-Seq.

The global ‘omics approach promises to decipher the complex interacting molecular mechanisms of TLR9 activation and BATF mediated immune regulation in pDCs from the transcriptomic as well as the epigenetic angle.

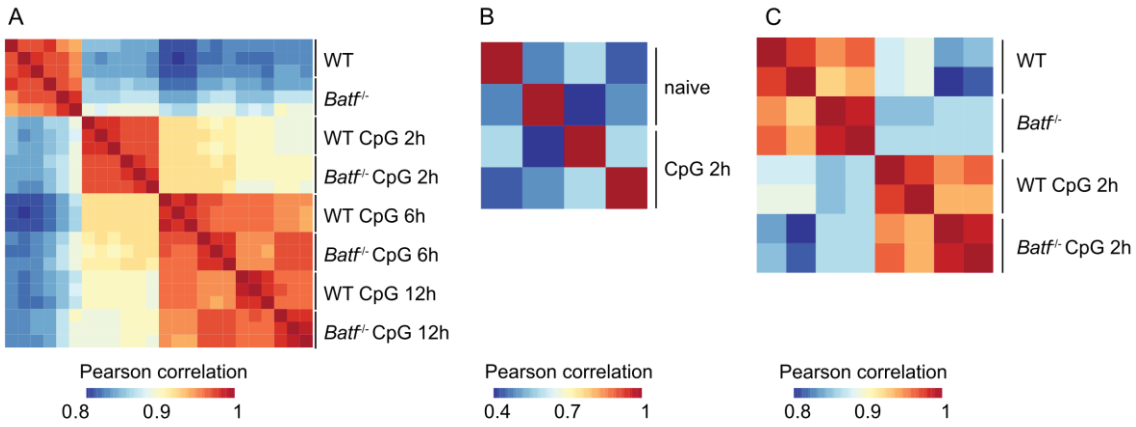

Figure 2 Quality control of samples used for the global ‘omics approach. Pearson correlation of biological replicates for RNA-Seq (WT and *Batf*$^{-/-}$ pDCs, **A**), BATF ChIP-Seq (WT pDCs, **B**) and ATAC-Seq (WT and *Batf*$^{-/-}$ pDCs, **C**) plotted as a heatmap.

Quality control of the samples used for the ‘omics approach was performed by calculating Pearson correlation coefficients in RStudio and plotting the results as a heatmap. Our results reveal high similarity (<95%) for the biological replicates used in the respective conditions of the RNA-Seq data set. Notably, the differences between the stimulation time points (naïve, CpG2h, 6h and 12h) were higher than the differences observed between the two genotypes (WT and *Batf*-deficiency). Furthermore, the differences observed between steady state and 2h stimulation as well as 2h vs 6h stimulation were bigger than the differences observed between the latest activation time points of 6h vs 12h (**Fig. 2A**). As for ChIP-Seq, two biological replicates were used but did not reach the standard 95% similarity score. Therefore, a so called Drosophila spike in has been used to normalize and standardize the data. Hence, we continued to use the ChIP-Seq data for analysis, always paying attention to possible differences between biological replicates for each analyzed genomic region (**Fig. 2B**). Lastly, Pearson correlation for the ATAC-Seq data mounted to >95% similarity for all biological replicates, indicating very good quality of our data (**Fig. 2C**). We used all datasets to perform a quantitative

analysis of peak intensities across sample conditions, and further used the RNA-Seq and ATAC-Seq data to perform a differential analysis to determine *Batf*-dependent gene expression and to quantify the number of BATF-dependent accessible chromatin peaks.

3.2 Impact of TLR9 activation on the transcription factor reservoir and chromatin landscape in pDCs

The first aim of this thesis was to characterize the changes in expression and chromatin accessibility for the complete set of all known TFs in pDCs in an early time course study after activation. In detail, we wanted to evaluate the unique patterns of TF expression to define epigenetic and transcriptional states in pDCs 2, 6, and 12h after TLR9 activation as compared to the steady state situation. To this purpose, global gene expression (RNA-Seq) and chromatin landscape modulations (ATAC-Seq) have been analysed in purified BM-derived Flt3-L cultured pDCs. A Gene Ontology (GO) analysis was performed to identify the involvement of TLR9-induced TFs in various biological processes. Lastly, an integrative `omics approach was used to identify possibly important players in pDCs after cell activation.

We found that 70% of all genes annotated as TFs in the mouse genome (1,014 out of 1,636) are expressed in naïve or TLR9-activated pDCs (2h, 6h, 12h) in at least one condition, and are covering a wide range of TF classes defined by their specific DNA binding mechanisms. pDC activation correlated with a time dependent increase or decrease in the expression of distinct sets of TFs in pDCs. To unravel the biological processes underlying the changes in TF expression on a global scale downstream gene ontology (GO) analyses were performed and revealed involvement of CpG-induced TFs in epigenetic modulation, NFκB and JAK-STAT signaling, and protein production in the endoplasmic reticulum, amongst others. Evaluating the chromatin landscape in 2h CpG stimulated vs naïve pDCs we found that pDC activation substantially altered the chromatin landscape, leading to upwards of ~16,000 altered accessible regions (p=5%, |FC|>2) in the pDC genome. Among these, more than 750 altered accessible regions are associated with TF promoter and or intronic regions. Strikingly, roughly 80% of all CpG-dependent changes in chromatin regions in pDCs exhibit increased

DNA accessibility, suggesting that more of the chromatin landscape associated with TF genes is „turned on“ than is „turned off“ early after pDC activation. In these *in silico* analyses we identified the AP-1 family of TFs, which are so far less well characterized in pDC biology, as possibly important players in these cells after activation. Members of the AP-1 family exhibit (1) increased gene expression, (2) enhanced chromatin accessibility in their promoter region, and (3) a TF DNA binding motif found globally enriched in the genomic regions that are more accessible in pDCs 2h after TLR9 activation.

The results of these analyses are described in detail in the manuscript titled *The transcription factor reservoir and chromatin landscape in activated plasmacytoid dendritic cells* by Mann-Nüttel et al. (Appendix 7.1). This manuscript has been accepted for publication in the Journal BMC Genomic Data.

In summary, our results for the first time comprehensively define the global transcriptional and epigenetic state of TFs in pDCs in a longitudinal study comparing steady state with time points at 2h, 6h and 12h after TLR9 stimulation representing early events in virus infection. We suggest a novel biological classification of all CpG-stimulated TFs in pDCs and identify the AP-1 family as a set of TFs which warrant further investigation regarding their role in pDC development and function.

3.3 BATF represses type I IFN expression in pDCs

In previous studies from our lab the cellular source of IFNβ in the spleen during virus infection or TLR9 stimulation has been defined as a distinct subset of pDCs. Although pDCs have been known to have the ability to secrete high amounts of type I IFN we found that only 10% of pDCs produced IFNβ (Bauer et al., 2016). A microarray experiment has been performed to compare the gene expression patterns between IFNβ-producing pDCs and non IFNβ-producing pDCs from mice infected with the murine cytomegalovirus or directly stimulated with the TLR9 ligand CpG. This transcriptome analysis revealed *Batf* as a gene with a high differential expression in IFNβ-producing pDCs (**Fig. 3**).

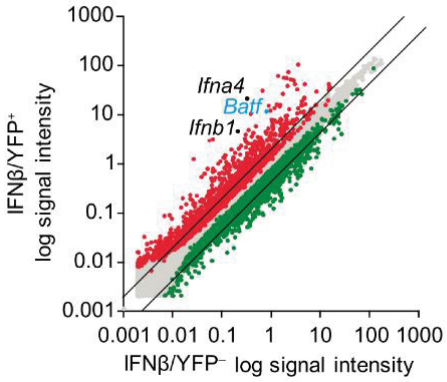

Figure 3 Higher expression of type I IFN and *Batf* in IFNβ/YFP$^+$ pDCs from the spleen. Microarray data showing red and green dots that represent genes differentially expressed between IFNβ/YFP$^+$ and IFNβ/YFP$^-$ *in vivo* CpG stimulated pDCs, respectively. Modified from (Bauer et al., 2016).

The role of BATF for cell development and function has been well described for T helper cell subsets and B cells (Murphy et al., 2013; Sahoo et al., 2015; Schraml et al., 2009). However, functional implications of BATF in pDC development or function have not been described up to now. The following chapter aims to better understand the role of BATF in IFNβ production by pDCs.

3.3.1 BATF is co-expressed with type I IFN in mouse and human pDCs

The BATF protein is conserved between human and mouse (85% protein identity) according to an analysis performed on Protein BLAST (https://blast.ncbi.nlm.nih.gov/Blast.cgi?PAGE=Proteins, 08.12.2019). We visualized the conservation of different genomic elements of the mouse *Batf* gene including downstream and upstream regions as compared to the human genome using the ECR (Evolutionary Conserved Regions) browser (**Fig. 4A**). We found that both exonic regions and non coding sequences in the promoter of the *Batf* gene are very well conserved between human and mouse (stretches larger than 100 base pairs have sequence identity above 70%). This suggests that the encoded BATF protein in humans is indeed very similar to mouse, and as the promoter regions are well conserved as well that regulatory mechanism of transcription initiation may be similar in mouse and human. We next went back to our initial finding that *Batf* is co-expressed with type I IFN genes in WT mouse pDCs stimulated with CpG. We wondered whether the same expression profile can

be observed in human pDCs. To this end we re-analyzed previously published RNA-Seq data from Caielli et al. who isolated human pDCs from PBMCs of healthy donors and *ex vivo* stimulated human pDCs with CpG for 18 h or left them untreated (n=3 per group, GSE93679) (Caielli et al., 2019). The results showed that human BATF is >22 fold up-regulated along with type I IFN genes in stimulated pDCs as compared to non-stimulated pDCs, which is line with our observation of gene expression patterns in mouse pDCs upon CpG stimulation (**Fig. 4B**).

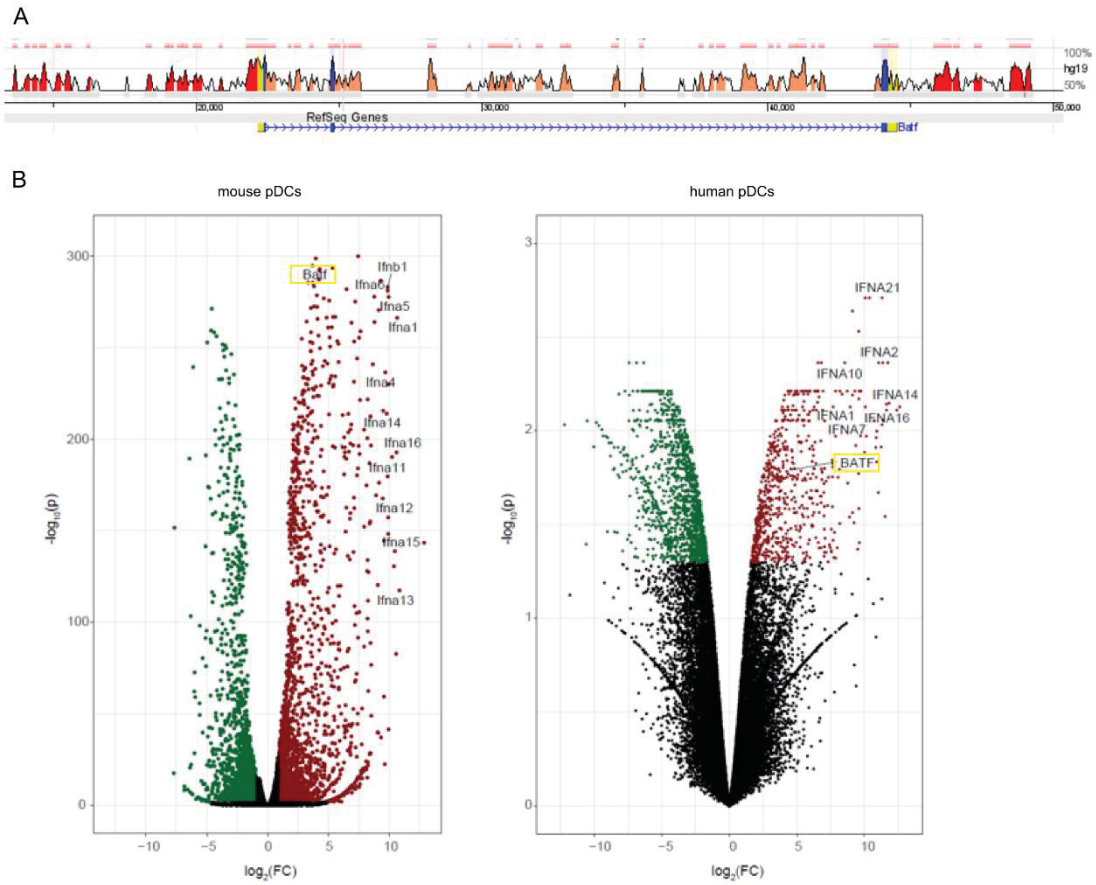

Figure 4 *Batf* is co-expressed with type I IFN in mouse and human pDCs. **A** Screen shot for evaluation of gene conservation from the ECR (evolutionary conserved regions) browser web site of the mouse as compared to the human *Batf* gene. Exonic regions are in blue, intronic regions in salmon, UTRs in yellow and CNS is in red. ECR regions are indicated by pink bars on top (ECR min length 100 base pairs and min identity 70%). **B** Volcano plots showing gene expression of naive vs CpG stimulated mouse (left) and human pDCs (right, GSE93679). The human data was re-analyzed using Biobase, GEOquery and limma R packages.

Taken together, BATF is well conserved in human and co-expressed along type I IFN in both mouse and human pDCs upon TLR9 stimulation, highlighting the

potential relevance of the investigated role of mouse BATF in DC development and function for human pDCs.

3.3.2 RNA-Seq reveals elevated type I IFN expression in *Batf*-deficient pDCs

To assess the impact of *Batf* on global gene expression in pDCs we performed RNA-Seq of sorted BM-derived Flt3-L pDCs from WT and *Batf*$^{-/-}$ mice that were left either naïve or treated with CpG (2h, 6h, 12h), a synthetic double-strand DNA that activates endosomal TLR9 when added directly to the culture medium, inducing a robust type I IFN production. In the untreated situation, there are 918 genes differentially expressed (DEGs) more than 2-fold between WT and *Batf*-deficient pDCs (**Fig. 5**). After CpG stimulation, 339 (2h), 1489 (6h) and 1570 (12h) genes are expressed at significantly different levels between the two genotypes, respectively. Compared to the untreated condition, we observe a reduction in the number of DEGs after pDCs are stimulated with CpG for 2h, which then increased again from 6h to 12h post CpG stimulation.

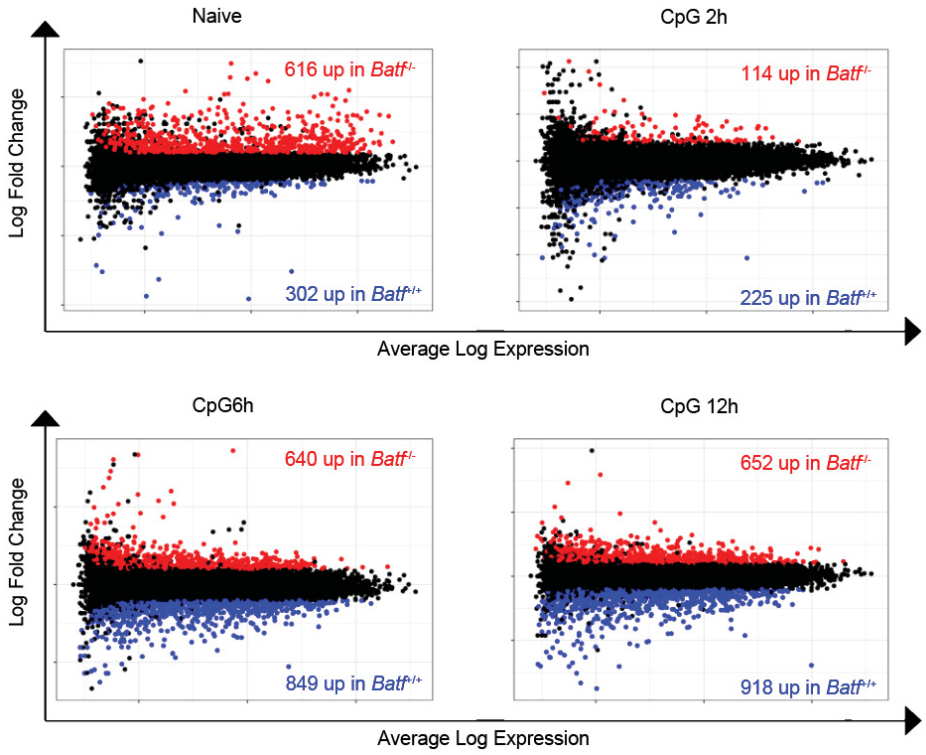

Figure 5 RNA-Seq reveals *Batf*-dependent gene expression in a longitudinal TLR9 activation study of pDCs. MA plots showing global expression of genes in sorted WT and *Batf*$^{-/-}$ pDCs at steady state and after 2h, 6h and 12h of CpG stimulation. Genes with a fold change |FC|≥2 and FDR ≤0.05 were considered significantly differentially expressed and are marked in colour (red and blue).

To better understand the biological impact of differential gene expression we next performed a Reactome pathway analysis. We observed that the IFNα/β and the cytokine signaling pathways are enriched in naïve pDCs in *Batf* absence. Further, the regulation of DDX58/IFIH1-mediated induction of type I IFN, IRF7 activation and TLR regulation are significantly enriched at 2h after CpG stimulation (**Fig. 6A**). In addition, a Gene Set Enrichment Analysis (GSEA) of the RNA-Seq experiments with naïve *Batf*-deficient vs WT pDCs was performed. While the Reactome pathway analysis takes into consideration only genes that are differentially expressed between two genotypes, the GSEA analysis requires an input of all expressed genes of the mouse genome to evaluate the influence of a genotype on biological pathways. The GSEA analysis for the Hallmark Pathways revealed a global up-regulation of type I IFN response genes (**Fig. 6B**). Hence the Reactome and GSEA pathway analyses suggest a significant impact of *Batf* on various pathways up- and down-stream of the type I IFN signaling cascade.

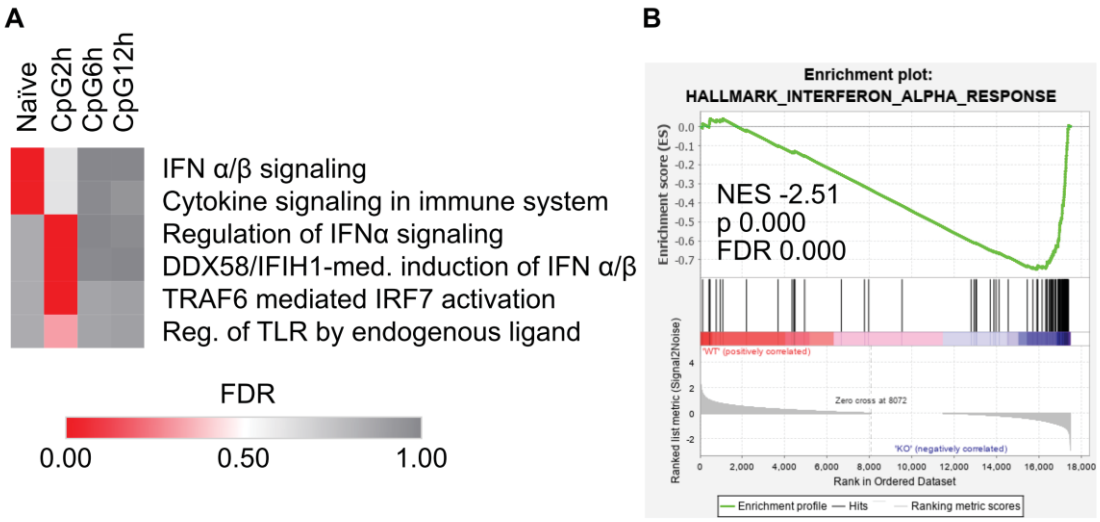

Figure 6 Reactome and GSEA analysis reveal underlying type I IFN signature in *Batf* deficiency. A Reactome pathway analysis of genes differentially expressed at the respective condition. Results are shown for the significance of the pathway (FDR) as heatmap. **B** GSEA of hallmark pathways for RNA-Seq data from naïve WT vs *Batf*$^{-/-}$ pDCs using normalized expression values and the gene set as permutation type.

An overall analysis of differentially expressed genes from our RNA-Seq revealed that more than half of the genes differentially expressed between naïve WT and *Batf*-deficient pDCs (504 out of 919) were annotated in the Interferome database as responsive to type I IFN (Interferome database v2.01) (Rusinova et al., 2013), and from these 68% were upregulated in *Batf*-deficient pDCs. At 2h after CpG

stimulation 339 genes were differentially expressed between WT and *Batf*-deficient pDCs. Among these, 184 were annotated in the Interferome database as responsive to type I IFN, and from these 33% were upregulated in *Batf*-deficient pDCs. At 6h and 12h after TLR9 activation of pDCs we found 1,489 and 1570 genes being differentially expressed between WT and *Batf*$^{-/-}$ pDCs. Strikingly, even at these later time points we found 622 and 667 genes to be annotated as responsive to type I IFN at 6h and 12h after CpG stimulation, respectively. Looking at the *Batf*-deficient states of 6h and 12h stimulated pDCs we discovered that 36% and 38% of ISGs were up-regulated in these states, respectively. We plotted all unique genes annotated as ISGs in at least one WT vs *Batf*$^{-/-}$ comparison (1,411 genes) in a clustered heatmap (**Fig. 7A**, selected genes highlighted). Discovering the pronounced ISG gene signature led us to speculate that BATF might block type I IFN expression. In line with this hypothesis, we found that pDCs stimulated with CpG showed a significant higher expression of all type I IFN genes except Ifna13 at 2h, but not at the later points of 6h and 12h (**Fig. 7B**). We were able to confirm key RNA-Seq results with an independent RT-PCR experiment on sorted BM-derived Flt3-L pDCs (data not shown). Absence of *Batf* did not affect the expression of most of the genes encoding components of the TLR9 signaling pathway (Tlr9 itself, Myd88, Trif1, among others) or the type I IFN receptor (Ifnar1, Ifnar2, Jak1, Jak2, among others) at any time point after CpG stimulation. However, Tlr9, Irf7, Atf3, Stat1 and Stat2 were significantly higher expressed in naïve pDCs in *Batf* absence (data not shown), which may explain a stronger type I IFN response after CpG stimulation in *Batf*-deficient pDCs as compared to WT cells. Also, this may already give insight into how BATF possibly regulates type I IFN expression by regulating the expression of certain components up and down-stream of the type I IFN signaling cascade.

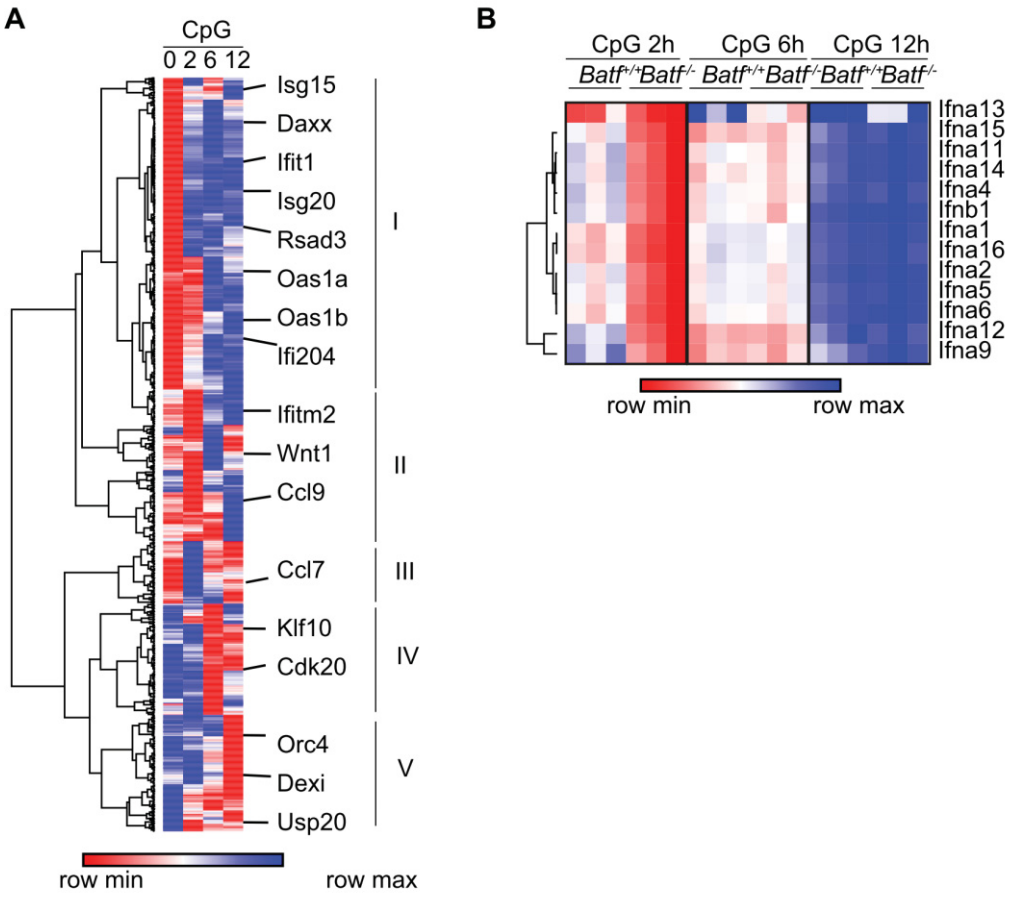

Figure 7 Elevated expression of type I IFN and ISGs in *Batf* absence. **A, B** Clustered heatmaps showing fold change (**A**) and normalized expression values (cpms, **B**) of type I IFN stimulated genes as annotated by the Interferome database (**A**) and type I IFN genes (**B**) between sorted WT and *Batf*$^{-/-}$ pDCs 2h, 6h and 12h after CpG stimulation and at steady state, respectively.

Altogether, the analysis of the RNA-Seq data revealed an unexpected function of BATF, since it is well known to induce the expression of cytokines after pathogen receptor stimulations it could also restrain type I IFN production and responses in pDCs.

3.3.3 BATF does not directly regulate type I IFN expression

To assess the possible direct impact of *Batf* on type I IFN expression and regulation of other genes by binding onto DNA we performed BATF ChIP-Seq in naïve and 2h CpG stimulated pDCs. Of 15453 BATF ChIP-Seq peaks, 4470 and 10983 bound within genes annotated by RefSeq in naïve and CpG stimulated pDCs, respectively. Interestingly, BATF binds extensively to exon regions in addition to promoter regions (**Fig. 8A**), and as anticipated, analysis of BATF ChIP-Seq peaks from pDC libraries identified enrichment of the AP-1 and AICE1 motifs (**Fig. 8B**),

which BATF is known to bind to extensively in B and T cells (Murphy et al., 2013). Notably, both motifs were enriched to a more significant extent after CpG stimulation of pDCs (**Fig. 8B**).

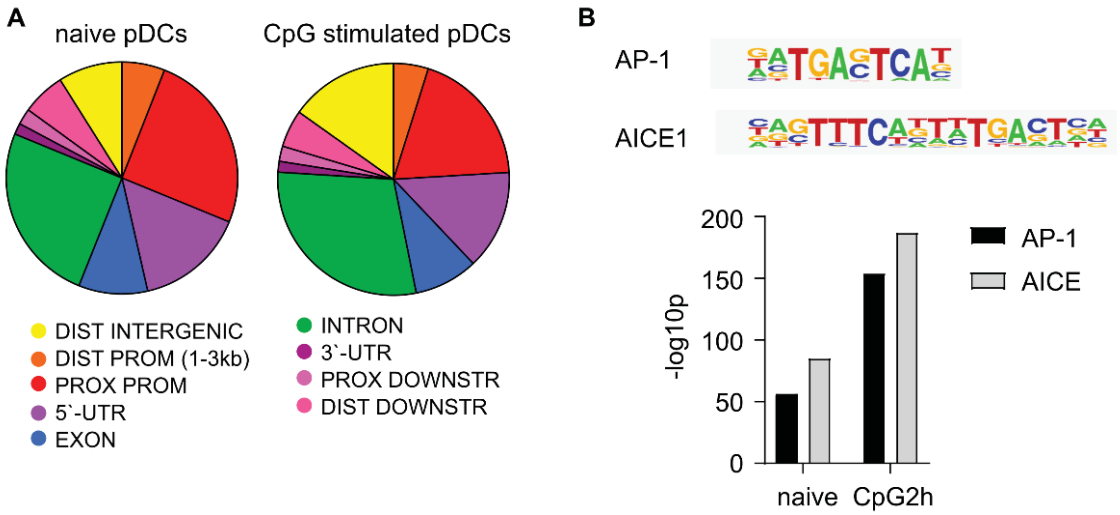

Figure 8 BATF extensively binds to AP-1 and AICE1 motifs in the pDC genome. A Genomic location distribution of BATF binding sites in naïve CpG stimulated pDCs according to BATF ChIP-Seq. Two biological replicates were used per condition, and results are shown for pooled samples per condition. **B** HOMER known motif analysis (JASPAR) for gene regions in naive and 2h CpG stimulated pDCs that interact with BATF according to ChIP-Seq.

However, our main hypothesis that BATF binds directly onto type I IFN genes to regulate their expression was not confirmed (**Fig. 9A**). BATF did not bind to *Ifnb1* associated genomic regions or regions associated with the gene loci of any IFNα subform except for IFNα13 and IFNα14 (**Fig. 9B**). The *Ifna14* gene is bound by BATF in the proximal promoter part under naïve and CpG 2h stimulated conditions, and *Ifna13* shows interaction with BATF in its distal promoter part after CpG stimulation of pDCs. When *Batf* is absent in pDCs we observe a higher expression of IFNα14, while IFNα13 is not expressed in pDCs, suggesting that BATF may inhibit IFNα14 expression by binding onto its promoter site.

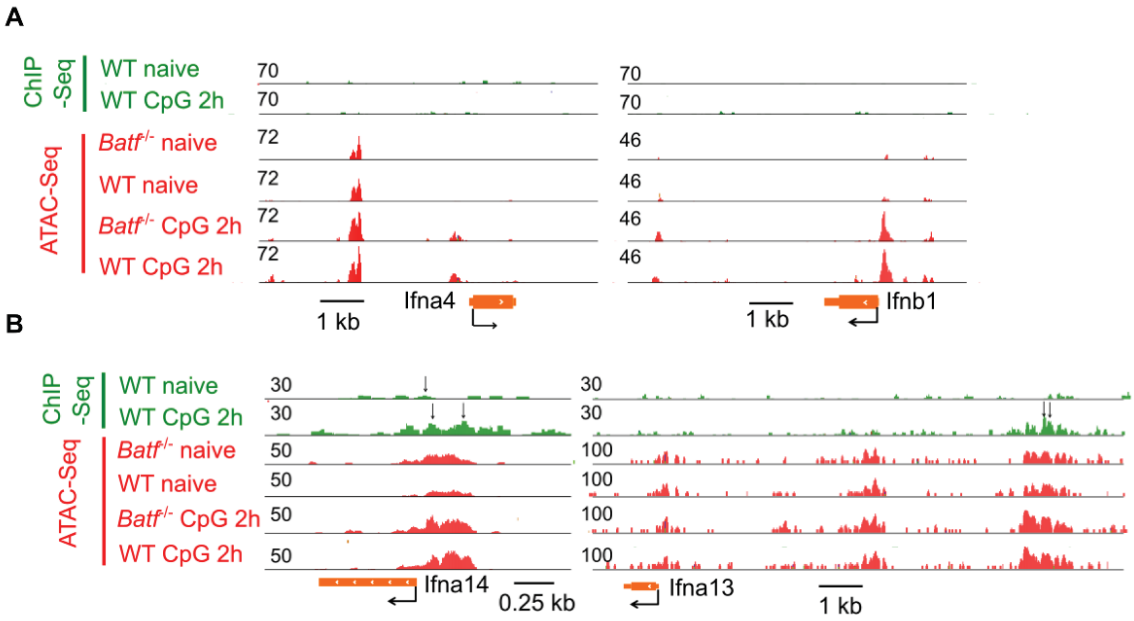

Figure 9 BATF does not bind onto type I IFN genes except *Ifna13* and *Ifna14*. A, B BATF ChIP-Seq (green) and ATAC-Seq (red) peaks visualized for the *Ifna4* and *Ifnb1* (**A**), and the *Ifna14* and *Ifna13* genes (**B**) using the IGV programme. Track height is shown by number on the left side. Arrows indicate significant BATF binding sites as calculated by the Model-based Analysis of ChIP-Seq (MACS) algorithm.

We further observed BATF targeting several type I IFN response genes (e.g. *Isg15*, *Isg20*), and all members of IRF family with the exception of *Irf3* (**Fig. 10**). This indicates possible direct regulation of signaling molecules important in the type I IFN signaling cascade by BATF.

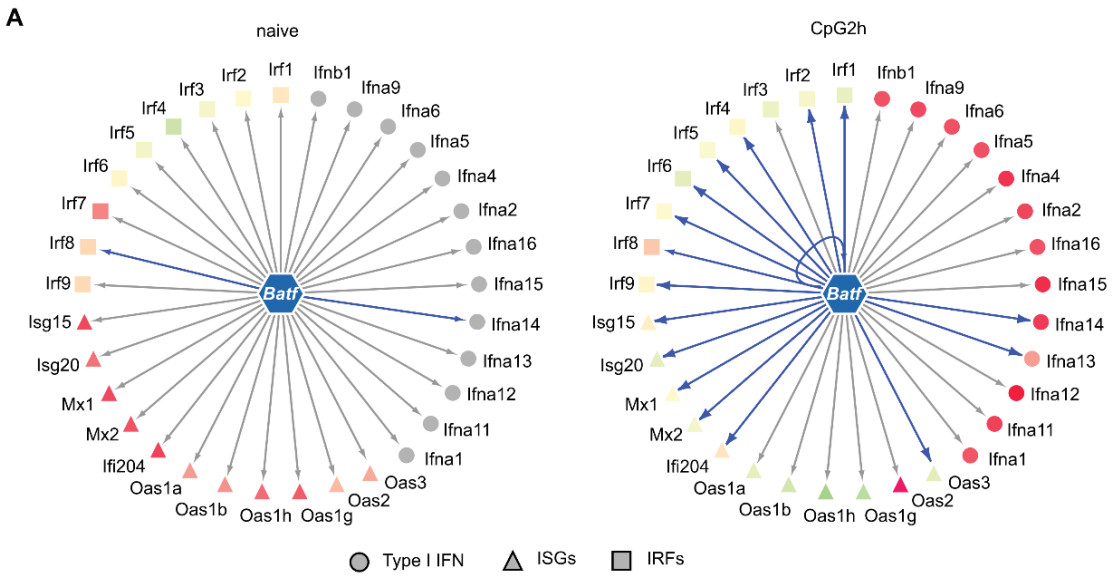

Figure 10 BATF does not directly regulate type I IFN genes but interacts with ISGs and IRFs. **A** Visualization of integrated RNA-Seq and ChIP-Seq data with Cytoscape. Gene shape represents gene groups, color of the gene shape indicates expression level (green: low expression, yellow: moderate expression, red: high expression, grey: no expression), and color of the arrow shows interaction (blue) or no interaction (grey) with BATF according to ChIP-Seq.

In summary, while BATF may directly target *Ifna14* and several ISGs its main mode of action to regulate type I IFN production in pDCs is not as a DNA interacting transcriptional regulator of promoter activity of type I IFN genes.

3.3.4 BATF controls type I IFN via Zfp366 (DC-SCRIPT)

We established in the last chapter that BATF does not directly regulate type I IFN expression by binding onto the promoter sites of these genes as determined by ChIP-Seq. We therefore sought to identify other factors that could explain the increased type I IFN production in *Batf*$^{-/-}$ vs WT pDCs after TLR9 activation. To restrict our search, we hypothesized that the factor(s) involved should fulfil the following criteria: (1) it must have BATF-dependent expression, (2) BATF must bind in the promoter of the factor in pDCs, and (3) the chromatin accessibility of the gene must be significantly altered by the loss of BATF in pDCs. Mining our dataset (**Fig. 11A, B**) revealed 12 and 19 genes fulfilling these criteria at steady state and after TLR9 activation, respectively. Strikingly, two genes, namely *Jdp2* and *Zfp366*, fulfilled the criteria in both pDC states. *Jdp2*, however, is a neighbouring gene directly upstream of *Batf*, which may be affected by the mutation in the *Batf* gene itself and has therefore been excluded from further

analysis. Instead, we decided to pay attention to *Zfp366*, also known as DC-SCRIPT. It is known from literature that Zfp366 is expressed in the nucleus of myeloid dendritic cells, pDCs and Langerhans cells (Triantis et al., 2006). Additionally it could be shown that Zfp366 induces the differentiation of cDC1 (Chopin et al., 2019).

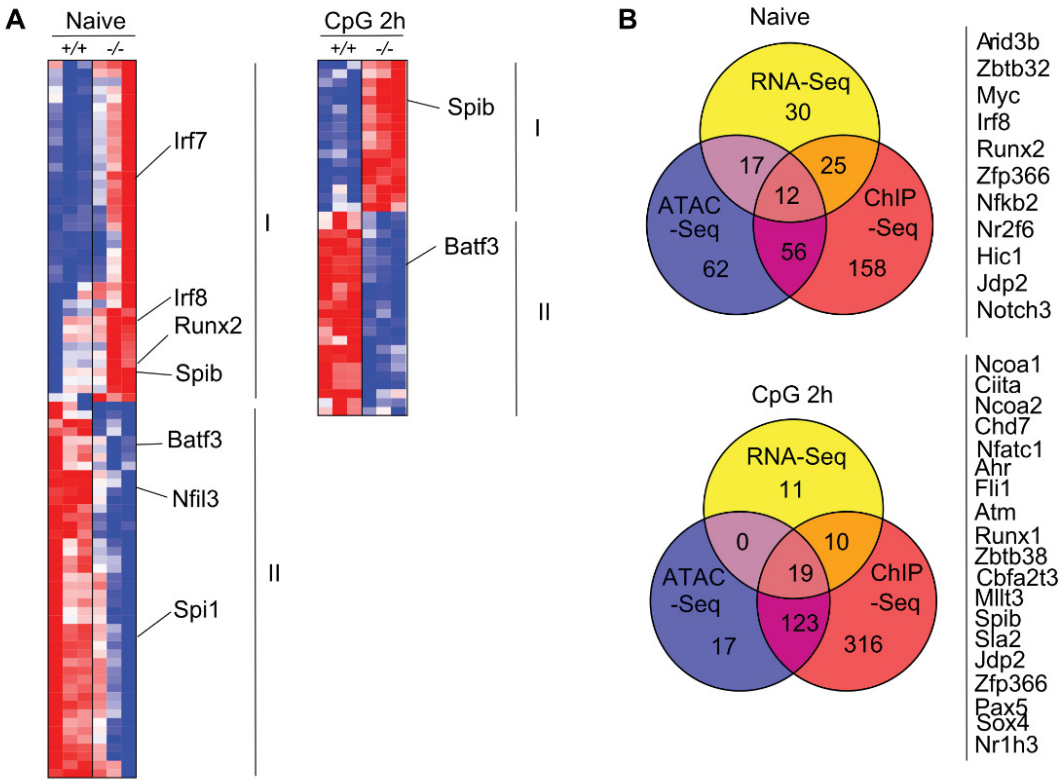

Figure 11 Differential expression of transcription factors in *Batf* absence. A Heatmaps showing significantly differentially expressed TFs between naïve (left) and 2h CpG stimulated (right) WT (+/+) and *Batf*$^{-/-}$ (-/-) pDCs from the RNA-Seq. TFs relevant for DC biology are highlighted. **B** Integrated RNA-Seq, ChIP-Seq and ATAC-Seq data for all mouse TFs (TRRUST ver2, https://www.grnpedia.org/trrust/) in naive (top) and 2h CpG stimulated (down) pDCs visualized in Venn diagrams. Total number of genes and the percentage thereof among all mouse TFs is shown for expression of genes between WT and *Batf*$^{-/-}$ pDCs (RNA-Seq, |fold change| ≥1.5 and FDR ≤0.05, EdgeR), direct BATF interaction with DNA (ChIP-Seq peaks called after MACS) and a differentially opening of chromatin between WT and *Batf*$^{-/-}$ pDCs (ATAC-Seq, |FC| ≥1.5 and FDR ≤0.05, DESEq2).

Our RT-PCR results revealed a reduced expression of Zfp366 in *Batf*-deficient pDCs both at steady state and 2h after CpG stimulation (**Fig. 12A**). In addition, we saw a significant reduction of Zfp366 expression in *Batf* absence as compared to WT pDCs at later time points of CpG stimulation (6h, 12h) in our RNA-Seq data (**Fig. 12B**). Zfp366 is well known to play an important role for cDC development at

steady state (Chopin et al., 2019) but no involvement in pDC biology or type I IFN production has been reported to date. Notably, the overall expression of Zfp366 increased in WT cells after CpG stimulation (**Fig. 12A**), which suggests a potential, important influence of Zfp366 for immunological processes after TLR9 stimulation, in addition to its already well known role in naïve cell conditions.

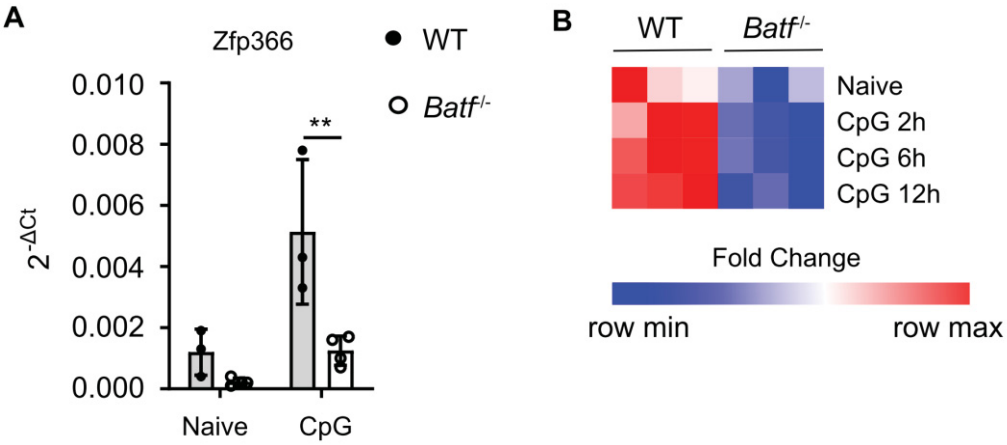

Figure 12 Reduced expression of Zfp366 (DC-SCRIPT) in naive and activated *Batf*$^{-/-}$ pDCs. A Quantitative RT-PCR for the expression of Zfp366 in sorted naive and CpG stimulated WT and *Batf*$^{-/-}$ pDCs. Data are the mean expression from four biological replicates (normalized to β-Actin) ± SD. **B** Heatmap showing the normalized expression (cpm) of Zfp366 in WT and *Batf*$^{-/-}$ pDCs at steady state and after CpG stimulation (2h, 6h, 12h).

When we focused on BATF binding positions in the Zfp366 gene, we observed a binding of BATF to three positions in its promoter at −1345, -2573 and −3464, respectively. Interestingly, BATF interactions on the Zfp366 gene are located in conserved CNS of this gene (**Fig. 13A**). Moreover, BATF binding was observed at positions where the chromatin is widely open in WT pDCs according to our ATAC-Seq data. However, when *Batf* is absent the chromatin closed up significantly within several regions upstream of the *Zfp366* gene (p≤0.05, FC≤-2, DESeq2 of ATAC-Seq data, **Fig. 13A**). In line with this we see a reduced expression of Zfp366 in *Batf*-deficient pDCs, suggesting that regulation of the chromatin structure in combination with direct binding of BATF onto the Zfp366 gene may constitute the mechanism of how BATF regulates Zfp366 expression. We next looked at the conservation of Zfp366 in other species. The core structure of elements regulating Zfp366 expression is well conserved between the proximal mouse and human gene promoters. Interestingly, this homology extends to the genomes of other mammal species. In particular, elements displaying a strong degree of

conservation across multiple species include the AP-1 motif known to be bound by BATF (Murphy et al., 2013) (**Fig. 13B**).

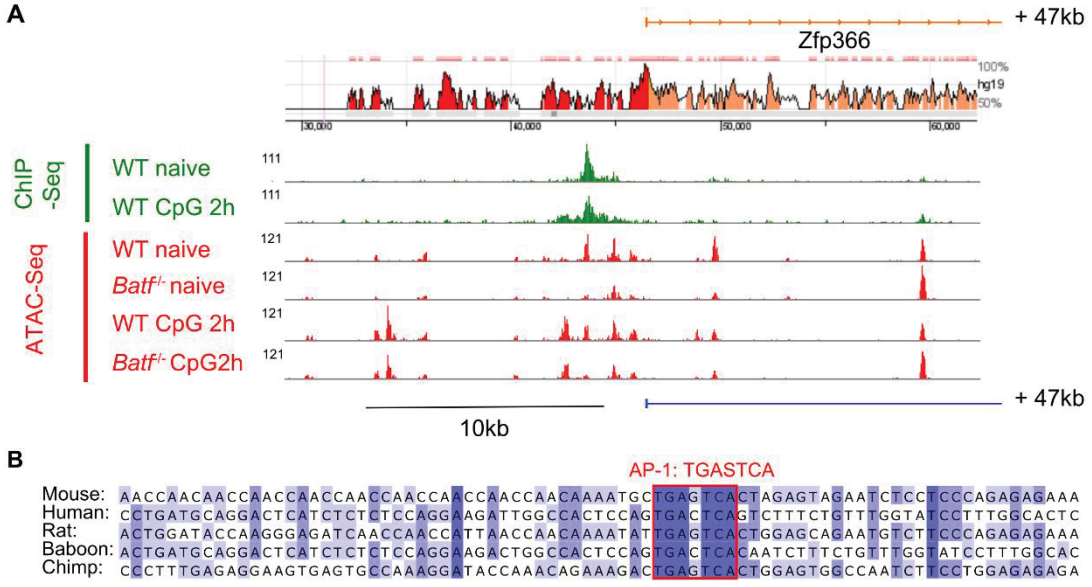

Figure 13 BATF directly binds onto the Zfp366 gene and modulates its chromatin. A Top panel presents a screen shot from the ECR (evolutionary conserved regions) Browser web site of the mouse *Zfp366* gene to evaluate gene conservation between mouse and human. Exonic regions are in blue, intronic regions in pink, UTRs in yellow and CNS is in red. Bottom panels present BATF ChIP-Seq in sorted WT naive and CpG stimulated (2h) pDCs, as well as ATAC-Seq peaks in WT and *Batf*$^{-/-}$ naive and CpG stimulated (2h) pDCs for the Zfp366 gene visualized with IGV. **B** Alignment of the BATF binding position at -3,464 of the TSS of the Zfp366 gene in different mammalian species. Alignment of the indicated genomic regions was done with Jalview with the blue coloring representing percentage identity. The position of the BATF binding to the AP-1 motif is marked with a red box.

In summary, we have identified a promising TF, Zfp366, that is directly regulated by BATF. First investigations on its possible impact for type I IFN expression have been performed by Shafaqat Ali using Ifnb- and Ifna4-promoter luciferase reporter assays (data not shown) that indicate a repressive function for type I IFN production. This suggests that BATF may repress type I IFN expression in pDCs via regulating Zfp366.

3.3.5 BATF reduces pDC mediated LCMV infection control

Type I IFN is known for its anti-viral effect to help clear infections from our body. As BATF represses type I IFN expression in pDCs we hypothesized that *Batf*$^{-/-}$ pDCs may exhibit enhanced antiviral effects *in vitro*. To evaluate the impact of increased type I IFN levels in pDCs during *Batf* absence for virus control we

assayed Lymphocytic choriomeningitis virus (LCMV) titres and plaque formation in an *in vitro* setting. Presence of *Batf*-deficient pDCs was associated with a reduced infection rate of MC57 fibroblasts as compared to the equivalent number of WT pDCs (**Fig. 14**).

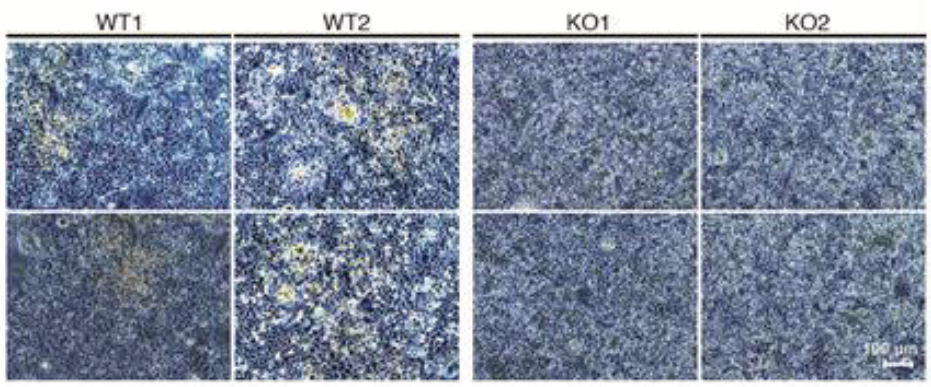

Figure 14 BATF reduces pDC mediated LCMV infection control. Representative pictures of MC57 fibroblasts infected with LCMV-WE for 4h. 18h prior to infection 50,000 purified WT or *Batf*$^{-/-}$ pDCs from BM-derived Flt3-L cultures were added. Staining was performed with VL-4 rat anti-LCMV mAb.

These findings suggest a modulatory role of BATF in pDCs for the type I IFN response leading to reduced virus control.

3.4 BATF negatively impacts pDC development

It had been assumed from previous studies that pDCs can differentiate from a common DC progenitor (CDP) within the myeloid branch (Naik et al., 2006). Recently, however, pDCs have been reported to develop predominantly from IL-7R^{+} lymphoid progenitors rather than CDPs (Dress et al., 2019; Rodrigues et al., 2018). The TFs IRF8 and E2-2, among others, were shown to be crucial in inducing pDC commitment (Ghosh et al., 2010; Reizis et al., 2011; Sichien et al., 2016). However, the detailed mechanisms of control of pDC development, and in particular whether they are of myeloid versus lymphoid origin, remains poorly understood. The following chapter aims at illuminating the impact of BATF on pDC cell fate TFs and pDC development in different secondary lymphoid organs.

3.4.1 Splenomegaly and lymph node enlargement in *Batf*-deficient animals

While the phenotype and numbers of B, T, iNKT cells and cDCs have been well described for *Batf*$^{-/-}$ mice (Schraml et al., 2009), no alterations have been reported for the pDC department or the development of secondary lymphoid organs. Therefore, we performed a comprehensive analysis of pDCs in different tissues of *Batf*$^{-/-}$ mice. Firstly, we observed that naïve *Batf*$^{-/-}$ mice held under SPF conditions had enlarged spleens and lymph nodes as compared to WT littermates (**Fig. 15A**). However, the frequency of pDCs (~0.4% and 1% in spleen and lymph nodes, respectively) was not elevated in these organs (**Fig. 15B**). Of note, overall absolute cell numbers in spleen and lymph nodes of *Batf*$^{-/-}$ mice were increased as compared to WT mice. Organ size correlated with a higher absolute number of cells per organ including a higher absolute number of pDCs in spleen and lymph nodes of *Batf*$^{-/-}$ mice (**Fig. 15B**).

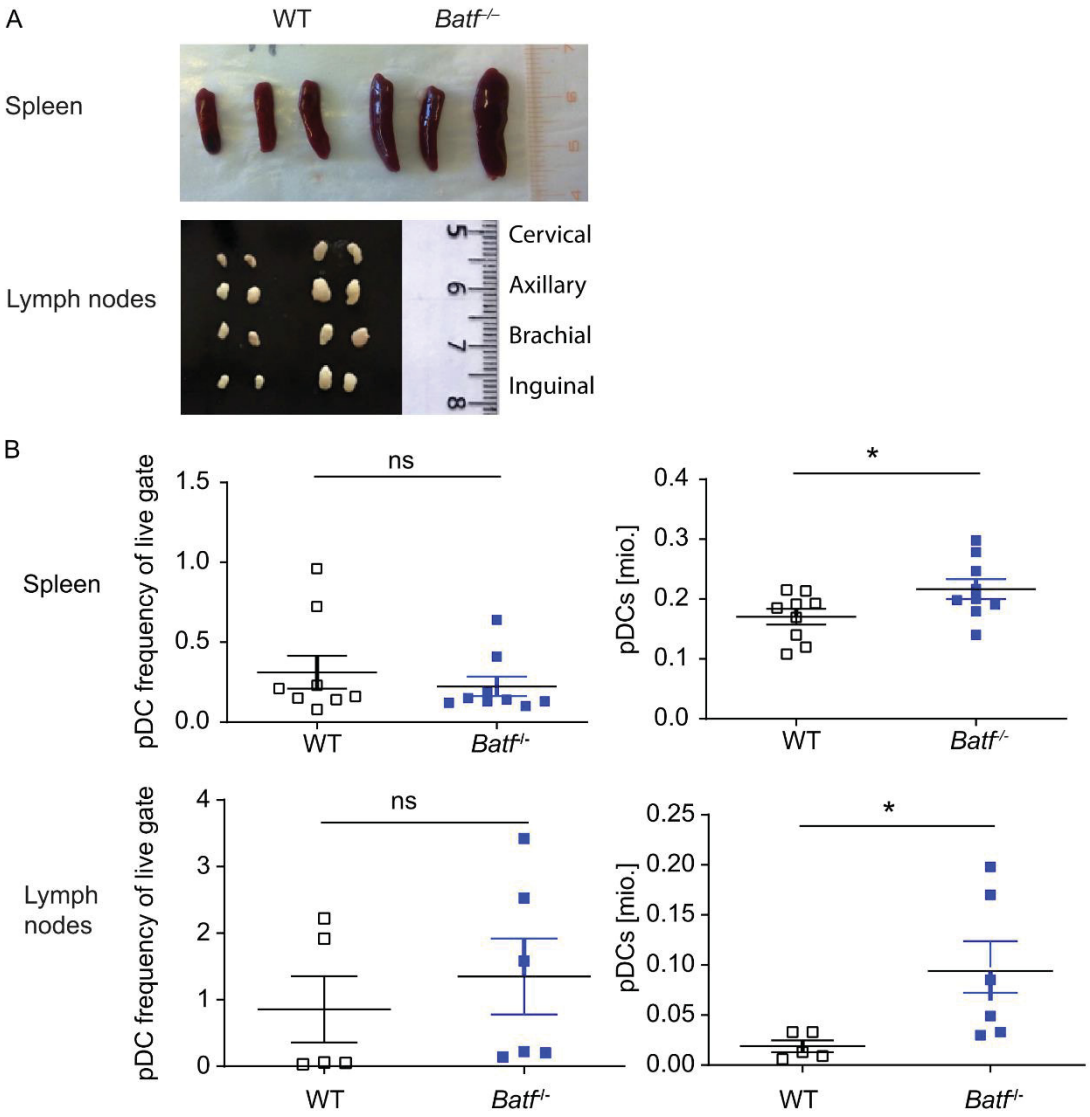

Figure 15 Enlarged spleen and lymph nodes without altered pDC numbers in *Batf*-deficient animals. A Spleen and lymph nodes from naïve WT and *Batf*$^{-/-}$ mice. **B** FACS analysis of pDC populations in the spleen and lymph nodes of naïve WT and *Batf*$^{-/-}$ mice.

In addition, an immunohistological staining for B cells (B220^{+}) and pDCs (SiglecH^{+}) was performed for the spleen and peripheral lymph nodes. We observed no obvious changes in the organ substructure as both the red and white pulp maintained its typical structural features in *Batf*-deficiency. pDCs were located in the marginal zone with no apparent differences in frequency between genotypes (**Fig. 16A**). Comparable results were obtained with an alternative staining for B cells (B220^{+}) and pDCs (mPDCA^{+}) (data not shown). While there is no impact of *Batf* on pDC numbers or localization in secondary lymphoid organs of *Batf*-deficient mice the question remains as to why the secondary lymphoid organs are enlarged

in these animals. One explanation would be the increased type I IFN expression that has been observed by *Batf*$^{-/-}$ pDCs. Possibly, an underlying type I IFN signature *in vivo* might explain the increased organ size. To discriminate between the effect of *Batf* vs type I IFN on organ size we morphologically evaluated spleens in Ifnar$^{-/-}$ and newly bred *Batf*$^{-/-}$ Ifnar$^{-/-}$ mice. We found that Ifnar$^{-/-}$ mice exhibited the smallest spleens. *Batf*$^{-/-}$ mice had significantly increased spleens as compared to WT and Ifnar$^{-/-}$ mice. Strikingly, the *Batf*$^{-/-}$ Ifnar$^{-/-}$ double knock out mice showed spleen sizes comparable to *Batf*-deficient mice (**Fig. 16B**), suggesting that the increase of spleen size in *Batf* absence is independent of Ifnar signaling.

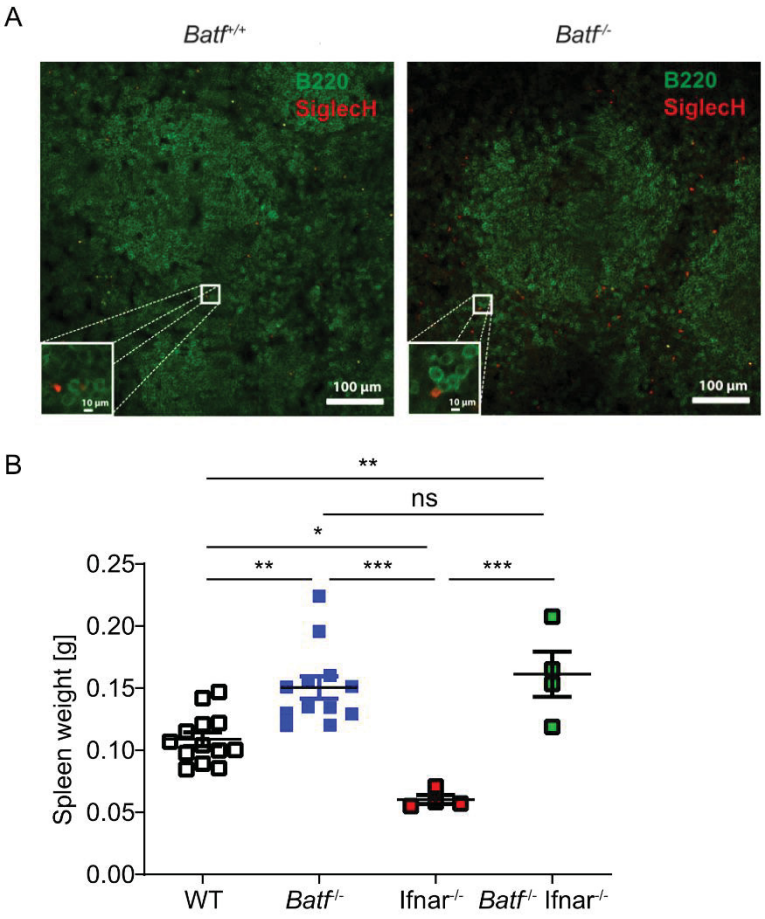

Figure 16 Impact of *Batf* on spleen structure and weight. **A** Immunofluorescent staining (B220^{+} in green and SiglecH^{+} in red) of the spleen of naïve WT and *Batf*$^{-/-}$ mice. **B** Spleen weight in g from comparable WT, *Batf*$^{-/-}$, Ifnar$^{-/-}$ and *Batf*$^{-/-}$ Ifnar$^{-/-}$ mice. Data is shown from one representative experiment out of a series of 3 (A, B). Differences between two groups were tested using two-paired t-test.

In summary, we have observed an Ifnar independent effect of BATF on spleen and lymph node size, which does not alter the substructure of the organs, or the pDC localization and frequency. Understanding how BATF impacts the size of secondary lymphoid organs remains to be elucidated.

3.4.2 BATF represses the expression of pDC specific TFs

TFs are well known for their role in the regulation of gene transcription, the conversion of DNA into RNA. They bind to specific sequences of DNA, usually enhancer or promoter sequences. Transcription may be either stimulated or repressed, allowing a unique expression of each gene in different cell types and during development. Some TFs are so called master regulatory TFs which tightly control the expression of a set of other TFs. The regulatory impact of BATF on the expression of TFs in pDCs at steady state or after CpG stimulation (2h, 6h, 12h) has been studied in a genome wide approach. For this purpose we analyzed all mouse TFs as defined in the TRRUST2 database (Han et al., 2018). In here 828 genes are defined as TFs in the mouse genome. We next performed a k-means clustering of these TFs using the fold change in expression between WT and *Batf*$^{-/-}$ pDCs using the pheatmap package in R (Kolde, 2019) (**Fig. 17A**). We found that our TFs cluster into 4 groups: Cluster 1 contains 45 TFs which are less expressed in *Batf* absence under all conditions, starting from naïve with an increase in average fold change leading up to CpG 12h. Cluster 2 consists of 88 TFs which are all expressed more in *Batf* absence with a similar increase in difference of gene expression between the genotypes over the duration of CpG stimulation. Cluster 3, interestingly, has 84 TFs that are expressed more *Batf*-deficient pDCs as compared to the WT control only under naïve condition, but not after CpG stimulation. Lastly, we have the large Cluster 4 that contains 364 TFs that are not very much affected by *Batf* presence or absence. We take from this that *Batf* does indeed affect the expression of a large set of TFs (Cluster 1-3) and can both suppress or initiate the expression of TFs under various conditions. To better understand the biology behind our clusters we next plotted the average of the normalized count (cpms) of all genes for each Cluster against the time points for CpG stimulation (0h, 2h, 6h, 12h) and have highlighted a few hallmark genes known for their importance in pDC biology (in orange, **Fig. 17B**). It is well known

that a set of TFs (e.g. Id2, Nfil3) drives the development of cDCs while another set of TFs (e.g. Tcf4, Irf8, Runx2, Bcl11a, Spib) drives precursor cells to differentiate toward pDCs (Chopin et al., 2016; Cisse et al., 2008; Sichien et al., 2016). Strikingly, we found that cDC driving TFs are less expressed in *Batf*-deficient pDCs (Cluster 1) while pDC driving TFs are expressed more in *Batf* absence (Cluster 2). This suggests a negative role of *Batf* for the expression of pDC driving TFs, possibly negatively regulating pDC development. Cluster 3 contains e.g. Irf7, a TF that is essential for type I IFN signaling in pDCs. Surprisingly, this factor is already expressed at higher levels in *Batf*-deficient pDCs at steady state, so before the cell receives the signal to produce type I IFN via CpG stimulation. Hence Irf7 may explain the more robust induction of type I IFN in naïve, *Batf*-deficient pDCs as compared to WT pDCs. Cluster 4 contains genes that show little impact by *Batf* absence regarding their expression, many of which also do not have any known role for pDC development or effector function. As *Batf* presence or absence is affecting mostly prominent TFs known for their requirement to ensure proper pDC functions and differentiation we can assume that BATF is an important factor in pDC biology itself.

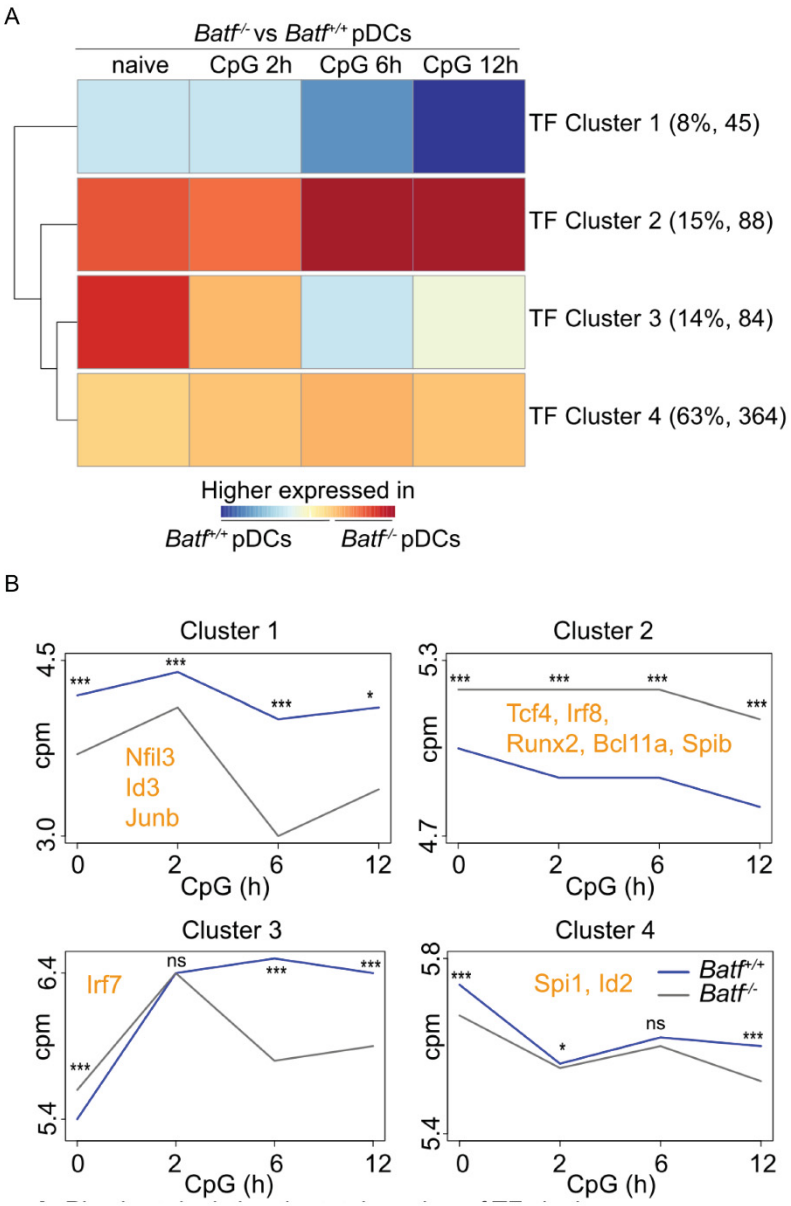

Figure 17 Clustering of differentially expressed TFs between WT and *Batf*$^{-/-}$ pDCs in a longitudinal pDC activation study. A k-means clustering of all in pDCs expressed mouse TFs between WT and *Batf*$^{-/-}$ pDCs in naïve condition and after CpG stimulation at different time points (2h, 6h, 12h). Differential expression was determined using edgeR (FDR<5%, |FC|>2). **B** Counts-per-million (cpm) of cluster genes from **A** shown for WT and *Batf*$^{-/-}$ pDCs. Statistics were performed using the Wilcoxon matched-pairs signed rank test.

Lastly, we evaluated the direct vs indirect impact of *Batf* on TF gene expression regulation. To this end we integrated our RNA-Seq with out BATF ChIP-Seq and ATAC-Seq data (**Fig. 18**). Overall, we found in RNA-Seq that 26% of all TFs (153 genes) expressed in pDCs are dependent on *Batf* regarding their expression under the tested conditions (naïve, CpG 2h, 6h, 12h). Further, 81% of all TFs (469 genes) interact directly with BATF. Against our expectation much of the BATF binding onto

genes seems to be non-functional as we see no impact on gene expression when BATF is absent: Only 110 genes out of 469 show both BATF binding onto their promoter and or enhancer site and changes in gene expression when BATF is not expressed. However, TFs do not only regulate gene expression by direct DNA interaction, but they may also modulate the chromatin landscape to regulate expression as so called pioneering TFs. When the chromatin is open at a specific genomic location other TFs can be recruited and bind to the accessible DNA stretch to regulate gene expression. When the chromatin is closed the DNA becomes inaccessible in that particular genomic region. The opening and closing of chromatin is known to be regulated by direct interaction of pioneering TFs with chromatin. BATF has been reported to have a pioneering function in Type I regulatory T (Tr1) cells (Karwacz et al., 2017). We found that BATF modulated the chromatin of 162 TFs, and that 47 of these have an altered expression in BATF absence. Further, 139 of the TFs that have an altered chromatin opening in *Batf*-deficient pDCs as compared to WT pDCs also indicate direct binding of BATF onto their DNA. This suggests that BATF may exert both a pioneering function and direct DNA binding function to regulate gene expression of TFs. It has not been well studied whether pioneering factors commonly also bind to gene regulatory sequences of the genes that they modulate the chromatin structure of. But we became in interested in genes that would be very strongly regulated by BATF and hence looked for genes that fulfilled three criteria: (1) They are differentially expressed between WT and *Batf*$^{-/-}$ pDCs, (2) BATF directly interacts with their DNA, and (3) their chromatin structure is altered in *Batf* absence (including the promoter and downstream region of the respective gene for ~10,000 nucleotides). We found 6 genes that fulfil all three criteria, intriguingly among them Irf8, which is well known to be required for inducing pDC differentiation (Sichien et al., 2016). The direct impact of *Batf* on expression and epigenetic state of a TF essential for pDC development once more stresses the potential role of *Batf* itself for pDC differentiation.

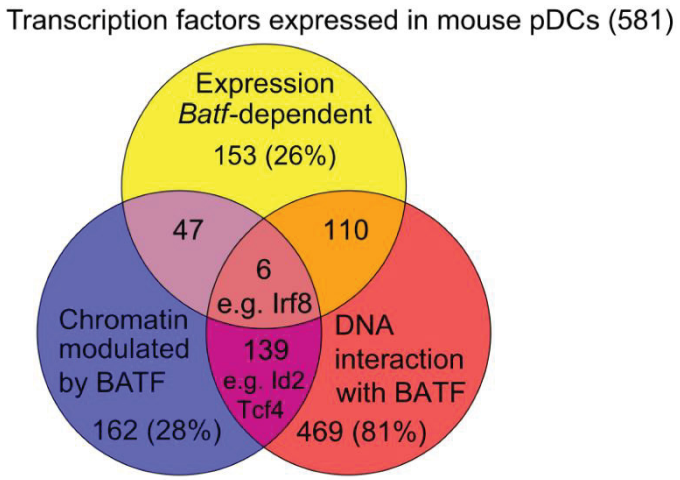

Figure 18 Impact of *Batf* on the epigenetic state and expression of TFs in pDCs. Venn diagram showing the actual and overlapping numbers and percentages of TFs which are regulated by BATF regarding expression (RNA-Seq), chromatin structure (ATAC-Seq) and by direct DNA interaction (ChIP-Seq).

Taken together as a first summary, BATF influences the expression of hundreds of TFs by direct interaction with their DNA (intergenic and promoter regions) and by modulation of their chromatin landscape, suggesting BATF is a master transcriptional regulator of other TFs in pDCs.

As we have just discussed we found that pDC specific TFs such as E2-2 and Irf8 are significantly increased in expression in naïve *Batf*-deficient vs WT pDCs (**Fig. 17B**), indicating a possible role for BATF in pDC differentiation. At the same time, cDC specific TFs such as Nfil3 were significantly reduced in *Batf*-deficient pDCs. Notably, BATF also binds to promoter and/or enhancer elements of most of these genes. In line with this BATF seems to also regulate the chromatin of the respective gene groups in a favorable manner: pDC specific factors have a more open chromatin structure in *Batf* absence, which facilitates the access of various TFs including BATF to this DNA stretch to induce gene transcription. On the other hand, cDC specific factors such as Id2 and Zfp366 have a reduced chromatin opening in *Batf* absence, which decreases their access of DNA for other TFs and leads to a reduced expression in *Batf*-deficiency (**Fig. 19A**). So far, we could show the role of BATF for binding onto DNA regulatory sequences and the chromatin structure to be significant in statistical terms. We next looked at the sequencing peaks from our global ‘omics data to evaluate the visual peaks for the impact of *Batf* on gene

expression of pDC and cDC specific factors. We found that Id2, a cDC driving TF, shows reduced expression in *Batf*$^{-/-}$ pDCs (**Fig. 19B**). Also, we see BATF binding onto its proximal promoter part after CpG stimulation but not at steady state. Most strikingly, the chromatin of Id2 was almost completely closed up in *Batf*-deficient pDCs, explaining the reduced expression in *Batf* absence. Interestingly, we see that the chromatin also closes up in WT pDCs after CpG stimulation, highlighting here an additional impact of CpG on the expression of the cDC driving TF Id2. We also show here one exemplary gene of the pDC driving TFs: The *Tcf4* gene that encodes the E2-2 protein. As the gene is rather large (~38kb) we show here the transcriptional start site (TSS) and proximal promoter. We have a slightly enhanced expression of Tcf4 in *Batf* absence, and direct binding of BATF onto its promoter and enhancer elements in naïve as well as CpG stimulated condition. However, the before as statistically significant calculated chromatin changes between WT and *Batf*$^{-/-}$ pDCs are not very convincing by the eye, suggesting that BATF regulates Tcf4 expression in pDCs by direct DNA interaction rather than by modulation of its chromatin structure.

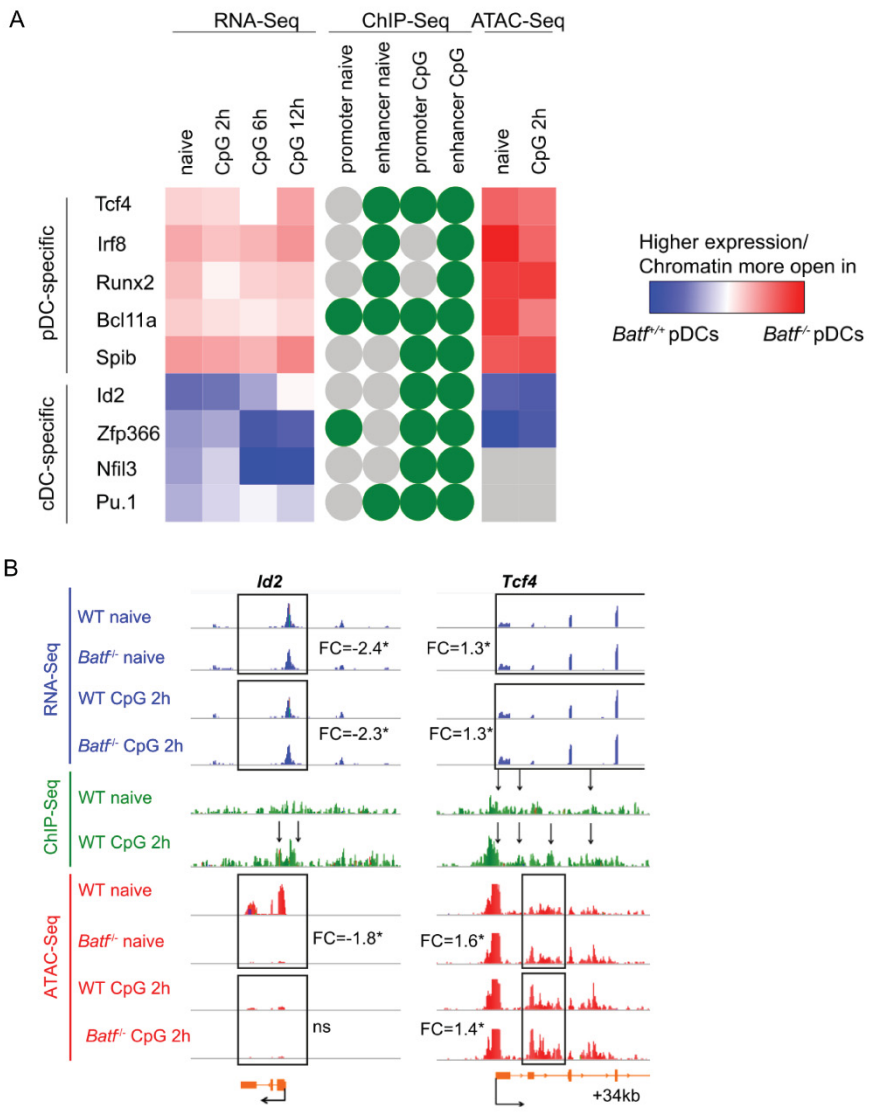

Figure 19 pDC and cDC-specific cell fate TFs are regulated by BATF. A, B RNA-Seq, BATF ChIP-Seq and ATAC-Seq signals in sorted BM-derived Flt3-L WT and *Batf*$^{-/-}$ pDCs for pDC and cDC-specific TFs visualized as a heatmap (**A**) and peaks of the *Id2* and *Tcf4* gene (**B**).

We next confirmed our results from RNA-Seq with RT-PCR using sorted pDCs from BM-derived Flt3-L cultures. We found that the pDC driving factors Tcf4, Irf8 and Runx2 are significantly more expressed in *Batf*-deficiency, while the cDC driving factors Id2 and Nfil3 were reduced in their expression in *Batf* absence (**Fig. 20A**). A higher expression of pDC driving TFs in fully differentiated *Batf*-deficient as compared to WT pDCs indicates a “super pDC” state. The hallmark of DC driving factors is their increased expression in precursor cells that can differentiate into different DC subtypes. We wanted to evaluate the expression of pDC driving TFs in whole *ex vivo* bone marrow, which contains various precursor cells from

lymphoid and myeloid origin. To this purpose we first depleted *ex vivo* BM of fully differentiated immune cells other than pDCs, namely T, B and NK cells using MACS. Next Tcf4 (E2-2) expression was evaluated with RT-PCR. Strikingly, we found higher expression of Tcf4 in *Batf*-deficient T, B and NK cell depleted *ex vivo* BM (**Fig. 20B**), opening up questions about the impact pf BATF on differentiation of pDCs that need to be answered with additional wet lab experiments.

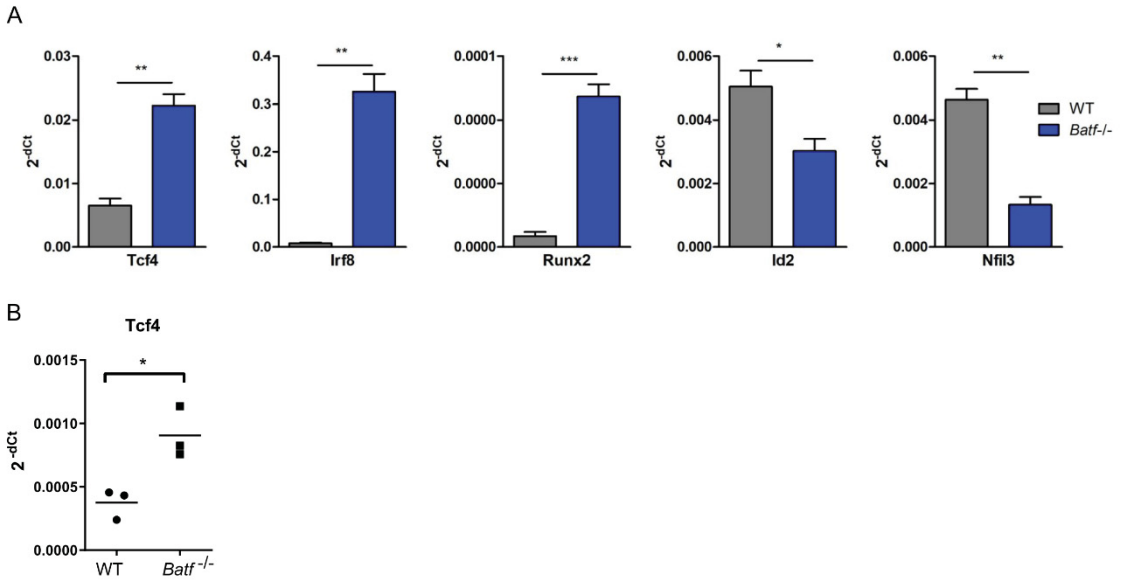

Figure 20 RT-PCR of pDC cell fate TFs in fully differentiated pDCs and depleted bone marrow of *Batf*$^{-/-}$ mice. A Expression of pDC and cDC-specific TFs in *in vitro* BM-derived Flt3-L FACS-purified pDCs in *Batf*-deficiency and WT controls (RT-PCR, two-sided students t-test). **B** Expression of Tcf4 in B, T, NK cell depleted *ex vivo* BM of *Batf*$^{-/-}$ and WT mice determined by RT-PCR (n=3).

In summary, we found that BATF repressed expression of pDC cell fate driving TFs and activated cDC driving TFs by direct interaction with the promoter and intergenic elements of the respective genes, as well as modulation of their chromatin landscape upon TLR9 activation of pDCs.

3.4.3 BATF negatively impacts pDC development *in vitro*

BM-derived Flt3-L cultures were used to investigate the impact of *Batf* on pDC differentiation *in vitro*. We observed a general trend of elevated pDC frequencies and decreased cDC frequencies in BM-derived Flt3-L cultures from *Batf*$^{-/-}$ mice (**Fig. 21A**). In fact, significantly elevated numbers of pDCs were present in the *Batf*-deficient cultures already at day 3 of culture, and with an increasing duration of

culture time the difference in pDC numbers between the genotypes increased even more (**Fig. 21B**).

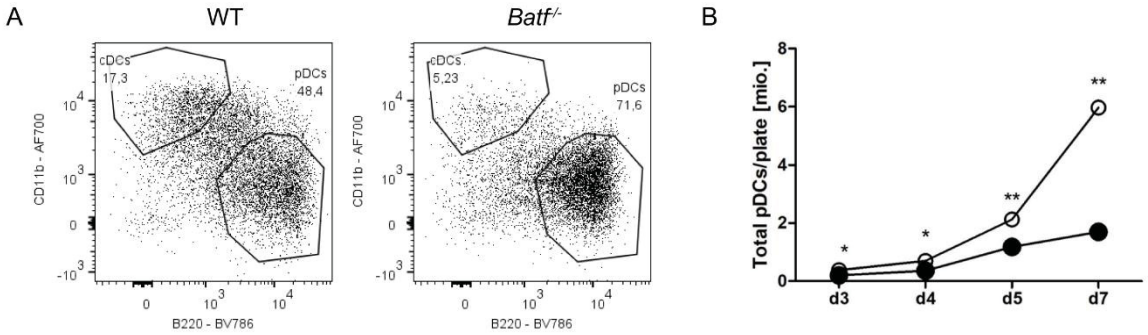

Figure 21 Increased frequency and total number of pDCs in BATF absence *in vitro* A Percentages of pDCs and cDCs in BM-derived Flt3-L cultured DCs from WT and *Batf*$^{-/-}$ mice as analyzed by FACS. **B** Total number of pDCs per BM-derived Flt3-L culture from WT and *Batf*$^{-/-}$ mice shown over a time course of the naïve Flt3-L culture (d3 to d7).

Hence, BATF clearly has an influence on pDC frequencies and numbers in BM-derived Flt3-L cultures, confirming a biological impact of BATF expression for pDC differentiation.

3.4.4 BATF regulates pDC development independent of IFNAR-mediated signaling

We wanted to explain the increase in pDC numbers. One explanation is the increased expression of pDC cell fate TFs that we have seen in our RNA-Seq and RT-PCR experiments. Another explanation could be type I IFN that is known to drive pDC differentiation and numbers (Chen et al., 2013). As we observed more type I IFN production in pDCs in *Batf* absence, we had to discriminate between the possible impact of *Batf* vs activation of the type I IFN receptor pathways on increased pDC numbers in our BM-derived Flt3-L cultures. For this purpose, we made use of the Ifnar$^{-/-}$ mice (Muller et al., 1994) which lack the receptor that recognizes type I IFN and hence cannot activate the JAK-STAT pathway. In addition we bred a new mouse genotype, the Ifnar$^{-/-}$ *Batf*$^{-/-}$ double knock out mouse. We next created BM-derived Flt3-L cultures and determined pDC frequencies and total numbers per culture via FACS. We were able to confirm our previous results showing that BM-derived Flt3-L cultures from *Batf*$^{-/-}$ mice have a significantly increased number of total pDCs as compared to cultures from WT controls (**Fig. 22A**). Notably, we see this effect not only at naïve condition but also after 12h of CpG stimulation (**Fig. 22B**). As type I IFN has a driving role for pDC differentiation

we find in accordance with this that the smallest number of pDCs can be found in both naïve CpG stimulated cultures from Ifnar$^{-/-}$ mice. Knocking out *Batf* in addition to Ifnar, however, shows a dramatic increase in pDC numbers as compared to the single Ifnar-knock out, once again, demonstrating that the impact of BATF on pDC development is independent of Ifnar signaling in both steady state and after CpG stimulation.

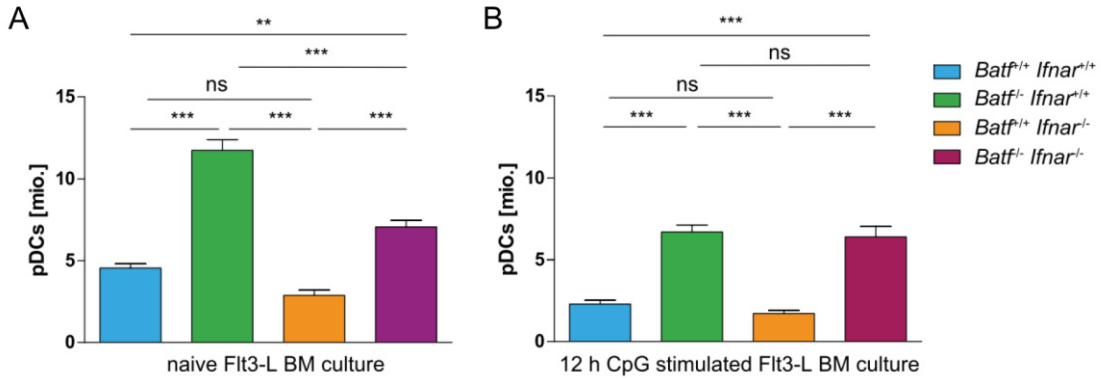

Figure 22 Increase of pDC numbers in *Batf* absence is independent of Ifnar signaling. Total number of pDCs in naïve (**A**) and 12h CpG stimulated (**B**) BM-derived Flt3-L cultures of WT, *Batf*$^{-/-}$, Ifnar$^{-/-}$ and Ifnar$^{-/-}$ *Batf*$^{-/-}$ mice as determined by FACS (1-way ANOVA, Tukey's multiple comparison test).

In summary, BATF negatively impacts the expression of pDC driving TFs and pDC numbers in BM-derived Flt3-L cultures independently of Ifnar signaling.

3.5 BATF is a pioneering transcription factor in pDCs

The previous chapters showed that the TF BATF extensively binds onto intergenic and non coding sequences of genes in mouse pDCs according to ChIP-Seq. Interestingly, BATF together with members of the IRF family has been shown to regulate chromatin accessibility and act as pioneer factors in Tr1, Th17 and $CD8^+$ T cells (Ciofani et al., 2012; Karwacz et al., 2017; Kurachi et al., 2014). Pioneering factors can either “turn on” genes by making a genomic region more accessible, or “turn off” genes by decreasing chromatin accessibility. It is tempting to speculate that BATF might fulfil similar pioneering but yet unknown functions in pDCs.

To assess potential pioneering roles of BATF during pDC differentiation, we measured chromatin accessibility using ATAC-seq in pDCs deficient for *Batf* in naive conditions and at 2h after CpG stimulation and the respective WT controls (n=2). We detected ~116,000 accessible regions (peaks) across samples, and next performed a differential analysis with DESeq2 to quantify the number of BATF-dependent accessible peaks, subsampling to ensure equal statistical power for each condition. BATF deficiency substantially altered the chromatin landscape, leading to upwards of ~2,500 altered accessible regions (FDR=10%, $\log_2$|fold-change|>1, **Fig. 23A, B**). In detail, BATF deficiency in naive pDCs resulted in 880 peaks with increased accessibility and 287 peaks with decreased accessibility. After CpG stimulation we observed 1358 peaks with increased accessibility and 488 peaks with decreased accessibility (**Fig. 23A, B**), showing first of all that TLR9 signaling increases the impact of BATF on the number of differentially accessible genomic regions in pDCs. Additionally, we see that ~75% of all BATF-dependent chromatin regions in both naive and 2h CpG stimulated pDCs have increased accessibility in *Batf*$^{-/-}$ cells, suggesting that most of the pDC chromatin landscape is „turned on“ rather than being „turned off“ in *Batf* absence (**Fig. 23A, B**). We further compared the specific genomic location with accessible chromatin between *Batf*$^{-/-}$ and WT pDCs. We found no apparent shift in the distribution of genomic locations where chromatin is accessible in pDCs in *Batf* absence (**Fig. 23C**), suggesting BATF regulates chromatin accessibility globally in pDCs but yet does not induce shifts in the chromatin landscape per se.

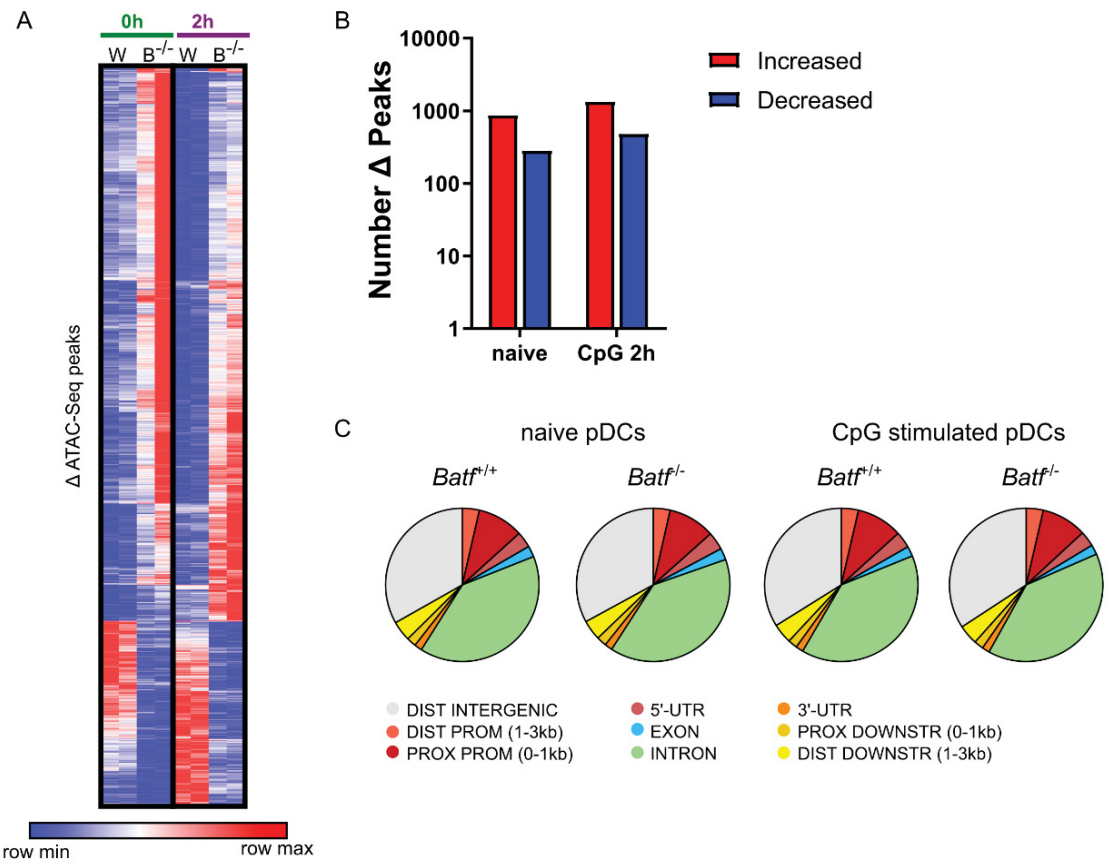

Figure 23 BATF increases and decreases chromatin accessibility of hundreds of regions in pDCs. A Heatmap of normalized ATAC-Seq peak intensities (log_2-fold changes relative to the mean for each peak). Limited to (2410) peaks that are condition-dependent with log2|FC|>1 and FDR=5% for eat least one pairwise comparison of interest. **B** Number of differentially accessible peaks detected using DESeq2, comparing *Batf*$^{-/-}$ to control pDCs at steady state and 2h after CpG stimulation, log2|FC|>1 and FDR=10% (Subsampled, each comparison had n=2). **C** Genomic location distribution of open chromatin sites in naïve and CpG stimulated WT and *Batf*$^{-/-}$ pDCs according to ATAC-Seq. Two biological replicates were used per condition, and results are shown for pooled samples per condition. W, *Batf*$^{+/+}$: WT; B: *Batf*.

In summary, the differences in chromatin landscapes of *Batf*$^{-/-}$ and WT pDCs at steady state and after TLR9 activation point to a role of BATF in epigenetic modulation of pDC differentiation and function as a pioneering factor in pDCs for the first time.

4. Author Contributions

The microarray data was generated and analyzed by Philipp Dresing, Regine Dress and Jens Bauer (Lab of Prof. Scheu, Institute of Medical Microbiology and Hospital Hygiene, Heinrich Heine University Düsseldorf). BM-derived Flt3-L cultures of DCs and subsequent FACS sort of WT and *Batf*$^{-/-}$ pDCs for RNA-Seq, BATF ChIP-Seq and ATAC-Seq assays were performed by Shafaqat Ali (Lab of Prof. Scheu, Institute of Medical Microbiology and Hospital Hygiene, Heinrich Heine University Düsseldorf). NGS was performed by Patrick Petzsch (Biological and Medical Research Centre (BMFZ), Heinrich Heine University Düsseldorf) and ChIP-Seq, ATAC-Seq was performed by Active Motif (Belgium). Raw data was then annotated to the mouse genome by Patrick Petzsch (RNA-Seq) and Active Motif (ChIP-Seq, ATAC-Seq). Calculation of normalized expression values and differentially expressed genes, as well as all further downstream analyses (quality controls, heatmaps, volcano plots, venn diagrams, pathway analyses, visualization of peaks etc.) of the RNA-Seq was performed by me. Also, all downstream analyses and visualizations for ChIP-Seq and ATAC-Seq as well as the analysis of publicly available data was performed by me. I generated and analysed all FACS data for cell numbers, surface marker expression and activation analysis of naïve and CpG-stimulated BM-Flt3-L-derived pDCs from WT, *Batf*$^{-/-}$, Ifnar$^{-/-}$ and *Batf*$^{-/-}$ Ifnar$^{-/-}$ mice. I prepared and stained all spleen and lymph node sections from *Batf*$^{-/-}$ and WT mice for immunofluorescence analysis, took the images and analysed them. Further, bone marrow cultures, RNA isolation and qRT-PCRs were performed by me, while Shafaqat Ali sorted the pDCs used for qRT-PCR. Likewise, the pDC sort for the LCMV infection assay was performed by Shafaqat Ali but the assay itself including feeder cell culture and LCMV staining was performed by me.

5. Discussion

TFs control gene expression by direct binding to regulatory regions of target genes but also by impacting chromatin landscapes and modulating DNA accessibility for other TFs. In recent decades several TFs have been defined that control cell fate decisions and effector functions in the immune system. pDCs are an immune cell type with the unique capacity to produce unmatched amounts of type I IFNs quickly in response to contact with viral components. Hereby, this cell type is involved in anti-infectious immune responses but also in the development of inflammatory and autoimmune diseases. To date, the global TF reservoir in pDCs remains to be fully characterized. For the first part of this doctoral thesis we performed a detailed analysis on the changes in expression and chromatin accessibility for the complete set of all known TFs in pDCs in an early time course after activation. This work has been published on bioRxiv, (https://doi.org/10.1101/2021.04.14.439791) and a revised version is under review with the Journal BMC Genomic Data. Therefore the results on this work will be discussed only shortly in this thesis.

In the second part of this doctoral work we evaluated the role of the TF BATF on pDC effector function and development. In a previous publication we showed that IFNβ is produced by a very small subpopulation of pDCs after TLR9 stimulation (Bauer et al., 2016; Scheu et al., 2008) which highly expressed the TF BATF. In this study we show that BATF is a dual negative regulator of type I IFN production and pDC differentiation, influencing thousands of genomic regions by binding to cis regulatory and enhancer regions and exerting pioneering functions to modulate the chromatin landscape.

5.1 The transcription factor reservoir and chromatin landscape in activated pDCs

We used as the basis of our study the definition of the murine TF reservoir in the AnimalTFDB (Hu et al., 2019) and found that 70% of all genes annotated as TFs in the mouse genome (1014 out of 1636) are expressed in naïve or specifically activated pDCs (CpG 2h, 6h, 12h), covering a wide range of TF classes based on different DNA binding mechanisms. Global TF expression analysis led to the definition of the identification of 661 unique TFs, which show a significant change in expression in at least one condition compared to another ($|FC|>2$, $p<0.05$, pDC

at steady state, or after CpG activation at 2h, 6h, 12h). Downstream gene ontology (GO) analyses of RNA-Seq data allowed a biological evaluation of all TFs, showing involvement in a wide variety of biological processes, such as the NFκB and JAK-STAT signaling, circadian regulation of gene expression, and sumoylation, among others. We hereby provide identify CpG-dependent TFs involved in particular biological processes that may require further investigation for their role in activated pDCs. Hence the global transcriptomics approach allows a comparison for the expression patterns of TFs belonging to the same TF family or involved in the same biological process, which may help to further narrow down interesting candidates for follow up investigations.

We further found that the activation of pDCs significantly altered the global expression patterns of the TF reservoir in the cell. Also, pDC activation modulated the chromatin landscape and DNA accessibility for different TF families. Using CpG as an optimal TLR9 agonist representing early events after virus infection we found that after pDC activation most of the pDC chromatin landscape is „turned on“ rather than being „turned off“ both globally in the genome and also among the regions associated with TF genes themselves. An extensive motif analysis revealed that TFs belonging to the JAK-STAT and the NFκB signaling pathway have increased accessibility to DNA binding regions after pDC stimulation. This underlines the importance of the JAK-STAT and NFκB signaling pathways in activated pDCs, as known from literature. Surprisingly, the AP-1 family of TFs which have little to no mention in literature in pDCs after pathogen infection or in chronic autoimmune state also have increased access to DNA in pDCs after activation as compared to the naïve state.

Focusing on a few key candidates we unravelled that IRF7, NFκB1, and RELA as well as ATF3 and JUN, two AP-1 family members, fulfil three criteria: They have (1) increased gene expression, (2) enhanced chromatin accessibility to their DNA, and (3) an enriched TF DNA binding motif in the genomic regions that are more accessible after TLR9 activation of pDCs. We used this integrative `omics approach to identify potential novel players important in pDC biology after cell activation. While the role for IRF7, NFκB1 and RELA have been described in activated pDCs, there is little known about any function of AP-1 factors in pDCs.

Strikingly, a connection has been made between NFκB and AP-1 activity, which may be regulated by NFκB (Fujioka et al., 2004), suggesting a possible common molecular mechanism in activated pDCs of the TFs involved in the NFκB signaling and AP-1 factors. Looking more closely at our key AP-1 candidates we found that ATF3 has been described as a negative regulator of antiviral signaling in induced Japanese encephalitis virus infection in mouse neuronal cells (Sood et al., 2017). The hallmark of pDCs is their importance in antiviral signaling, making ATF3 even more interesting as a candidate to evaluate in TLR9 activated pDCs that receive a microbial stimulus. JUN was the first described oncogene (Curran and Franza, 1988) and has been studied in detail in the context of various cancer. However, its study in the context of infection is more limited: It has e.g. been shown to have a regulatory role in H5N1 influenza virus replication and host inflammation in mice (Xie et al., 2014). Thus, the *in silico* analyses of the global TF reservoir in pDCs from our study provide novel candidates that warrant further investigation regarding their role in pDC biology, in particular after cell activation, which may lead to the development of novel therapeutics to treat infection, autoimmune disease and or cancer.

A more detailed discussion on our findings can be found in the attached manuscript that is under review for the Journal BMC Genomic Data and has been posted on the bioRxiv preprint server under the following DOI: https://doi.org/10.1101/2021.04.14.439791.

5.2 Negative regulation of type I IFN by BATF

BATF is known to play a role in development and function of immune cell types such as T and B cells (Edelson et al., 2010; Ise et al., 2011; Schraml et al., 2009). However, no impact of BATF on development or effector function of pDCs has been reported so far. In this study, we show that BATF is a negative regulator of type I IFN production in pDCs.

In previous findings we could demonstrate that IFNβ-producing pDCs have a distinct gene expression profile compared to non-IFNβ-producing pDCs, with BATF being highly upregulated in IFNβ-producing pDCs. This finding suggests a potential role of BATF in pDC transcriptional induction of IFNβ. We used *Batf*$^{-/-}$ mice (Schraml et al., 2009) in order to investigate the impact of BATF on pDC

development and effector function. In line with Tussiwand et al. we found that fully differentiated pDCs in *Batf*$^{-/-}$ mice are functional and morphologically comparable to WT pDCs (Tussiwand et al., 2012).

Using sorted BM-derived Flt3-L pDCs from *Batf*$^{-/-}$ mice we employed RNA-Seq to assess *Batf*-dependent gene expression in naïve and TLR9 activated pDCs. The RNA-Seq set up constituted a longitudinal study of pDCs activated with CpG, a synthetic double-strand DNA that specifically activated endosomal TLR9 and is known to induce a robust type I IFN production. CpG can further be considered as an optimal and specific microbial stimulus for pDCs which induces TLR9 mediated signaling that leads to the activation of the JAK-STAT and NF-κB signaling pathways (Volpi et al., 2013) and represents early events in virus infection. Before using the RNA-Seq data for biological interpretation we performed a quality control of the samples using Spearman correlation. We found high similarity (<95%) for the biological replicates used in the respective conditions of the RNA-Seq data set, suggesting that the culture and sorting of pDCs from distinct mice resulted in cells of high biological similarity. Notably, the differences between the stimulation time points (naïve, CpG 2h, 6h and 12h) were higher than the differences observed between the two genotypes (WT and *Batf*-deficiency). This gives a hint that the overall transcriptional changes induced by the TLR9 agonist CpG outweigh the expressional changes induced by *Batf* absence in pDCs at the respective condition. Lastly, we observed that the differences between steady state and 2h stimulation as well as 2h vs 6h stimulation were bigger than the differences observed between the latest activation time points of 6h vs 12h. Hence, the global pDC transcriptome seems to be altered significantly early after pDC activation (2h) while at later time points (6h, 12h) the additional transcriptional changes between WT and *Batf*$^{-/-}$ pDCs induced by longer stimulation time are diminishing.

Using the global RNA-Seq approach we found that *Batf* is co-expressed with type I IFN genes in murine WT pDCs after CpG stimulation, suggesting either a positive role of BATF in the induction of type I IFN, or a negative role as its up-regulation might represent the onset of a negative feedback loop to keep the production of type I IFN in pDCs after TLR9 activation under control. As we found BATF to be well conserved between mouse and human (Protein BLAST, ECR analyses) we next wanted to investigate whether our observed phenotype exists in human pDCs

before determining a potentially positive or negative role of BATF for type I IFN induction in pDCs. To this end we re-analyzed published RNA-Seq data from Caielli et al. who isolated human pDCs from PBMCs of healthy donors and *ex vivo* stimulated human pDCs with CpG for 18 h or left them naïve (n=3 per group, GSE93679) (Caielli et al., 2019). The results showed that human BATF is > 22 fold significantly up-regulated along with type I IFN genes in stimulated pDCs as compared to non-stimulated pDCs, which is line with our observation of gene expression patterns in mouse pDCs upon CpG stimulation. This suggests a potentially similar function of human and mouse BATF after TLR9 activation of pDCs. While an increased expression of the AP-1 family member BATF has been reported in various human cancers (Feng et al., 2020; Gil et al., 2015) no connection between an heightened BATF expression and type I IFN expression has been made to our knowledge. The dimeric AP-1 protein, however, has been shown to be required for spontaneous type I IFN production in pDCs, whereas type I IFN production triggered by pathogen receptor recognition such as TLR stimulation was not affected by AP-1 inhibition (Kim et al., 2014).

Going back to our longitudinal RNA-Seq study we found that there are 918 genes differentially expressed for more than 2-fold between WT and *Batf*$^{-/-}$ pDCs. After CpG stimulation 339 (2h), 1489 (6h) and 1570 (12h) genes expressed at significantly different levels between the two genotypes. This indicates a significant *Batf*-dependent global gene expression in pDCs both at steady state and after activation with CpG which represents early events after virus infection and hence hints at a possibly important role of BATF for global gene expression in pDCs during virus infection. To reveal the biological impact of the differentially expressed genes we performed a Reactome pathway analysis. We observed that the IFN α/β and different cytokine signaling pathways are enriched in naïve pDCs in *Batf* absence. In addition GSEA revealed a global up-regulation of type I IFN response genes. These results indicate a significant impact of *Batf* on various pathways up- and down-stream of the type I IFN signaling cascade. Strikingly, 68% and 33% of all differentially expressed genes at steady state or at 2h after TLR9 activation, respectively, are annotated in the Interferome database as responsive to type I IFN (Interferome database v2.01) (Rusinova et al., 2013). We hypothesized that BATF might block type I IFN expression as we see a more pronounced type I IFN

signature in *Batf* absence. We therefore next looked at the expression of type I IFN genes in our longitudinal RNA-Seq study and found an elevated type I IFN production of *Batf*$^{-/-}$ pDCs 2h after CpG stimulation as compared to WT pDCs, but not at 6h or 12h, confirming a negative impact of BATF on type I IFN production in pDCs. So far, no effect of BATF on type I IFN production has been shown in pDCs or any other cell type. However, since we found earlier that IFNβ-producing pDCs represent only ~5% of the overall splenic pDC population (Bauer et al., 2016), we reckon that a potential role of BATF for pDC differentiation and function might have gone unnoticed in previous studies with *Batf*$^{-/-}$ mice. To explain the impact of BATF on type I IFN production we speculated that BATF might be binding onto type I IFN promoter sites thereby exerting control of gene expression. Direct BATF interaction with DNA in pDCs was tested globally using BATF ChIP-Seq on naïve and 2h CpG stimulated pDCs. Here, the quality control did not pass the criteria of >95% similarity between the biological replicates. We did, however, use the data, always carefully comparing the two biological replicates used at the respective condition, to rule out biases from our side. We found that BATF did not directly regulate type I IFN expression by binding to type I IFN promoter or intergenic elements, except for the IFNα13 and IFNα14 genes, one of which is not even expressed in pDCs upon CpG stimulation. Before ruling out the direct control of BATF for type I IFN expression we investigated one last mechanism we could think of, which is the alteration of chromatin accessibility of type I IFN genes by BATF. A more or less accessible chromatin may facilitate or inhibit DNA binding of certain TFs to the respective DNA stretches, which may impact gene transcription. To this end we performed ATAC-Seq of WT and *Batf*$^{-/-}$ pDCs at steady state and 2h after CpG stimulation. Here, the biological replicates showed >95% similarity and were therefore used for a quantitative differential analysis (DESeq2). We found that BATF did not alter the chromatin accessibility of type I IFN genes in pDCs as the chromatin peaks were neither visually affected by *Batf* absence nor did the statistical analysis of differential chromatin opening reveal any significant changes for chromatin regions associated with type I IFN genes. The ChIP-Seq and ATAC-Seq data taken together suggest that BATF is not directly involved in the control of type I IFN gene transcription in pDCs. One explanation might be that the altered cDC frequency observed in our BM-derived Flt3-L system (WT ~17%, *Batf*$^{-/-}$ ~5%)

may reflect a developmental and functional defect in cDCs that impacts type I IFN production by pDCs. Another explanation for BATF's negative impact on type I IFN production may be that BATF does directly regulate another factor that affects type I IFN levels in pDCs. This latter explanation was tested using our 'omics data to identify potential candidates that fulfil three criteria: (1) they must have *Batf*-dependent expression, (2) BATF must bind in the promoter of the factor(s) in pDCs, and (3) the chromatin accessibility of the gene must be significantly altered by the loss of BATF in pDCs. Mining our dataset we were able to narrow down the list of potential candidates, discovering Zfp366, also known as DC-SCRIPT that not only fulfilled the criteria but is already known for its role in DC biology, as it is required to induce cDC differentiation (Chopin et al., 2019). Zhang et al. recently showed that DC-SCRIPT was required for cDC1 cells to effectively cross-present antigen and produce IL-12. Interestingly, DC-SCRIPT was able to control expression of IRF8 in cDC1s (Zhang et al., 2021), which is an important cell fate TF required for pDC development (Sichien et al., 2016). Hence existing literature points to a first possible indirect role of DC-SCRIPT for pDC development, in response to which we started to evaluate the importance of DC-SCRIPT in the connection with BATF for the hallmark function of pDCs, the production of type I IFN. We were able to show that Zfp366 has significantly reduced expression in *Batf* absence in pDCs at steady state and after CpG activation (RNA-Seq, RT-PCR). BATF directly binds onto the Zfp366 proximal promoter site, which contains the AP-1 motif (TGAGTCA), suggesting BATF binding induces gene expression by binding. Further, ATAC-Seq showed decreased chromatin opening in the promoter site of Zfp366 in *Batf* absence, thereby reducing the accessibility of BATF and other TFs to the DNA of the Zfp366 gene. Intriguingly, data generated by another lab member has in the meanwhile shown that Zfp366 inhibits type I IFN promoter activity using a luciferase assay (data not shown). The underlying molecular mechanisms of these regulatory BATF and ZFP366-actions are focus of on-going studies in our lab and will help us to further understand the impact of these TFs on type I IFN production in pDCs.

Ultimately, we showed that the increase in type I IFN production in *Batf* absence reduced pDC mediated LCMV infection control *in vitro*. This suggests a detrimental effect of BATF on the outcome of virus infection, as its absence helped to clear the

infection. We would therefore like to speculate that *Batf* absence may help to clear virus infection by increased type I IFN production. However, since pDCs comprise approximately 0.2 to 0.8% of mononuclear cells in the blood they constitute a relatively small cell population, out of which another subpopulation constituting maybe 5-10% of all cells have been shown to produce type I IFN in infection (Bauer et al., 2016). One may therefore also speculate that the success of virus clearance in *Batf* absence in a mouse model may well be dependent on the initial virus dosage that the animal has to combat. Type I IFN is well known to have both beneficial and detrimental effects for human health. While its production is required to fight pathogens an excessive and chronic overproduction of type I IFN has been observed in several autoimmune diseases (Lee-Kirsch, 2017). Understanding how BATF and ZFP366 regulate type I IFN production in pDCs may help to develop strategies to manipulate protein or protein levels of these TFs to both treat infection and autoimmune disease in the future.

In summary, we identified a novel function of BATF in pDCs where it could restrain type I IFN production. We further identified Zfp366 as a possible link to explain the impact of *Batf* absence on increased type I IFN levels, as we found Zfp366 expression to be regulated by BATF binding and *Batf*-dependent chromatin changes. Lastly, we showed an impact of BATF on virus clearance *in vitro*.

5.3 BATF blocks pDC development

In order to investigate the development of pDCs lacking BATF we made again use of *Batf*$^{-/-}$ mice (Schraml et al., 2010). We investigated pDC development in different secondary lymphoid organs of WT and *Batf*$^{-/-}$ mice. We observed the striking phenotype that naïve *Batf*$^{-/-}$ mice held under SPF conditions had enlarged spleens and lymph nodes as compared to WT littermates which has not been described before. In fact, Logan et al. observed quite the opposite, as transgenic mice overexpressing human BATF in T cells showed an enlargement of lymph nodes (Logan et al., 2012). We next investigated different immune cell populations in frequency and absolute numbers in the organs, as well as the organ structure using histology. We found that the frequency of pDCs (~0.4% and 1% in spleen and lymph nodes, respectively) was not elevated in these *Batf*$^{-/-}$ organs, while overall

absolute cell numbers in spleen and lymph nodes of *Batf*$^{-/-}$ mice were increased as compared to WT mice. Neither did the immunohistological staining for B cells (B220^{+}) and pDCs (SiglecH^{+}) reveal any obvious changes in organ substructure of the red and white pulp. These results established that *Batf* had no impact on pDC numbers or localization in the spleen and lymph nodes. Nonetheless, one open question remains as to why these organs are increased in size in *Batf* absence. One explanation is that the capacity of *Batf*-deficient pDCs to produce increased amounts of type I IFN may cause a basal elevated type I IFN signature in the mouse *in vivo* which leads to inflammation and enlargement of the organs. Splenomegaly has been shown occur during *in vivo* virus infection of mice and TLR7 stimulation with imiquimod (Grine et al., 2016; Halemano et al., 2013), both of which induce type I IFN. To test the hypothesis that type I IFN may be responsible for increased organ size in *Batf* absence we evaluated the effect of *Batf* vs type I IFN on spleen size in Ifnar$^{-/-}$ and *Batf*$^{-/-}$ Ifnar$^{-/-}$ mice. We found that Ifnar$^{-/-}$ mice exhibited the smallest spleens. *Batf*$^{-/-}$ had significantly increased spleens as compared to WT and Ifnar$^{-/-}$ mice. Strikingly, the *Batf*$^{-/-}$ Ifnar$^{-/-}$ double knock out mice showed spleen sizes comparable to *Batf*-deficient mice, suggesting that the increase of spleen size in *Batf* absence is independent of Ifnar signaling. These results suggest that BATF is responsible for the increase in organ sizes independent of Ifnar signaling, possibly inducing enhanced cell proliferation of spleen and lymph nodes in *Batf*$^{-/-}$ animals. Therefore, it should be subject of further studies to unravel the mechanism behind the increased organ sizes in *Batf*$^{-/-}$ animals.

We next focused on pDC ontogeny. The differentiation of distinct cell types from pluripotent stem cells is enabled by the expression of cell fate determining TFs in progenitor cells. Over the years, different TFs could be determined as cell fate TFs in pDCs. In particular, IRF8, Spi-B, Runx2 and E2-2 have been shown to be required for pDC development (Cisse et al., 2008; Sasaki et al., 2012; Sawai et al., 2013; Tsujimura et al., 2003). We wanted to evaluate the expression of pDC driving cell fate TFs in fully differentiated pDCs using our longitudinal RNA-Seq study. But instead of handpicking TFs known from literature to affect pDC differentiation and evaluating their expression we made use of a genome wide approach analyzing all 828 mouse TFs as defined in the TRRUST2 database (Han et al., 2018). *Batf*-

dependent clustering revealed that ~220 TFs show significant changes in expression pattern in *Batf* absence as compared to WT pDCs. This narrows down the list of TFs that are affected by BATF regarding their expression and may play a role in BATF-mediated biology by e.g. being involved in processes affected by BATF or by interacting with BATF. Looking more closely, we found that cDC driving TFs (e.g. Nfil3, Zfp366) are less expressed in *Batf*-deficient pDCs while pDC driving TFs (e.g. Runx2, Tcf4, Spi-B) are expressed more in *Batf* absence. This suggests a negative role of *Batf* for the expression of pDC driving TFs, possibly negatively regulating pDC development, which we investigated at a later point using *in vitro* cell culture. For some DC cell fate TFs it is known how they are regulated, e.g. pDC driving TFs such as SPI-B and IRF8 are activated by E2-2, the protein encoded by *Tcf4(Cisse et al., 2008)*, and the cDC driving TF DC-SCRIPT is a key transcriptional target of PU.1 (Chopin et al., 2019). Thus, after evaluating the impact of *Batf* expression on the expression levels of well known DC cell fate factors we next looked at the role of BATF for transcriptional control of DC cell fate factors. To this end, we hypothesized that BATF may directly regulate the expression of the TFs which change their expression in *Batf* absence, and in particular the expression of pDC cell fate driving TFs. In detail, this direct control of BATF could be exerted by binding onto promoter elements of TFs (BATF ChIP-Seq) or by regulating the chromatin accessibility of promoter regions (ATAC-Seq) of the respective TF. We found that 110 TFs show both BATF binding onto their promoter and or enhancer site and changes in gene expression when *Batf* is not expressed. Further, BATF modulated the chromatin of 162 TFs, and 47 of these have an altered expression in *Batf* absence. These results indicate that BATF makes use of both mechanisms, direct DNA interaction and chromatin modulation, to exert control of gene expression of TFs. Transcriptional regulation of genes by both direct DNA binding and altering chromatin accessibility has been shown for BATF in various immune cells (Iwata et al., 2017; Karwacz et al., 2017), but never in pDCs or the context of a global analysis of all TFs in the mouse genome. As of particular interest for pDC biology we next focused in detail on pDC cell fate TFs. TFs known to positively induce pDC differentiation (e.g. Tcf4, Irf8, Runx2, Bcl11a, Spib) not only showed increased expression in *Batf* absence at steady state and after TLR9 activation in pDCs (RNA-Seq, RT-PCR) but they also showed

increased chromatin accessibility within their gene or promoter region in ATAC-Seq. In addition, BATF showed direct interaction with the DNA of these TFs in enhancer regions and for some, also in the promoter region. On the hand, cDC driving TFs (e.g. Id2, Zfp366, Nfil3, Pu.1) exhibited decreased expression in *Batf* absence in pDCs (RNA-Seq, RT-PCR), while two in particular, Id2 and Zfp366, were also characterized by diminished chromatin opening in *Batf* absence. Similar to pDC cell fate TFs this set of TFs also indicated great direct interaction of BATF with their DNA. These data suggest that BATF directly manipulates and controls the expression of DC fate factors, driving the expression of cDC factors in its presence. We show according to our knowledge of the literature for the first time that one TF, namely BATF, controls a whole range of important DC cell fate TFs, suggesting BATF as a possible master regulator of Flt3-L dependent cDC vs pDC development in the bone marrow. We wondered whether this altered expression of DC fate factors in fully differentiated pDCs may also be present in DC precursor cells. We have conducted some initial experiments to address this possibility. In a first experiment we used *ex vivo* BM from WT and *Batf*$^{-/-}$ mice which was depleted for T, B and NK cells, leaving a pool of fully differentiated pDCs and cDCs and all their precursor cells in the myeloid and lymphoid department in our depleted BM. Using RT-PCR we discovered a significantly increased expression of Tcf4 in depleted *Batf*$^{-/-}$ BM, opening up questions about the differentiation of pDCs in *Batf*-deficient mice that needed to be answered with laboratory experiments. Hence BM-derived Flt3-L cultures were used to investigate the impact of BATF on pDC differentiation *in vitro*. We observed a general trend of elevated pDC frequencies and decreased cDC frequencies in BM-derived Flt3-L cultures from *Batf*$^{-/-}$ mice. This result showed an altered ratio of cDC to pDCs in BM-derived Flt3-L cultures in *Batf* absence. Looking at total cell numbers we found that significantly elevated numbers of pDCs were present in the *Batf*-deficient cultures already at day 3 of culture, and with an increasing duration of culture time the difference in pDC numbers between the genotypes increased even more. Hence *Batf* absence not only altered the pDC to cDC ratio but enhanced pDC differentiation resulting in more pDCs when starting the BM-derived Flt3-L culture from the same cell numbers per plate as compared to the WT cultures. These results confirm a negative role of BATF for pDC differentiation using *in vitro* culture. This is quite

intriguing as existing literature on the role of BATF for the development of immune cells has so far shown a requirement of BATF presence for complete and functional development of B cells, various T cell subsets and cDCs (Ise et al., 2011; Kurachi et al., 2014; Sahoo et al., 2015; Tussiwand et al., 2012). Here, we identify for the first time a negative role of BATF for the development of a cell type, namely pDCs. One obvious explanation for enhanced pDC differentiation is the increased expression of pDC driving TFs in whole *ex vivo* BM of *Batf*$^{-/-}$ mice (depleted for T, B and NK cells). Another explanation may be the capacity of *Batf*$^{-/-}$ pDC to produce more type I IFN than WT pDCs, as type I IFN is known to drive pDC differentiation and numbers (Chen et al., 2013). We wanted to discriminate between the possible impact of BATF vs activation of the type I IFN receptor pathways on increased pDC numbers in naïve and CpG stimulated BM-derived Flt3-L cultures. To this end we made use of the Ifnar$^{-/-}$ mice (Muller et al., 1994) and the newly bred Ifnar$^{-/-}$ *Batf*$^{-/-}$ double knock out mouse. We observed that Ifnar$^{-/-}$ cultures showed less pDC differentiation than WT cultures, and that knocking out *Batf* in addition to Ifnar resulted in a dramatic increase in pDC numbers as compared to the single Ifnar-knockout. These results show that the impact of BATF on pDC development is independent of Ifnar signaling in both steady state and CpG stimulated BM-derived Flt3-L cultures. However, using BM-derived Flt3-L cultures one has to keep in mind that we create an artificial situation using the growth and differentiation factor Flt3-L which enriches fully differentiated pDCs. Also, the direct TLR9 stimulation with CpG further facilitates maturation of the pDCs in the *in vitro* dish. This might skew more *Batf*-deficient pDCs to become fully differentiated and mature pDCs able to produce type I IFN than it is likely to happen in the *in vivo* situation. These possibilities will be tested *in vivo* using a newly bred pDC-specific *Batf*-knock out mouse model that has been created in our facility (Batf$^{fl/fl}$ SiglecH^{Cre}) in future studies. The Batf$^{fl/fl}$ mouse (Betz et al., 2010) has a floxed *Batf* allele and shows the phenotype of wildtype mice. The SiglecH^{Cre} mouse (Puttur et al., 2013) expressed the Cre recombinase under the control of the SiglecH promoter. Puttur et al. crossed the SiglecH^{Cre} mouse with the RFP reporter mouse, allowing the evaluation of the distribution of the reporter expression from BM and spleen. They found that SiglecH^{+} pDCs were targeted very efficiently. By crossing the Batf$^{fl/fl}$ mice with the SiglecH^{Cre} mouse we generated a novel mouse model (Batf$^{fl/fl}$

SiglecH^{Cre}) which has a *Batf* deficiency in all cells which are SiglecH^{+}, including pDCs but not excluding other SiglecH^{+} cell types. Therefore, the BATF expression in various immune cells of our newly generated pDC-specific *Batf*-knock out mouse model will be determined to evaluate the mouse phenotype before proceeding with *in vivo* studies to investigate the role of BATF on pDC development and effector function. In addition, the impact of BATF on differentiation of pDCs from the myeloid vs the lymphoid origin from the hematopoietic stem cell in the bone marrow is currently under investigation. The differentiation of pDCs from CDPs in the myeloid branch (Naik et al., 2006) has been taken for granted for many years. However recently, pDCs have been reported to develop predominantly from IL-7R^{+} lymphoid progenitors rather than from CDPs (Dress et al., 2019; Rodrigues et al., 2018). Rodrigues et al. purified pDCs derived from the myeloid vs the lymphoid branch to perform global gene expression analysis, which allowed them to characterize differences between pDCs developing from these two branches. They found that myeloid-derived pDCs exhibit more cDC-like characteristics such as an efficient antigen presenting capability. Lymphoid-derived pDCs, on the other hand, were more efficient at producing type I IFN as compared to myeloid-derived pDCs (Rodrigues et al., 2018). Also, Dress et al. compared myeloid vs lymphoid derived pDCs. They conclude that their cell sorting procedure may have led to a contamination of myeloid-derived pDCs with cDCs, and that “real” pDCs develop within the lymphoid branch only (Dress et al., 2019). The different results and opinions of the scientific community on the origin of pDCs makes the question of how BATF may impact pDC differentiation from different precursor cells and in particular in the myeloid vs lymphoid branch of great importance. To this end CMPs, LMPPs and CDPs have been purified from *ex vivo* BM of WT and *Batf*$^{-/-}$ mice that were re-cultured with Flt3-L to evaluate pDC numbers via FACS. First experiments that require repetition indicate that the increased number of pDCs in BM-derived Flt-3L cultures of *Batf*$^{-/-}$ mice originate from the lymphoid rather than the myeloid branch, showing for one that in our hands pDCs as defined by the expression of typical surface markers (SiglecH^{+} mPDCA^{+} B220^{+} CD11c^{int} CD11b^{-} CD19^{-} CD3^{-}) do develop from the myeloid CDP and CMP precursors, and second that BATF blocks pDC development in the lymphoid branch. Further experiments will help to understand the mechanism of BATF control for pDC differentiation in

the BM, possibly even opening up opportunities for manipulation of pDC differentiation using protein therapeutics. This could be of particular interest for diseases like blastic pDC neoplasm, an aggressive malignancy affecting primarily the skin

Taken together, the data of our studies have shown that BATF negatively drives the expression of pDC cell fate factors and pDC frequencies as well as total numbers in BM-derived Flt3-L cultures independent of Ifnar signaling.

5.4 Pioneering function of BATF

BATF has been shown to regulate chromatin accessibility and act as a chromatin accessibility modulating pioneer factor in Tr1, Th17 and $CD8^+$ T cells (Ciofani et al., 2012; Karwacz et al., 2017; Kurachi et al., 2014). We speculated that BATF might fulfil similar pioneering but yet unknown functions in pDCs. To assess potential pioneering roles of BATF during pDC differentiation, we measured chromatin accessibility using ATAC-seq in naive and TLR9 stimulated pDCs. *Batf* deficiency altered the chromatin landscape leading to upwards of ~2,500 altered accessible regions (FDR=10%, $\log_2$|fold-change|>1). In detail, *Batf* deficiency in naive pDCs resulted in 880 and 1358 peaks with increased accessibility and 287 and 488 peaks with decreased accessibility in naive and 2h CpG stimulated pDCs, respectively. Karwacz et al. performed a similar analysis for BATF in Tr1 cells, discovering that Batf deficiency led to ~20.000 altered accessible chromatin regions (FDR=10%, $\log_2$|fold-change|>1). We can conclude from this that BATF affects a smaller number of chromatin regions in pDCs as compared to Tr1 cells. Notably, while we performed the same statistical analysis as Karwacz et al. their ATAC-Seq library preparation and sequencing was performed under different conditions, which requires caution when comparing numbers from ATAC-Seq results. Although the scale of BATF-induced chromatin changes in Tr1 cells and pDCs differs we would classify BATF as a pioneering TF in pDCs as well as the deficiency of other TFs such as Irf1 in Tr1 cells resulted in ~1200 altered chromatin regions which yet led to a classification of Irf1 as a pioneering factor in Tr1 cells. The number of altered regions by Irf1 in Tr1 cells constitutes half of the number of regions that BATF affects in pDCs. Another striking observation is that BATF both „turned on“ and turned off“ regions in pDCs, similar to the Tr1 chromatin landscape.

In contrast, some TFs such as Irf1 more strongly affect the chromatin landscape in one or the other way, either strongly decreasing or increasing DNA accessibility in their absence (Irf1 decreases accessibility) (Karwacz et al., 2017). This work is further in line with the observation that the BATF protein has no DNA transactivation domain, suggesting it rather inhibits than induces gene expression. Our ATAC-Seq data shows that the chromatin landscape is less accessible in BATF presence in pDCs, and assuming that in general less accessible chromatin rather leads to inhibition of gene expression we have hereby defined a so far not recognized mechanism by BATF to globally modulate gene expression in pDCs as a pioneering factor.

In summary, BATF could be shown to play pioneering role in pDCs both increasing and decreasing chromatin accessibility for thousands of regions globally. As could be shown in Tr1 cells (Karwacz et al., 2017) BATF is not a so called focused/small-scale pioneering TF but acts globally in pDCs.

Taken together, our data demonstrate that TLR9 activation of pDCs with CpG significantly altered the global TF reservoir and chromatin landscape of the cell. In addition, we found the TF BATF to have a dual negative role for pDC development and type I IFN production. The underlying molecular mechanisms of BATF mediated regulatory actions are focus of on-going studies in our lab and will help to further understand the impact of this TF on pDC differentiation and cell effector functions. Ultimately this work could be of great importance for guiding therapeutic strategies to control infection and autoimmune disease using CpG, BATF and or type I IFNs in the future.

6. References

Afgan, E., Baker, D., van den Beek, M., Blankenberg, D., Bouvier, D., Cech, M., Chilton, J., Clements, D., Coraor, N., Eberhard, C.*, et al.* (2016). The Galaxy platform for accessible, reproducible and collaborative biomedical analyses: 2016 update. Nucleic Acids Res *44*, W3-W10.

Ali, S., Mann-Nuttel, R., Schulze, A., Richter, L., Alferink, J., and Scheu, S. (2019). Sources of Type I Interferons in Infectious Immunity: Plasmacytoid Dendritic Cells Not Always in the Driver's Seat. Front Immunol *10*, 778.

Arendt, A.D.a.C. (2020). xlsx: Read, Write, Format Excel 2007 and Excel 97/2000/XP/2003 Files.

Asselin-Paturel, C., Boonstra, A., Dalod, M., Durand, I., Yessaad, N., Dezutter-Dambuyant, C., Vicari, A., O'Garra, A., Biron, C., Briere, F., and Trinchieri, G. (2001). Mouse type I IFN-producing cells are immature APCs with plasmacytoid morphology. Nat Immunol *2*, 1144-1150.

Balamuta, D.E.a.J.J. (2017). Extending R with C++: A Brief Introduction to Rcpp. PeerJ Preprints *5:e3188v1*.

Bauer, J., Dress, R.J., Schulze, A., Dresing, P., Ali, S., Deenen, R., Alferink, J., and Scheu, S. (2016). Cutting Edge: IFN-beta Expression in the Spleen Is Restricted to a Subpopulation of Plasmacytoid Dendritic Cells Exhibiting a Specific Immune Modulatory Transcriptome Signature. J Immunol *196*, 4447-4451.

Betz, B.C., Jordan-Williams, K.L., Wang, C., Kang, S.G., Liao, J., Logan, M.R., Kim, C.H., and Taparowsky, E.J. (2010). Batf coordinates multiple aspects of B and T cell function required for normal antibody responses. J Exp Med *207*, 933-942.

Bindea, G., Mlecnik, B., Hackl, H., Charoentong, P., Tosolini, M., Kirilovsky, A., Fridman, W.H., Pages, F., Trajanoski, Z., and Galon, J. (2009). ClueGO: a Cytoscape plug-in to decipher functionally grouped gene ontology and pathway annotation networks. Bioinformatics *25*, 1091-1093.

Bjorck, P. (2001). Isolation and characterization of plasmacytoid dendritic cells from Flt3 ligand and granulocyte-macrophage colony-stimulating factor-treated mice. Blood *98*, 3520-3526.

Blasius, A.L., Cella, M., Maldonado, J., Takai, T., and Colonna, M. (2006a). Siglec-H is an IPC-specific receptor that modulates type I IFN secretion through DAP12. Blood *107*, 2474-2476.

Blasius, A.L., Giurisato, E., Cella, M., Schreiber, R.D., Shaw, A.S., and Colonna, M. (2006b). Bone marrow stromal cell antigen 2 is a specific marker of type I IFN-producing cells in the naive mouse, but a promiscuous cell surface antigen following IFN stimulation. J Immunol *177*, 3260-3265.

Bornstein, C., Winter, D., Barnett-Itzhaki, Z., David, E., Kadri, S., Garber, M., and Amit, I. (2014). A negative feedback loop of transcription factors specifies alternative dendritic cell chromatin States. Mol Cell *56*, 749-762.

Buenrostro, J.D., Giresi, P.G., Zaba, L.C., Chang, H.Y., and Greenleaf, W.J. (2013). Transposition of native chromatin for fast and sensitive epigenomic profiling of open chromatin, DNA-binding proteins and nucleosome position. Nat Methods *10*, 1213-1218.

Caielli, S., Veiga, D.T., Balasubramanian, P., Athale, S., Domic, B., Murat, E., Banchereau, R., Xu, Z., Chandra, M., Chung, C.H.*, et al.* (2019). A CD4(+) T cell population expanded in lupus blood provides B cell help through interleukin-10 and succinate. Nat Med *25*, 75-81.

Carotta, S., Dakic, A., D'Amico, A., Pang, S.H., Greig, K.T., Nutt, S.L., and Wu, L. (2010). The transcription factor PU.1 controls dendritic cell development and Flt3 cytokine receptor expression in a dose-dependent manner. Immunity *32*, 628-641.

Chen, Y., Lun, A.T., and Smyth, G.K. (2016). From reads to genes to pathways: differential expression analysis of RNA-Seq experiments using Rsubread and the edgeR quasi-likelihood pipeline. F1000Res *5*, 1438.

Chen, Y.L., Chen, T.T., Pai, L.M., Wesoly, J., Bluyssen, H.A., and Lee, C.K. (2013). A type I IFN-Flt3 ligand axis augments plasmacytoid dendritic cell development from common lymphoid progenitors. J Exp Med *210*, 2515-2522.

Chopin, M., Lun, A.T., Zhan, Y., Schreuder, J., Coughlan, H., D'Amico, A., Mielke, L.A., Almeida, F.F., Kueh, A.J., Dickins, R.A.*, et al.* (2019). Transcription Factor PU.1 Promotes Conventional Dendritic Cell Identity and Function via Induction of Transcriptional Regulator DC-SCRIPT. Immunity *50*, 77-90 e75.

Chopin, M., Preston, S.P., Lun, A.T.L., Tellier, J., Smyth, G.K., Pellegrini, M., Belz, G.T., Corcoran, L.M., Visvader, J.E., Wu, L., and Nutt, S.L. (2016). RUNX2 Mediates Plasmacytoid Dendritic Cell Egress from the Bone Marrow and Controls Viral Immunity. Cell Rep *15*, 866-878.

Ciofani, M., Madar, A., Galan, C., Sellars, M., Mace, K., Pauli, F., Agarwal, A., Huang, W., Parkhurst, C.N., Muratet, M.*, et al.* (2012). A validated regulatory network for Th17 cell specification. Cell *151*, 289-303.

Cisse, B., Caton, M.L., Lehner, M., Maeda, T., Scheu, S., Locksley, R., Holmberg, D., Zweier, C., den Hollander, N.S., Kant, S.G.*, et al.* (2008). Transcription factor E2-2 is an essential and specific regulator of plasmacytoid dendritic cell development. Cell *135*, 37-48.

Corces, M.R., Trevino, A.E., Hamilton, E.G., Greenside, P.G., Sinnott-Armstrong, N.A., Vesuna, S., Satpathy, A.T., Rubin, A.J., Montine, K.S., Wu, B.*, et al.* (2017). An improved ATAC-seq protocol reduces background and enables interrogation of frozen tissues. Nat Methods *14*, 959-962.

Curran, T., and Franza, B.R., Jr. (1988). Fos and Jun: the AP-1 connection. Cell *55*, 395-397.

Davis, S., and Meltzer, P.S. (2007). GEOquery: a bridge between the Gene Expression Omnibus (GEO) and BioConductor. Bioinformatics *23*, 1846-1847.

Deaton, A.M., and Bird, A. (2011). CpG islands and the regulation of transcription. Genes Dev *25*, 1010-1022.

Deppmann, C.D., Thornton, T.M., Utama, F.E., and Taparowsky, E.J. (2003). Phosphorylation of BATF regulates DNA binding: a novel mechanism for AP-1 (activator protein-1) regulation. Biochem J *374*, 423-431.

Diebold, S.S., Kaisho, T., Hemmi, H., Akira, S., and Reis e Sousa, C. (2004). Innate antiviral responses by means of TLR7-mediated recognition of single-stranded RNA. Science *303*, 1529-1531.

Dorsey, M.J., Tae, H.J., Sollenberger, K.G., Mascarenhas, N.T., Johansen, L.M., and Taparowsky, E.J. (1995). B-ATF: a novel human bZIP protein that associates with members of the AP-1 transcription factor family. Oncogene *11*, 2255-2265.

Dragulescu, A.A. (2014). xlsxjars: Package required POI jars for the xlsx package.

Dress, R.J., Dutertre, C.A., Giladi, A., Schlitzer, A., Low, I., Shadan, N.B., Tay, A., Lum, J., Kairi, M., Hwang, Y.Y.*, et al.* (2019). Plasmacytoid dendritic cells develop from Ly6D(+) lymphoid progenitors distinct from the myeloid lineage. Nat Immunol *20*, 852-864.

Drouin, J. (2014). Minireview: pioneer transcription factors in cell fate specification. Mol Endocrinol *28*, 989-998.

Echlin, D.R., Tae, H.J., Mitin, N., and Taparowsky, E.J. (2000). B-ATF functions as a negative regulator of AP-1 mediated transcription and blocks cellular transformation by Ras and Fos. Oncogene *19*, 1752-1763.

Edelson, B.T., Kc, W., Juang, R., Kohyama, M., Benoit, L.A., Klekotka, P.A., Moon, C., Albring, J.C., Ise, W., Michael, D.G.*, et al.* (2010). Peripheral CD103+ dendritic cells form a unified subset developmentally related to CD8alpha+ conventional dendritic cells. J Exp Med *207*, 823-836.

Egan, B., Yuan, C.C., Craske, M.L., Labhart, P., Guler, G.D., Arnott, D., Maile, T.M., Busby, J., Henry, C., Kelly, T.K.*, et al.* (2016). An Alternative Approach to ChIP-Seq Normalization Enables Detection of Genome-Wide Changes in Histone H3 Lysine 27 Trimethylation upon EZH2 Inhibition. PLoS One *11*, e0166438.

Elkon, K.B., and Wiedeman, A. (2012). Type I IFN system in the development and manifestations of SLE. Curr Opin Rheumatol *24*, 499-505.

Ellyard, J.I., and Vinuesa, C.G. (2011). A BATF-ling connection between B cells and follicular helper T cells. Nat Immunol *12*, 519-520.

Feng, Y., Pan, L., Zhang, B., Huang, H., and Ma, H. (2020). BATF acts as an oncogene in non-small cell lung cancer. Oncol Lett *19*, 205-210.

Fujioka, S., Niu, J., Schmidt, C., Sclabas, G.M., Peng, B., Uwagawa, T., Li, Z., Evans, D.B., Abbruzzese, J.L., and Chiao, P.J. (2004). NF-kappaB and AP-1 connection: mechanism of NF-kappaB-dependent regulation of AP-1 activity. Mol Cell Biol *24*, 7806-7819.

Fulton, D.L., Sundararajan, S., Badis, G., Hughes, T.R., Wasserman, W.W., Roach, J.C., and Sladek, R. (2009). TFCat: the curated catalog of mouse and human transcription factors. Genome Biol *10*, R29.

Gaudino, S.J., and Kumar, P. (2019). Cross-Talk Between Antigen Presenting Cells and T Cells Impacts Intestinal Homeostasis, Bacterial Infections, and Tumorigenesis. Front Immunol *10*, 360.

Ghosh, H.S., Cisse, B., Bunin, A., Lewis, K.L., and Reizis, B. (2010). Continuous expression of the transcription factor e2-2 maintains the cell fate of mature plasmacytoid dendritic cells. Immunity *33*, 905-916.

Gil, M., Pak, H.K., Park, S.J., Lee, A.N., Park, Y.S., Lee, H., Lee, H., Kim, K.E., Lee, K.J., Yoon, D.H.*, et al.* (2015). Engagement of CD99 Reduces AP-1 Activity by Inducing BATF in the Human Multiple Myeloma Cell Line RPMI8226. Immune Netw *15*, 260-267.

Glasmacher, E., Agrawal, S., Chang, A.B., Murphy, T.L., Zeng, W., Vander Lugt, B., Khan, A.A., Ciofani, M., Spooner, C.J., Rutz, S.*, et al.* (2012). A genomic regulatory element that directs assembly and function of immune-specific AP-1-IRF complexes. Science *338*, 975-980.

Gregory R. Warnes, B.B., Lodewijk Bonebakker, Robert Gentleman, Wolfgang Huber, Andy Liaw, Thomas Lumley, Martin Maechler, Arni Magnusson, Steffen Moeller, Marc Schwartz and Bill Venables (2020). gplots: Various R Programming Tools for Plotting Data. ScienceOpen.

Grine, L., Steeland, S., Van Ryckeghem, S., Ballegeer, M., Lienenklaus, S., Weiss, S., Sanders, N.N., Vandenbroucke, R.E., and Libert, C. (2016). Topical imiquimod yields systemic effects due to unintended oral uptake. Sci Rep *6*, 20134.

Grusdat, M., McIlwain, D.R., Xu, H.C., Pozdeev, V.I., Knievel, J., Crome, S.Q., Robert-Tissot, C., Dress, R.J., Pandyra, A.A., Speiser, D.E.*, et al.* (2014). IRF4 and BATF are critical for CD8(+) T-cell function following infection with LCMV. Cell Death Differ *21*, 1050-1060.

Hadley Wickham, J.H.a.R.F. (2018). readr: Read Rectangular Text Data.

Hadley Wickham, R.F., Lionel Henry and Kirill Müller (2020). dplyr: A Grammar of Data Manipulation.

Halemano, K., Harper, M.S., Guo, K., Li, S.X., Heilman, K.J., Barrett, B.S., and Santiago, M.L. (2013). Humoral immunity in the Friend retrovirus infection model. Immunol Res *55*, 249-260.

Han, H., Cho, J.W., Lee, S., Yun, A., Kim, H., Bae, D., Yang, S., Kim, C.Y., Lee, M., Kim, E.*, et al.* (2018). TRRUST v2: an expanded reference database of human and mouse transcriptional regulatory interactions. Nucleic Acids Res *46*, D380-D386.

Honda, K., Ohba, Y., Yanai, H., Negishi, H., Mizutani, T., Takaoka, A., Taya, C., and Taniguchi, T. (2005). Spatiotemporal regulation of MyD88-IRF-7 signalling for robust type-I interferon induction. Nature *434*, 1035-1040.

Hornung, V., Rothenfusser, S., Britsch, S., Krug, A., Jahrsdorfer, B., Giese, T., Endres, S., and Hartmann, G. (2002). Quantitative expression of toll-like receptor 1-10 mRNA in cellular subsets of human peripheral blood mononuclear cells and sensitivity to CpG oligodeoxynucleotides. J Immunol *168*, 4531-4537.

Hu, H., Miao, Y.R., Jia, L.H., Yu, Q.Y., Zhang, Q., and Guo, A.Y. (2019). AnimalTFDB 3.0: a comprehensive resource for annotation and prediction of animal transcription factors. Nucleic Acids Res *47*, D33-D38.

Ise, W., Kohyama, M., Schraml, B.U., Zhang, T., Schwer, B., Basu, U., Alt, F.W., Tang, J., Oltz, E.M., Murphy, T.L., and Murphy, K.M. (2011). The transcription

factor BATF controls the global regulators of class-switch recombination in both B cells and T cells. Nat Immunol *12*, 536-543.

Ishii, K.J., and Akira, S. (2006). Innate immune recognition of, and regulation by, DNA. Trends Immunol *27*, 525-532.

Ivashkiv, L.B., and Donlin, L.T. (2014). Regulation of type I interferon responses. Nat Rev Immunol *14*, 36-49.

Iwata, A., Durai, V., Tussiwand, R., Briseno, C.G., Wu, X., Grajales-Reyes, G.E., Egawa, T., Murphy, T.L., and Murphy, K.M. (2017). Quality of TCR signaling determined by differential affinities of enhancers for the composite BATF-IRF4 transcription factor complex. Nat Immunol *18*, 563-572.

Jabeen, R., Goswami, R., Awe, O., Kulkarni, A., Nguyen, E.T., Attenasio, A., Walsh, D., Olson, M.R., Kim, M.H., Tepper, R.S.*, et al.* (2013). Th9 cell development requires a BATF-regulated transcriptional network. The Journal of clinical investigation *123*, 4641-4653.

Jordan-Williams, K.L., Poston, S., and Taparowsky, E.J. (2013). BATF regulates the development and function of IL-17 producing iNKT cells. BMC Immunol *14*, 16.

Kanamori, M., Konno, H., Osato, N., Kawai, J., Hayashizaki, Y., and Suzuki, H. (2004). A genome-wide and nonredundant mouse transcription factor database. Biochem Biophys Res Commun *322*, 787-793.

Karsunky, H., Merad, M., Cozzio, A., Weissman, I.L., and Manz, M.G. (2003). Flt3 ligand regulates dendritic cell development from Flt3+ lymphoid and myeloid-committed progenitors to Flt3+ dendritic cells in vivo. J Exp Med *198*, 305-313.

Karwacz, K., Miraldi, E.R., Pokrovskii, M., Madi, A., Yosef, N., Wortman, I., Chen, X., Watters, A., Carriero, N., Awasthi, A.*, et al.* (2017). Critical role of IRF1 and BATF in forming chromatin landscape during type 1 regulatory cell differentiation. Nat Immunol *18*, 412-421.

Kim, S., Kaiser, V., Beier, E., Bechheim, M., Guenthner-Biller, M., Ablasser, A., Berger, M., Endres, S., Hartmann, G., and Hornung, V. (2014). Self-priming

determines high type I IFN production by plasmacytoid dendritic cells. Eur J Immunol *44*, 807-818.

Kolde, R. (2019). pheatmap: Pretty Heatmaps. R package version 1.0.12.

Kretschmer, S., and Lee-Kirsch, M.A. (2017). Type I interferon-mediated autoinflammation and autoimmunity. Curr Opin Immunol *49*, 96-102.

Kurachi, M., Barnitz, R.A., Yosef, N., Odorizzi, P.M., DiIorio, M.A., Lemieux, M.E., Yates, K., Godec, J., Klatt, M.G., Regev, A.*, et al.* (2014). The transcription factor BATF operates as an essential differentiation checkpoint in early effector CD8+ T cells. Nat Immunol *15*, 373-383.

Kuwahara, M., Ise, W., Ochi, M., Suzuki, J., Kometani, K., Maruyama, S., Izumoto, M., Matsumoto, A., Takemori, N., Takemori, A.*, et al.* (2016). Bach2-Batf interactions control Th2-type immune response by regulating the IL-4 amplification loop. Nat Commun *7*, 12596.

Larsson, J. (2018). eulerr: Area-Proportional Euler and Venn Diagrams with Ellipses.

Le Mercier, I., Poujol, D., Sanlaville, A., Sisirak, V., Gobert, M., Durand, I., Dubois, B., Treilleux, I., Marvel, J., Vlach, J.*, et al.* (2013). Tumor promotion by intratumoral plasmacytoid dendritic cells is reversed by TLR7 ligand treatment. Cancer Res *73*, 4629-4640.

Lee-Kirsch, M.A. (2017). The Type I Interferonopathies. Annu Rev Med *68*, 297-315.

Lee, W., Mitchell, P., and Tjian, R. (1987). Purified transcription factor AP-1 interacts with TPA-inducible enhancer elements. Cell *49*, 741-752.

Li, P., Spolski, R., Liao, W., Wang, L., Murphy, T.L., Murphy, K.M., and Leonard, W.J. (2012). BATF-JUN is critical for IRF4-mediated transcription in T cells. Nature *490*, 543-546.

Li, S., Wu, J., Zhu, S., Liu, Y.J., and Chen, J. (2017). Disease-Associated Plasmacytoid Dendritic Cells. Front Immunol *8*, 1268.

Liao, J., Humphrey, S.E., Poston, S., and Taparowsky, E.J. (2011). Batf promotes growth arrest and terminal differentiation of mouse myeloid leukemia cells. Mol Cancer Res *9*, 350-363.

Liu, R., Holik, A.Z., Su, S., Jansz, N., Chen, K., Leong, H.S., Blewitt, M.E., Asselin-Labat, M.L., Smyth, G.K., and Ritchie, M.E. (2015). Why weight? Modelling sample and observational level variability improves power in RNA-seq analyses. Nucleic Acids Res *43*, e97.

Logan, M.R., Jordan-Williams, K.L., Poston, S., Liao, J., and Taparowsky, E.J. (2012). Overexpression of Batf induces an apoptotic defect and an associated lymphoproliferative disorder in mice. Cell Death Dis *3*, e310.

Manz, M.G., Traver, D., Akashi, K., Merad, M., Miyamoto, T., Engleman, E.G., and Weissman, I.L. (2001). Dendritic cell development from common myeloid progenitors. Ann N Y Acad Sci *938*, 167-173; discussion 173-164.

Mashayekhi, M., Sandau, M.M., Dunay, I.R., Frickel, E.M., Khan, A., Goldszmid, R.S., Sher, A., Ploegh, H.L., Murphy, T.L., Sibley, L.D., and Murphy, K.M. (2011). CD8alpha(+) dendritic cells are the critical source of interleukin-12 that controls acute infection by Toxoplasma gondii tachyzoites. Immunity *35*, 249-259.

Muller, U., Steinhoff, U., Reis, L.F., Hemmi, S., Pavlovic, J., Zinkernagel, R.M., and Aguet, M. (1994). Functional role of type I and type II interferons in antiviral defense. Science *264*, 1918-1921.

Murphy, T.L., Tussiwand, R., and Murphy, K.M. (2013). Specificity through cooperation: BATF-IRF interactions control immune-regulatory networks. Nat Rev Immunol *13*, 499-509.

Naik, S.H., Metcalf, D., van Nieuwenhuijze, A., Wicks, I., Wu, L., O'Keeffe, M., and Shortman, K. (2006). Intrasplenic steady-state dendritic cell precursors that are distinct from monocytes. Nat Immunol *7*, 663-671.

Nakano, H., Yanagita, M., and Gunn, M.D. (2001). CD11c(+)B220(+)Gr-1(+) cells in mouse lymph nodes and spleen display characteristics of plasmacytoid dendritic cells. J Exp Med *194*, 1171-1178.

Neuwirth, E. (2014). RColorBrewer: ColorBrewer Palettes.

O'Shea, E.K., Rutkowski, R., and Kim, P.S. (1992). Mechanism of specificity in the Fos-Jun oncoprotein heterodimer. Cell *68*, 699-708.

O'Shea, E.K., Rutkowski, R., Stafford, W.F., 3rd, and Kim, P.S. (1989). Preferential heterodimer formation by isolated leucine zippers from fos and jun. Science *245*, 646-648.

Pfaffl, M.W. (2001). A new mathematical model for relative quantification in real-time RT-PCR. Nucleic Acids Res *29*, e45.

Platanias, L.C. (2005). Mechanisms of type-I- and type-II-interferon-mediated signalling. Nat Rev Immunol *5*, 375-386.

Puttur, F., Arnold-Schrauf, C., Lahl, K., Solmaz, G., Lindenberg, M., Mayer, C.T., Gohmert, M., Swallow, M., van Helt, C., Schmitt, H.*, et al.* (2013). Absence of Siglec-H in MCMV infection elevates interferon alpha production but does not enhance viral clearance. PLoS Pathog *9*, e1003648.

Reizis, B. (2019). Plasmacytoid Dendritic Cells: Development, Regulation, and Function. Immunity *50*, 37-50.

Reizis, B., Bunin, A., Ghosh, H.S., Lewis, K.L., and Sisirak, V. (2011). Plasmacytoid dendritic cells: recent progress and open questions. Annu Rev Immunol *29*, 163-183.

Robinson, J.T., Thorvaldsdottir, H., Winckler, W., Guttman, M., Lander, E.S., Getz, G., and Mesirov, J.P. (2011). Integrative genomics viewer. Nat Biotechnol *29*, 24-26.

Robinson, M.D., McCarthy, D.J., and Smyth, G.K. (2010). edgeR: a Bioconductor package for differential expression analysis of digital gene expression data. Bioinformatics *26*, 139-140.

Rodrigues, P.F., Alberti-Servera, L., Eremin, A., Grajales-Reyes, G.E., Ivanek, R., and Tussiwand, R. (2018). Distinct progenitor lineages contribute to the heterogeneity of plasmacytoid dendritic cells. Nat Immunol *19*, 711-722.

Rusinova, I., Forster, S., Yu, S., Kannan, A., Masse, M., Cumming, H., Chapman, R., and Hertzog, P.J. (2013). Interferome v2.0: an updated database of annotated interferon-regulated genes. Nucleic Acids Res *41*, D1040-1046.

Sahoo, A., Alekseev, A., Tanaka, K., Obertas, L., Lerman, B., Haymaker, C., Clise-Dwyer, K., McMurray, J.S., and Nurieva, R. (2015). Batf is important for IL-4 expression in T follicular helper cells. Nat Commun *6*, 7997.

Salio, M., Palmowski, M.J., Atzberger, A., Hermans, I.F., and Cerundolo, V. (2004). CpG-matured murine plasmacytoid dendritic cells are capable of in vivo priming of functional CD8 T cell responses to endogenous but not exogenous antigens. J Exp Med *199*, 567-579.

Sasaki, I., Hoshino, K., Sugiyama, T., Yamazaki, C., Yano, T., Iizuka, A., Hemmi, H., Tanaka, T., Saito, M., Sugiyama, M.*, et al.* (2012). Spi-B is critical for plasmacytoid dendritic cell function and development. Blood *120*, 4733-4743.

Sawai, C.M., Sisirak, V., Ghosh, H.S., Hou, E.Z., Ceribelli, M., Staudt, L.M., and Reizis, B. (2013). Transcription factor Runx2 controls the development and migration of plasmacytoid dendritic cells. J Exp Med *210*, 2151-2159.

Scheu, S., Dresing, P., and Locksley, R.M. (2008). Visualization of IFNbeta production by plasmacytoid versus conventional dendritic cells under specific stimulation conditions in vivo. Proc Natl Acad Sci U S A *105*, 20416-20421.

Schraml, B.U., Hildner, K., Ise, W., Lee, W.L., Smith, W.A., Solomon, B., Sahota, G., Sim, J., Mukasa, R., Cemerski, S.*, et al.* (2009). The AP-1 transcription factor Batf controls T(H)17 differentiation. Nature *460*, 405-409.

Senga, T., Iwamoto, T., Humphrey, S.E., Yokota, T., Taparowsky, E.J., and Hamaguchi, M. (2002). Stat3-dependent induction of BATF in M1 mouse myeloid leukemia cells. Oncogene *21*, 8186-8191.

Seth, S., Qiu, Q., Danisch, S., Maier, M.K., Braun, A., Ravens, I., Czeloth, N., Hyde, R., Dittrich-Breiholz, O., Forster, R., and Bernhardt, G. (2011). Intranodal interaction with dendritic cells dynamically regulates surface expression of the co-

stimulatory receptor CD226 protein on murine T cells. J Biol Chem *286*, 39153-39163.

Shannon, P., Markiel, A., Ozier, O., Baliga, N.S., Wang, J.T., Ramage, D., Amin, N., Schwikowski, B., and Ideker, T. (2003). Cytoscape: a software environment for integrated models of biomolecular interaction networks. Genome Res *13*, 2498-2504.

Sichien, D., Scott, C.L., Martens, L., Vanderkerken, M., Van Gassen, S., Plantinga, M., Joeris, T., De Prijck, S., Vanhoutte, L., Vanheerswynghels, M.*, et al.* (2016). IRF8 Transcription Factor Controls Survival and Function of Terminally Differentiated Conventional and Plasmacytoid Dendritic Cells, Respectively. Immunity *45*, 626-640.

Slowikowski, K. (2020). ggrepel: Automatically Position Non-Overlapping Text Labels with 'ggplot2'.

Smyth, G.K. (2004). Linear models and empirical bayes methods for assessing differential expression in microarray experiments. Stat Appl Genet Mol Biol *3*, Article3.

Sood, V., Sharma, K.B., Gupta, V., Saha, D., Dhapola, P., Sharma, M., Sen, U., Kitajima, S., Chowdhury, S., Kalia, M., and Vrati, S. (2017). ATF3 negatively regulates cellular antiviral signaling and autophagy in the absence of type I interferons. Sci Rep *7*, 8789.

Sopel, N., Graser, A., Mousset, S., and Finotto, S. (2016). The transcription factor BATF modulates cytokine-mediated responses in T cells. Cytokine Growth Factor Rev *30*, 39-45.

Swiecki, M., and Colonna, M. (2015). The multifaceted biology of plasmacytoid dendritic cells. Nat Rev Immunol *15*, 471-485.

Tailor, P., Tamura, T., Kong, H.J., Kubota, T., Kubota, M., Borghi, P., Gabriele, L., and Ozato, K. (2007). The feedback phase of type I interferon induction in dendritic cells requires interferon regulatory factor 8. Immunity *27*, 228-239.

Tamura, T., Tailor, P., Yamaoka, K., Kong, H.J., Tsujimura, H., O'Shea, J.J., Singh, H., and Ozato, K. (2005). IFN regulatory factor-4 and -8 govern dendritic cell subset development and their functional diversity. J Immunol *174*, 2573-2581.

Team, R. (2020). RStudio: Integrated Development for R.

Triantis, V., Trancikova, D.E., Looman, M.W., Hartgers, F.C., Janssen, R.A., and Adema, G.J. (2006). Identification and characterization of DC-SCRIPT, a novel dendritic cell-expressed member of the zinc finger family of transcriptional regulators. J Immunol *176*, 1081-1089.

Trinchieri, G., and Santoli, D. (1978). Anti-viral activity induced by culturing lymphocytes with tumor-derived or virus-transformed cells. Enhancement of human natural killer cell activity by interferon and antagonistic inhibition of susceptibility of target cells to lysis. J Exp Med *147*, 1314-1333.

Tsujimura, H., Nagamura-Inoue, T., Tamura, T., and Ozato, K. (2002). IFN consensus sequence binding protein/IFN regulatory factor-8 guides bone marrow progenitor cells toward the macrophage lineage. J Immunol *169*, 1261-1269.

Tsujimura, H., Tamura, T., Gongora, C., Aliberti, J., Reis e Sousa, C., Sher, A., and Ozato, K. (2003). ICSBP/IRF-8 retrovirus transduction rescues dendritic cell development in vitro. Blood *101*, 961-969.

Tussiwand, R., Lee, W.L., Murphy, T.L., Mashayekhi, M., Kc, W., Albring, J.C., Satpathy, A.T., Rotondo, J.A., Edelson, B.T., Kretzer, N.M.*, et al.* (2012). Compensatory dendritic cell development mediated by BATF-IRF interactions. Nature *490*, 502-507.

Ubel, C., Sopel, N., Graser, A., Hildner, K., Reinhardt, C., Zimmermann, T., Rieker, R.J., Maier, A., Neurath, M.F., Murphy, K.M., and Finotto, S. (2014). The activating protein 1 transcription factor basic leucine zipper transcription factor, ATF-like (BATF), regulates lymphocyte- and mast cell-driven immune responses in the setting of allergic asthma. The Journal of allergy and clinical immunology *133*, 198-206 e191-199.

Volpi, C., Fallarino, F., Pallotta, M.T., Bianchi, R., Vacca, C., Belladonna, M.L., Orabona, C., De Luca, A., Boon, L., Romani, L.*, et al.* (2013). High doses of CpG oligodeoxynucleotides stimulate a tolerogenic TLR9-TRIF pathway. Nat Commun *4*, 1852.

Wagner, E.F., and Eferl, R. (2005). Fos/AP-1 proteins in bone and the immune system. Immunol Rev *208*, 126-140.

Wang, J., Sun, Q., Morita, Y., Jiang, H., Gross, A., Lechel, A., Hildner, K., Guachalla, L.M., Gompf, A., Hartmann, D.*, et al.* (2012). A differentiation checkpoint limits hematopoietic stem cell self-renewal in response to DNA damage. Cell *148*, 1001-1014.

Wickham, H. (2016). ggplot2: Elegant Graphics for Data Analysis. Springer-Verlag New York.

Williams, K.L., Nanda, I., Lyons, G.E., Kuo, C.T., Schmid, M., Leiden, J.M., Kaplan, M.H., and Taparowsky, E.J. (2001). Characterization of murine BATF: a negative regulator of activator protein-1 activity in the thymus. Eur J Immunol *31*, 1620-1627.

Williams, K.L., Zullo, A.J., Kaplan, M.H., Brutkiewicz, R.R., Deppmann, C.D., Vinson, C., and Taparowsky, E.J. (2003). BATF transgenic mice reveal a role for activator protein-1 in NKT cell development. Journal of immunology *170*, 2417-2426.

Wu, J., Li, S., Li, T., Lv, X., Zhang, M., Zang, G., Qi, C., Liu, Y.J., Xu, L., and Chen, J. (2019). pDC Activation by TLR7/8 Ligand CL097 Compared to TLR7 Ligand IMQ or TLR9 Ligand CpG. J Immunol Res *2019*, 1749803.

Xie, J., Zhang, S., Hu, Y., Li, D., Cui, J., Xue, J., Zhang, G., Khachigian, L.M., Wong, J., Sun, L., and Wang, M. (2014). Regulatory roles of c-jun in H5N1 influenza virus replication and host inflammation. Biochim Biophys Acta *1842*, 2479-2488.

Zhang, H.M., Chen, H., Liu, W., Liu, H., Gong, J., Wang, H., and Guo, A.Y. (2012). AnimalTFDB: a comprehensive animal transcription factor database. Nucleic Acids Res *40*, D144-149.

Zhang, S., Coughlan, H.D., Ashayeripanah, M., Seizova, S., Kueh, A.J., Brown, D.V., Cao, W., Jacquelot, N., D'Amico, A., Lew, A.M.*, et al.* (2021). Type 1 conventional dendritic cell fate and function are controlled by DC-SCRIPT. Sci Immunol *6*.

Zullo, A.J., Benlagha, K., Bendelac, A., and Taparowsky, E.J. (2007). Sensitivity of NK1.1-negative NKT cells to transgenic BATF defines a role for activator protein-1 in the expansion and maturation of immature NKT cells in the thymus. J Immunol *178*, 58-66.

7. Appendix

7.1 Publications

The results of the work presented here were in part published in scientific journals or presented at international conferences.

The paper titled *The transcription factor reservoir and chromatin landscape in activated plasmacytoid dendritic cells* by Mann-Nüttel et al. has been accepted for publication in the Journal BMC Genomic Data. The manuscript can be found below. It has also been posted on the bioRxiv preprint server (DOI: https://doi.org/10.1101/2021.04.14.439791).

The results from the type I IFN study will be submitted in a manuscript with me as co-author with Shafaqat Ali in the near future. The pDC development story will also be published with me as a first author in the future.

The transcription factor reservoir and chromatin landscape in activated plasmacytoid dendritic cells

Ritu Mann-Nüttel,[1] Shafaqat Ali,[1,2,3] Patrick Petzsch,[4] Karl Köhrer,[4] Judith Alferink,[2,3] and Stefanie Scheu[1,5,*]

[1]Institute of Medical Microbiology and Hospital Hygiene, University of Düsseldorf, Düsseldorf, Germany

[2]Cells in Motion Interfaculty Centre, Münster, Germany

[3]Department of Mental Health, University of Münster, Münster, Germany

[4]Biological and Medical Research Center (BMFZ), Medical Faculty, University of Düsseldorf, Düsseldorf, Germany

[5]Lead contact

[*]Correspondence: stefanie.scheu@hhu.de

Running title: Transcription factors in pDC activation

Abstract

Transcription factors (TFs) control gene expression by direct binding to regulatory regions of target genes but also by impacting chromatin landscapes and thereby modulating DNA accessibility for other TFs. To date, the global TF reservoir in plasmacytoid dendritic cells (pDCs), a cell type with the unique capacity to produce unmatched amounts of type I interferons, has not been fully characterized. To fill this gap, we have performed a comprehensive analysis in naïve and TLR9-activated pDCs in a time course study covering early timepoints after stimulation (2h, 6h, 12h) integrating gene expression (RNA-Seq), chromatin landscape (ATAC-Seq) and Gene Ontology studies. We found that 70% of all described TFs are expressed in pDCs for at least one stimulation time point and that activation predominantly “turned on” the chromatin regions associated with TF genes. We hereby define the complete set of TLR9-regulated TFs in pDCs. Further, this study identifies the AP-1 family of TFs as potentially important but so far less well characterized regulators of pDC function.

Keywords

Transcription factors, plasmacytoid dendritic cells, TLR9, gene expression analysis, next generation sequencing, ATAC-Seq

Introduction

Transcription factors (TFs) are known to bind to DNA-regulatory sequences to either enhance or inhibit gene transcription during cell differentiation, at steady state, and for exertion of cell effector functions (Vaquerizas et al., 2009; Wingender et al., 2018; Zhou et al., 2017). TFs also show unique expression patterns for different cell types and cellular states. The differentiation of distinct cell types from pluripotent stem cells is enabled by the expression of cell fate-determining TFs in progenitor cells. Transcription factors not only regulate cell development and effector functions by binding to *cis*-

regulatory elements but also impact the accessibility of chromatin in different cell states (Serebreni and Stark, 2020). These latter TFs are called pioneering TFs and have the ability to remodel chromatin and thus modify the epigenome (Drouin, 2014). Chromatin is dynamically modified during cell differentiation leading to a cell-type specific landscape (Chauvistre and Sere, 2020; Deaton and Bird, 2011), which may be altered after cell activation. This process changes DNA accessibility for a particular set of TFs, that in turn modulate the expression of other genes important for cell identity and function. Efforts have been made to list and integrate all known mouse TFs in dedicated databases (db), such as Riken mouse TFdb (Kanamori et al., 2004) and TFCat (Fulton et al., 2009), amongst others. However, most of these were built before 2010 and have not been updated. The AnimalTFDB, most recently updated in 2019, classifies the mouse TF reservoir based on the structure of the DNA binding domains (Hu et al., 2019; Zhang et al., 2012). This database provides an accurate TF family assignment combined with TF binding site information in 22 animal species which also allows insight into TF evolution.

Plasmacytoid dendritic cells (pDCs) comprise a rare population of 0.2 to 0.8% of peripheral blood mononuclear cells (Liu, 2005). They were first described more than 40 years ago as natural interferon (IFN)-producing cells (IPCS) that activate NK cells after virus recognition (Trinchieri and Santoli, 1978). As we and others have shown, pDCs are now known for their capacity to produce unmatched amounts of type I IFN in response to stimulation of their toll like receptors (TLRs) (Ali et al., 2019; Asselin-Paturel et al., 2001; Bauer et al., 2016; Gilliet et al., 2008; Reizis, 2019). In contrast to other dendritic cell (DC) subsets, pDCs express only a limited repertoire of TLRs, namely predominantly TLR7 and TLR9 (Hornung et al., 2002), which recognize guanosine- and uridine-rich ssRNA and DNA containing CpG motifs (Diebold et al., 2004; Ishii and Akira, 2006; Wu et al., 2019). After TLR7 and TLR9 activation, in addition to type I IFN production, pDCs acquire the ability to prime T cell responses (Salio et al., 2004). CpG can be considered as an optimal and specific microbial stimulus for pDCs which induces TLR9 mediated signaling that leads to activation of IRF7 and NF-kB signaling pathways (Swiecki and Colonna, 2015). With regard to immunopathologies, unremitting production of type I IFN by pDCs has been reported in autoimmune diseases like systemic lupus erythematosus (Elkon and Wiedeman, 2012). Moreover, when recruited to the tumor microenvironment pDCs may induce immune tolerance and thus contribute to tumor progression (Le Mercier et al., 2013; Li et al., 2017). Thus, exploiting CpG for immunotherapeutic treatment to both enhance and repress pDC responses to mediate antitumor activity (Lou et al., 2011), treat allergy (Hayashi et al., 2004), and autoimmunity (Christensen et al., 2006) has been attempted in recent years. In addition, targeting specific TFs with the aim to control immunity and autoimmune disease (Lee et al., 2018) or to enhance cancer gene therapy (Libermann and Zerbini, 2006) has become the focus of attention in recent decades to develop immunomodulatory drugs.

Over the last years, different TFs have been determined as cell fate-instructive TFs in DCs. In particular, absence of the interferon regulatory factor 8 (IRF8) resulted in pDC-deficient mice (Tamura et al., 2005; Tsujimura et al., 2002). Bornstein *et al.* further identified IRF8 as an inducer of cell-specific chromatin changes in thousands of pDC enhancers (Bornstein et al., 2014). Further, mice deficient in the Ets family transcription factor Spi-B showed decreased pDC numbers in the bone marrow (BM) while pDC numbers were increased in the periphery. This indicated an involvement of Spi-B in pDC development,

caused by a defective retainment of mature nondividing pDCs in the BM (Sasaki et al., 2012). In contrast to the phenotype of *Spi-B*-deficient mice, *Runx2*-deficient animals exhibited normal pDC development in the BM but reduced pDC numbers in the periphery due to a reduced egress of mature pDCs from the BM into the circulation (Chopin et al., 2016; Sawai et al., 2013). Finally, the *Tcf4*-encoded TF E2-2 is essentially required for pDC development as either its constitutive or inducible deletion in mice blocked pDC differentiation (Cisse et al., 2008). Using a combined approach to evaluate genome-wide expression and epigenetic marks a regulatory circuitry for pDC commitment within the overall DC subset specification has been devised (Lin et al., 2015). Even though the functions of selected cell fate TFs have been well described in pDCs, to our knowledge no global TF expression analysis after pDC activation has been performed for this cell type.

In the present study, we performed a detailed analysis on the changes in expression and chromatin accessibility for the complete set of all known TFs in pDCs in an early time course after activation. To this purpose, we used the AnimalTFDB data base and combined RNA-Seq, ATAC-Seq, and Gene Ontology analyses to define global TF gene expression, chromatin landscapes, and biological pathways in pDCs following activation. We defined epigenetic and transcriptional states using purified murine BM-derived Flt3-L cultured pDCs 2h, 6h, and 12h after TLR9 activation as compared to steady state. Based on our findings, we suggest a novel set of CpG-dependent TFs associated with pDC activation. We further identify the AP-1 family of TFs, which are so far less well characterized in pDC biology, as novel and possibly important players in these cells after activation.

Results

Expression of transcription factors in naïve and activated pDCs

To assess the impact of pDC activation on global TF expression in these cells, we simulated early events after virus infection in a time course study. To this end, we performed RNA-Seq of sorted BM-derived Flt3-L pDCs from C57BL/6N mice that were either left untreated or stimulated with CpG for 2h, 6h, or 12h. This synthetic double-strand DNA specifically activates endosomal TLR9 and is known to induce a robust type I IFN production (Gilliet et al., 2008). As the global definition of the mouse TF reservoir in this study we used 1,636 genes annotated by Hu *et al.* as TFs in the mouse genome (Hu et al., 2019). We evaluated the expression of all TFs in pDCs according to a formula by Chen *et al.,* which takes into consideration the library length of the RNA-Seq run and the gene length to determine whether the gene is expressed or not (Chen et al., 2016). We found that 1,014 TFs (70% of all annotated TFs) are expressed in at least one condition, naïve or after TLR9 activation (2h, 6h, 12h) (**Fig. 1A**). The TFs expressed in pDCs were allocated to the different TF classes based on their DNA binding domain as described in the AnimalTFDB (Hu et al., 2019) (**Fig. 1B**). We found that more than half of all TFs (55%, 558 TFs in total) expressed in pDCs belong to the Zinc-coordinating TF group which use zinc ions to stabilize its folding and classically consist of two-stranded β-sheets and a short α-helix. Helix-turn-helix factors, of which 158 (16%) were expressed in pDCs under the defined conditions, comprise several helices mediating multiple functions such as insertion into a major DNA groove, stabilization of the backbone and binding to the overall structure of the DNA (Aravind et al., 2005). Furthermore, 10%

(104 TFs) of all TFs expressed in pDCs belong to the Basic Domain group, which contains TFs that become α-helically folded upon DNA binding (Patel et al., 1990; Weiss et al., 1990). 44 expressed TFs (4%) belong to the Other α-Helix group exhibiting α-helically structured interfaces are required for DNA binding. In addition, 32 of the TFs (3%) found in pDCs are β-Scaffold factors which use a large β-sheet surface to recognize DNA by binding in the minor groove. Lastly, another ~100 TFs (12%) were of unclassified structure, meaning their mode of action for DNA binding is unknown. Strikingly, some TF families were not expressed in pDCs at all (**Fig. 1C**), such as the AP-2 family in the Basic Domain group, the GCM family in the β-Scaffold group, the Orthodenticle homeobox (Otx) TFs in the Helix-turn-helix group, Steroidgenic factor (SF)-like factors in the Zinc-coordinating group, and the DM group, first discovered in *Drosophila melanogaster*, among the unclassified TFs. Other TF families showed expression of all family members in at least one condition (steady state, or CpG 2h, 6h, 12h), such as the Transforming growth factor-β stimulated clone-22 (TSC22) family in the Basic Domain group, Runt and Signal Transducers and Activators of Transcription (STAT) factors from the β-scaffold classification, and E2F and Serum response factor (SRF) factors in the Helix-turn-helix group. In summary, 70% of all genes annotated as TFs in the mouse genome (1,014 out of 1,636) were expressed either in naïve or activated pDCs (CpG 2h, 6h, 12h), covering a wide range of TF classes based on different DNA binding mechanisms.

Activation-dependent TF expression changes

We next investigated the impact of pDC activation on changes in expression of TFs using our time course RNA-Seq study. The similarity of our biological replicates in each condition was evaluated with a Pearson correlation analysis. Our results revealed high similarity (<95%) for the biological replicates used in the respective conditions of the RNA-Seq data set. Notably, the differences in the Pearson correlation coefficient between the naïve and first stimulation time point (CpG 2h) were higher than the differences observed between the later CpG stimulation time points (6h, 12h) (**Fig. 2A**). We used the data for differential expression analysis of genes between pDC states, not only comparing TF expression levels between different CpG stimulation time points vs steady state but also between the different CpG stimulation time points between each other (**Fig. 2B**). The total number of differentially expressed TFs (DETFs) with a fold change $|FC|>2$ and a $p<0.05$ between stimulated vs naïve pDCs (452 DETFs in 2h vs 0h; 400 DETFs in 6h vs 0h; 335 DETFs in 12h vs 0h) was higher than the absolute number of TFs showing expression changes between the CpG conditions (270 DETFs in 6h vs 2h; 119 DETFs in 12h vs 6h; 358 DETFs in 12h vs 2h). This reflects the results from the Pearson correlation analysis (**Fig. 2A**). Interestingly, by comparing TF gene expression in 2h stimulated vs unstimulated pDCs, a higher number of TF genes were down-regulated in expression after TLR9 stimulation than were upregulated in these cells (271 vs 181). With increased duration of pDC stimulation, the difference in the number of TFs that were up- vs down-regulated diminished (208 down vs 192 up in 6h vs 0h). Finally, at the longest stimulation time used in this study (12h vs 0h), the number of up-regulated TF genes was higher than the number of down-regulated TF genes (179 vs 156). Comparing the CpG stimulated samples amongst each other, more TFs exhibited increased expression with longer stimulation times than there were TFs showing reduced expression levels (171 up vs 99 down in 6h vs

2h; 63 up vs 56 down in 12h vs 6h; 234 up vs 124 down in 12h vs 2h) (**Fig. 2B** and **C**). In total, we identified 661 unique TF genes that are differentially expressed between at least one of the compared pDC states |FC|>2, p<0.05, pDC at steady state, or after CpG activation at 2h, 6h, 12h). To evaluate patterns of expression changes for all 661 differentially expressed TFs, we next carried out hierarchical clustering of all TF genes based on the normalized expression in naïve and stimulated pDCs (**Fig. 2B**). This led to the definition of five different clusters of TFs according to their expression pattern (**Fig. 2D**). Cluster I, IV and V contained TFs with large expression changes after short duration of pDC stimulation (2h), while cluster II and III contained TFs that exhibit altered expression only with longer duration of cell stimulation (6h, 12h). Cluster V contained genes that were all down-regulated at any time point after CpG stimulation as compared to the unstimulated condition (**Fig. 2D**). In more detail, TFs driving either pDC (e.g. *Tcf4, Spib, Runx2*) or classical DC (cDC) (e.g. *Nfil3, Spi1, Id2*) development (Bornstein et al., 2014; Sasaki et al., 2012; Sawai et al., 2013; Tamura et al., 2005; Tsujimura et al., 2002) were distributed over all clusters I to V. This highlights variable expression patterns of DC cell fate TFs after pDC activation. In summary, in this time course study that models early events after virus infection, we identified in total 661 unique CpG-dependent TF genes that show significant differential expression in at least one condition compared to another |FC|>2, p<0.05, pDC at steady state, or after CpG activation at 2h, 6h, 12h). Further, pDC activation showed time dependent activating as well as inhibiting effects on the expression of TFs.

Gene ontology analysis of CpG-dependent TFs

Next, downstream gene ontology (GO) analyses of RNA-Seq data were performed to unravel the biological processes in which CpG-dependent TFs are involved. For this purpose, functional annotation clustering with the 661 TF encoding genes defined as CpG-dependent |FC|>2, p<0.05) was performed on DAVID including terms for biological processes (BP), molecular functions (MF), and cellular components (CC). The analysis produced 16 clusters, out of which the 9 non-redundant and most relevant in the context of innate immunity are depicted in **Fig. 3A** (complete list in **Table S1**). The GO analyses produced an individual fold enrichment for each GO term (**Fig. 3A**, right column), and in addition, an enrichment score for each cluster containing several GO terms (**Table S1**). The order of the clusters from top to bottom follows a decrease in the cluster enrichment score, establishing a hierarchy of importance for the biological processes affected. Cluster one contained GO terms for DNA binding, transcription, and nuclear localization with a ~5 fold enrichment comprising more than 400 genes in each term. This confirmed the inherent DNA binding capacity of the defined murine TF reservoir by Hu et al. (Hu et al., 2019) and proved the applicability of our approach. The following clusters comprised less than 25 unique genes per GO term but significant fold enrichments for most GO terms drawing attention to specific TFs involved in particular biological processes in pDC activation. Cluster 2 contained GO terms associated with the circadian rhythm and regulation of gene expression (e.g. *Klf10, Jun*). We further found GO terms enriched for the IκB/NFκB complex, NIK/NFκB signaling, and IκB kinase/NFκB signaling (e.g. *Nfkb1, Nfkb2, Rel*), which showed the highest fold enrichment (up to 25 fold) among all GO terms and clusters. In line with this, it is well known that CpG activates the canonical TLR9-Myd88-NFκB/IRF7 signaling pathway in pDCs (Tomasello et al., 2018). Another cluster

contained processes involving SMAD proteins (e.g. *Smad1, Smad2, Smad3*), signal transducers for TGFβ receptors, involved in receptor binding, signal transduction, and protein complex assembly. Of note, it is known that pDCs exposed to TGFβ lose their ability to produce type I IFN after TLR9 stimulation (Saas and Perruche, 2012). Another significantly enriched cluster comprised GO terms for various processes involving the endoplasmic reticulum (e.g. *Cebpb, Ddit3*), an important site of intracellular protein and lipid assembly. GO terms containing TFs that regulate sumoylation (e.g. *Pias4, Egr2*), posttranslational modifications that e.g. coordinate the repression of inflammatory gene expression during innate sensing (Decque et al., 2016), were also significantly enriched and clustered together. As expected, CpG-dependent TFs were enriched in GO terms for the JAK-STAT signaling pathway (e.g. *Stat1, Stat2, Stat3*) activated by binding of type I IFN to the type I IFN receptor. TFs affecting mRNA binding processes (e.g. *Mbd2, Ybx2*) which are required for synthesizing proteins at the ribosomes, were also affected. The fact that epigenetic modulators (e.g. *Prdm9, Kmt2c*) were enriched, highlights the importance of gene expression regulation of TFs in pDCs by modifications that alter the physical structure of the DNA after CpG stimulation. In summary, we find that CpG-dependent TFs are involved in a wide variety of biological processes, such as circadian regulation, mRNA binding, and signaling pathways such as the NFκB and JAK-STAT pathways. The analyses revealed the importance of these biological processes being affected by pDC activation in a hierarchical manner according to their attributed relevance. This opens up the opportunity to investigate specific TFs involved in processes that have not been fully elucidated for pDC biology.

pDC activation modulates chromatin accessibility for binding of TF families

Another hallmark of cell activation is the modification of the chromatin landscape. To better understand how the chromatin accessibility of different TF families is altered in pDCs in the course of activation, we performed ATAC-Seq in naïve and 2h CpG activated pDCs. Pearson correlation analysis for the ATAC-Seq data reveals >95% similarity for all biological replicates (**Fig. 4A**). A quantitative analysis of peak intensities across sample conditions and a differential analysis to determine the number and regions of activation-dependent accessible chromatin peaks was performed. Comparing the specific genomic locations such as introns, 3'-UTRs, distal (1-3kb) and proximal (0-1kb) promoter regions with accessible chromatin between naïve and 2h CpG stimulated pDCs, we found that chromatin is mostly open in distal intergenic and intron regions in both conditions. However, there was no apparent shift in the distribution of genomic locations where chromatin is accessible in pDCs after cell activation (**Fig. 4B**). This suggests that TLR9 activation regulates the chromatin accessibility globally in pDCs but does not induce shifts in the chromatin landscape per se. Overall, we detected ~116,000 accessible regions (peaks) across samples in naïve and activated states. Next, we performed a differential analysis using the DESeq2 algorithm to quantify the number of CpG-dependent accessible peaks. pDC activation substantially altered the chromatin landscape leading to ~16,600 altered accessible regions ($|FC|>2$, $p<0.05$, **Fig.4C, D**). In detail, 2h CpG stimulation of pDCs resulted in 13,226 peaks with increased accessibility and 3,381 peaks with decreased accessibility (**Fig. 4C, D**). Roughly 80% of all CpG-dependent chromatin regions in 2h stimulated pDCs exhibited increased DNA accessibility as compared to naïve pDCs. This suggests that more of the pDC chromatin landscape is „turned on" rather than being „turned off" after

pDC activation. To unravel the biological significance of the activation-dependent chromatin states for the more accessible vs the less accessible DNA regions in pDCs, a differential motif analysis using the HOCOMOCO database (Kulakovskiy et al., 2018) was performed (**Fig. 4E**). The purpose of the analysis was to identify TF families that gain or lose access to DNA after pDC activation which would hint at pathways being affected after activation. At the same time, this unbiased approach allows the identification of TFs that have not been associated with this cell type before. This motif analysis revealed that TFs belonging to the JAK-STAT and the NFκB signaling pathway have increased accessibility to their specific DNA binding regions after CpG stimulation. Besides the NFκB family, we identified the AP-1 family of TFs as one of the most significant hits to gain access to the DNA in our search. This type of TF remains so far less well characterized in pDCs after pathogen encounter or in pDC-specific functions in chronic inflammatory or autoimmune disorders. Albeit the AP-1 member c-Fos has been shown to be required for type I IFN induction, a hallmark function of pDCs, in osteoclast precursor cells after RANKL treatment (Takayanagi et al., 2002). On the other hand, Ets family members belonging to the Helix-turn-helix family of TFs and Zinc-coordinating zf-C2H2 TFs had less access to DNA. Strikingly, pDC-driving cell fate TFs such as IRF8 and RUNX2 showed motif enrichment in two sets of regions, one set with increased and another set with decreased chromatin accessibility after pDC activation. Hence, pDC-driving cell fate TFs both gained and lost access to specific DNA regions after TLR9 activation. We next performed a more detailed analysis searching for enrichment of TF motifs among all regions that contain the promoter sequence of one or more genes. As TFs can regulate gene expression by binding to the promoter site of genes this analysis hints at TF families that exert a functional binding occupancy in the investigated chromatin regions. We previously determined that 13,226 regions exhibit increased chromatin accessibility after pDC activation. Out of these, 2,174 regions were associated with the promoter of one or more genes. An unbiased motif enrichment search revealed that TFs belonging to the NFκB family (e.g. NFκB1, NFκB2, TF65), the AP-1 family (e.g. ATF3, JUN, FOSB), and the JAK-STAT family (e.g. STAT1, STAT2), as well as pDC cell fate TFs (e.g. RUNX2, IRF8) are among the top hits for TFs with DNA binding domains present in promoter associated chromatin regions which gain accessibility after pDC activation (**Table S2**). In summary, the differences in chromatin landscapes of naïve and 2h CpG stimulated pDCs point to a substantial amount of epigenetic modulation of thousands of pDC regions. Also, these analyses unravelled the AP-1 family of TFs, which have so far been less well characterized in pDC biology, as possibly important players in these cells after activation.

TFs show activation-dependent expression and chromatin accessibility

As shown above, pDC activation results in significant alterations of the chromatin landscape in pDCs making the DNA more or less accessible to specific TF families on a global level. We next analysed the impact of pDC activation on regions associated with TF genes themselves by evaluating regions ranging from 1kb upstream of the transcriptional start site (TSS) to 1kb downstream of the poly adenylation site. pDC activation altered the chromatin landscape of ~750 accessible regions associated with TF genes (|FC|>2, $p<0.05$, **Fig. 5A**). In detail, 2h stimulation of pDCs resulted in 627 peaks with increased accessibility and 126 peaks with decreased accessibility to regions associated with TF genes (**Fig. 5A**).

83% of all CpG-dependent chromatin regions in 2h stimulated pDCs exhibited increased DNA accessibility as compared to naïve pDCs. This suggests that most of the chromatin landscape associated with TF genes is „turned on“ rather than being „turned off“ after CpG stimulation. Finally, an integrative approach using the RNA-Seq and ATAC-Seq data was conducted analysing the differential chromatin states of regions associated with differentially expressed TF genes. This revealed 540 TF regions out of the overall ~750 chromatin regions that are significantly associated with a differential RNA expression of the respective TF gene (**Fig. 5B**). Out of these chromatin peaks we found 209 unique TF genes being associated with the differentially opened chromatin regions. Thus, pDC activation modulates the chromatin of most genes in more than one region associated with the respective gene, as shown here for the NFκB family members *Nfkb1* and *Rela* (**Fig. 5B**). To identify potential novel players in pDC biology after cell activation, we integrated the results of our motif analysis, the RNA expression levels, and chromatin states for all TFs. We focused our search on factors that fulfil the following criteria after pDC stimulation: (i) increased gene expression, (ii) enhanced chromatin accessibility, and (iii) enriched TF DNA binding motif in the genomic regions that are more accessible. Mining our dataset, we found that TFs already known to be important in TLR9-mediated signaling such as IRF and NFκB TFs met the requirement as expected. Additionally, members of the AP-1 family such as ATF3 and JUN, which received little mention for pDC biology in literature so far, also fulfilled these criteria. The candidates of all three families exhibited a significantly increased mRNA expression 2h after pDC activation as compared to naïve pDCs. At 6h after stimulation, expression remained at the same level (Jun, Rela), increased further (Irf7) or decreased (Atf3, Nfkb1). After 12h pDC stimulation, expression remained at the same level (Irf7, Atf3) or even decreased (Jun, Nfkb1, Rela) (**Fig. 5C**). In line with an increased expression of the selected TFs 2h after cell activation as compared to the naïve state, we found an increased accessibility of chromatin in the proximal promoter region of the *Irf7*, *Jun*, *Atf3*, *Nfkb1,* and *Rela* genes. Two regions of the *Nfkb1* gene, one proximal and another distal from the TSS of the gene, indicated increased DNA accessibility after CpG stimulation at 2h as compared to the naïve condition. While *Atf3*, *Nfkb1* and *Rela* are characterized by single or a small number of open chromatin peaks, several peaks in the *Irf7* and *Jun* gene were found, both proximal and after the TSS in the intergenic region. Of note, the core structural elements regulating gene expression for the proximal promoter and the intergenic regions were well conserved between mouse and human for all newly identified candidates (top panels, **Fig. 5D**). The potential relevance of the AP-1 factors for pDC biology was further investigated by searching for the common AP-1 motif (TGA[G/C]TCA) (Risse et al., 1989) among all open chromatin regions associated with pDC driving TF genes (*Runx2, Tcf4, Spib, Irf8, Bcl11a*). Using the MEME-FIMO search tool, we found an AP-1 motif in the proximal promoter site of the *Tcf4* gene which encodes the E2-2 protein (**Fig. 5E**). As AP-1 has not been implicated so far in E2-2 gene regulation this finding warrants further investigation. In summary, we found that pDC activation mostly “turns on” TF genes resulting in significant expression changes along with more accessible DNA in promoter and or intergenic regions. Moreover, we newly identified the AP-1 family as a set of TFs associated with pDC activation.

Discussion

In this study we investigated the yet unknown global expression patterns of the TF reservoir of pDCs in in a time course after activation in combination with DNA accessibility analysis for implicated TF families. Combining RNA-Seq, ATAC-Seq, and GO analyses, we defined specific sets of TLR9-modulated TFs with known roles in pDC differentiation and function, but also TFs so far not implicated in pDC biology.

We used as the basis of our study the definition of the murine TF reservoir in the AnimalTFDB (Hu et al., 2019) and found that 70% of all genes annotated as TFs in the mouse genome (1,014 out of 1,636) were expressed in at least one condition, naïve or CpG-activated pDCs (2h, 6h, or 12h). These covered a wide range of TF classes defined by their respective DNA binding mechanisms. Interestingly, some TF families showed expression of all family members. Among those, we found factors that have been shown to be of particular importance in pDC biology, such as Runx2 of the Runt family (Sawai et al., 2013). Downstream GO analyses of RNA-Seq data allowed a biological classification of all TFs showing involvement in a wide variety of biological processes, such as the NFκB and JAK-STAT signaling. It has been well established that the production of type I IFN by pDCs upon TLR9 activation depends on the canonical TLR9-Myd88-NFκB/IRF7 signaling pathway (Tomasello et al., 2018). In this regard, it has been reported that NFκB and cREL are key players in pDC differentiation and survival programs after TLR9 activation by CpG. *Nfkb1*$^{-/-}$ *cRel*$^{-/-}$ double knock-out pDCs were still able to produce type I IFN upon CpG administration but failed to produce IL-6 or IL-12 and did not acquire a dendritic phenotype but rather underwent apoptosis (O'Keeffe et al., 2005). Here, we show for the first time the time-dependent patterns of gene expression for TFs involved in NFκB and JAK-STAT signaling upon pDC stimulation. Not only expression of these factors was enhanced in pDCs after CpG treatment, but also DNA binding sites for factors from the NFκB and JAK-STAT signaling pathways were identified as globally enriched in a differential motif analysis comparing regions with increased vs decreased chromatin accessibility. In addition, we found changed expression patterns of TFs important for circadian gene regulation in activated pDCs over time. In this regard, it has been reported that up to 10% of the transcriptome is under circadian regulation (Panda et al., 2002; Storch et al., 2002), suggesting that some pDC activation-dependent changes in gene expression may be under circadian control of global TF expression. Along this line, Silver et al. showed that TLR9 function is controlled by the circadian molecular clock in a number of cell types including DCs (Silver et al., 2012). Another group of TFs that show significant changes in expression after pDC activation could be classified as SMAD proteins, classical effectors of TGFβ signaling. It is known that stimulating DC progenitors with TGFβ accelerates DC differentiation, directing development toward cDCs (Felker et al., 2010). Also, one of the SMAD proteins, SMAD3, has been determined as a key player in determining cDC versus pDC cell fates (Jeong-Hwan Yoon, 2019). Interaction of SMAD proteins with known pDC driving factors such as Zeb2 have also been described (Vandewalle et al., 2009; Wu et al., 2016). Other SMAD members do not affect pDC numbers, as shown *in vivo* in *Smad7*-deficient mice (Lukas et al., 2017). Further, TFs involved in various processes of the endoplasmic reticulum are differentially expressed in TLR9 activated pDCs. Notably, mouse and human pDCs are morphologically characterized by an extensive rough ER, enabling them to rapidly secrete copious amounts of type I IFN after TLR7 and TLR9 stimulation (Alculumbre et al., 2018; Fitzgerald-Bocarsly et al., 2008). The enrichment of TFs involved

in mRNA binding processes, sumoylation and epigenetic modifications further highlights the changing biology of pDCs in protein production, posttranslational protein modifications, and alteration of the physical DNA structure that regulates gene expression after cell activation. We hereby define a novel set of expressed TFs in TLR9 activated pDCs, thus identifying TFs involved in particular biological processes that may require further investigation for their functional role in activated pDCs. The global transcriptomics approach allows a comparison for the expression patterns of several TFs belonging to the same TF family or involved in the same biological process, which may help to further narrow down interesting candidates.

Using CpG as an optimal TLR9 agonist and focusing on early events after virus infection, we found that after pDC activation more of the pDC chromatin landscape is „turned on“ rather than „turned off“, both globally in the genome and also among the regions associated with TF genes themselves. Specifically, about 80% of all regions that show significant chromatin changes exhibited increased accessibility for TFs. However, with regard to gene expression, 2h after pDC activation more genes were down-regulated than up-regulated as compared to the naïve state. One explanation could be that while DNA is more accessible, the TFs that possibly bind to these DNA stretches may inhibit rather than activate gene expression. An extensive motif analysis revealed that TFs belonging to the JAK-STAT and the NFκB signaling pathways exhibit increased accessibility to DNA binding regions after pDC stimulation. This underlines the importance of the JAK-STAT and NFκB signaling pathways in activated pDCs.

In contrast, Ets family members belonging to the Helix-turn-helix family of TFs and Zinc-coordinating zf-C2H2 TFs were both found to have less access to DNA after pDC activation. Ets family members include SPI1, also known as PU.1, which has been shown to drive the development of precursor cells toward cDC rather than pDC development (Chopin et al., 2019). Regarding pDC-driving cell fate TFs, IRF8 and RUNX2 belonging to the helix-turn-helix and β-scaffold TF groups, respectively, show motif enrichment in two sets of regions exhibiting increased versus decreased chromatin accessibility after pDC activation. Hence, cell fate TFs that drive pDC development both gain and lose access to distinct DNA regions after TLR9 activation.

Gene expression of the key pDC cell fate TFs IRF8, E2-2, and RUNX2 has been shown to steadily increase in expression during pDC precursor development into fully differentiated pDCs (Bornstein et al., 2014; Sasaki et al., 2012; Sawai et al., 2013; Tamura et al., 2005; Tsujimura et al., 2002). However, the role of these TFs for pDC survival and differentiation has not been investigated in detail after TLR9 activation. Here we observed different gene expression patterns for E2-2, and RUNX2 after pDC activation. E2-2 expression is strongly up-regulated at 2h and 6h of CpG stimulation vs no stimulation, but not at 12h after CpG activation vs steady state. Runx2, on the other hand, is strongly down-regulated at each CpG stimulation time point as compared to the naïve state.

Our results therefore warrant further investigations of pDC cell fate TFs to explore the biological relevance of distinct expression patterns as well as the simultaneous gain and loss of accessibility to DNA by modulation of chromatin after pDC activation. We found that IRF7, NFκB1, and RELA as well as ATF3 and JUN, two AP-1 family members, fulfil three criteria relevant in this context: They exhibit (i) increased gene expression, (ii) enhanced chromatin accessibility for their gene regions, and (iii) enriched TF DNA binding motifs in the accessible genomic regions after pDC stimulation. We used this

integrative omics approach to identify potential novel players important in pDC biology after cell activation. While the role for IRF7, NFκB1, and RELA have been described in activated pDCs, there is little known about any function of AP-1 factors in pDCs. Activator Protein-1 (AP-1) was one of the first TFs to be described in the 1980s (Angel et al., 1987). It consists of a dimeric protein complex with members from the JUN, FOS, ATF, BATF, or MAF protein families (Eferl and Wagner, 2003; Shaulian and Karin, 2002). A shared feature between the members is a basic leucine-zipper (bZIP) domain which is required for dimerization and DNA binding. The AP-1 family of TFs are known to regulate various biological processes such as proliferation, differentiation, and cell survival (Eferl and Wagner, 2003; Murphy et al., 2013; Sopel et al., 2016; Wagner and Eferl, 2005). They have further been implicated in a variety of pathologies ranging from cardiovascular disease to cancer, hepatitis, and Parkinson's disease (Meijer et al., 2012; Muslin, 2008; Uchihashi et al., 2011). A connection has been established between NFκB and AP-1 activity, which may be regulated by NFκB (Fujioka et al., 2004) suggesting a possible common molecular mechanism of these TFs in activated pDCs. Further, AP-1 has been shown to be required for spontaneous type I IFN production in pDCs, whereas type I IFN production triggered by pathogen receptor recognition such as TLR stimulation was not affected by AP-1 inhibition (Kim et al., 2014). In contrast, our *in silico* analyses suggest a close link between AP-1 factors and pDC biology after TLR9 stimulation: The AP-1 motif is present within the open chromatin region of the proximal promoter site of the *Tcf4* gene, a prominent pDC cell fate TF. Grajkowska *et al.* showed that there are two *Tcf4* isoforms, the expression of which is controlled during pDC differentiation by two respective promoters as well as distal enhancer regions within 600-900 kb 5' and ~150 kb 3' of the *Tcf4* gene (Grajkowska et al., 2017). However, the binding site of specific TFs to these cis-regulatory sites has not been fully evaluated. This calls for further investigations on the AP-1 binding site in activated pDCs newly identified in our study. One of the key AP-1 candidates in our investigation, ATF3, has been described as a negative regulator of antiviral signaling in Japanese encephalitis virus infection in mouse neuronal cells (Sood et al., 2017). The hallmark of pDCs is their importance in antiviral immune responses, pointing toward ATF3 as an interesting candidate to investigate in TLR9 activated pDCs. Another AP-1 family member, JUN, was the first oncogene to be described (Curran and Franza, 1988) and has since been studied in detail in the context of various tumor entities. In contrast, knowledge about its role in the context of infection is limited. For example, it has been shown to have a regulatory role in H5N1 influenza virus replication and host inflammation in mice (Xie et al., 2014). Our analyses revealed a distinct regulation of *Jun* expression and chromatin structure combined with an increased global DNA binding accessibility in pDCs after activation. Further studies are required to assess the role of *Jun* regulation in pDCs upon a microbial stimulus or in a chronically activated state that might unravel unknown functions of this TF in immunity. While targeting TFs for therapeutic purpose has been proven difficult so far, recent advances have been made through novel chemistries and the use of staples peptides to disrupt protein-protein interactions (Ball et al., 2016; Rezaei Araghi et al., 2018). Thus, the *in silico* analyses of the global TF reservoir in pDCs from our study led to the identification of novel candidates that warrant further investigation regarding their role in pDC biology, in particular after cell activation, which may lead to the development of novel therapeutics to treat infection, autoimmune disease and cancer.

Author Contributions

RM analysed the data. SA performed BM Flt3-L pDC cultures and FACS sorted pDCs for the RNA-Seq and ATAC-Seq assays. PP and KK conducted RNA-Seq including primary analyses. RM, JA, and SS wrote the manuscript.

Declaration of Interests

The authors declare no conflict of interest.

Materials and Methods

Mice

C57BL/6N mice were housed under specific pathogen-free conditions in the animal research facility of the University of Düsseldorf according to German animal welfare guidelines. All experiments were performed with sex and age matched littermates between 7 to 14 weeks of age.

Generation and stimulation of BM-derived pDCs for RNA-Seq and ATAC-Seq

BM-derived Flt3-L cultured pDCs were generated as previously described (Scheu et al., 2008). For RNA-Seq, BM-derived pDCs ($CD3^-CD19^-CD11c^+CD11b^{low}B220^+SiglecH^+$ $CD317^+$) were FACS purified using FACS Aria III (BD). The pDCs were left untreated or stimulated with 1µM CpG 2216 (Tib Molbiol, Nr. 930507l) complexed to transfection reagent DOTAP (Roche) for 2h, 6h or 12 h. RNA was isolated by using the NucleoSpin II RNA mini kit (Macherey-Nagel) and subjected to RNA-Seq. For ATAC-Seq BM-derived pDCs ($CD3^-CD19^-CD11c^+CD11b^{low}B220^+SiglecH^+CD317^+$) were FACS purified using FACS Aria III (BD). The pDCs were left untreated or stimulated with 1µM CpG 2216 complexed to transfection reagent DOTAP (Roche) for 2h. At the end of stimulation time, cells were kept on ice and stained for 7AAD (BD). Live cells ($7AAD^-$) were further purified by FACS and kept frozen in complete RPMI medium containing 5% DMSO. The frozen cells were transported on dry ice to Active Motif (Belgium) for ATAC-Seq.

The following antibodies have been used: CD3-PerCP (BD Bioscience, Clone: 145-2C11), CD19-PerCP-Cy5.5 (BD Bioscience, Clone:1D3), CD11c-PE-Cy7 (BioLegend, Clone: N418), CD11b-APC-Cy7 (BD Bioscience, Clone: M1/70), B220-FITC (BD Bioscience, Clone: RA3-6B2), SiglecH-APC (BioLegend, Clone 551), CD317-PE (eBioscience/Thermoscientific, Clone: ebio927).

RNA-Seq Analyses

DNase digested total RNA samples used for transcriptome analyses were quantified (Qubit RNA HS Assay, Thermo Fisher Scientific) and quality measured by capillary electrophoresis using the Fragment Analyzer and the 'Total RNA Standard Sensitivity Assay' (Agilent Technologies, Inc. Santa Clara, USA). All samples in this study showed high RNA Quality Numbers (RQN; mean = 9.9). The library preparation was performed according to the manufacturer's protocol using the Illumina® 'TruSeq Stranded mRNA Library Prep Kit'. Briefly, 200 ng total RNA were used for mRNA capturing, fragmentation, the synthesis

of cDNA, adapter ligation and library amplification. Bead purified libraries were normalized and sequenced on the HiSeq 3000/4000 system (Illumina Inc. San Diego, USA) with a read setup of SR 1x150 bp. The bcl2fastq tool was used to convert the bcl files to fastq files as well for adapter trimming and demultiplexing.

Data analyses on fastq files were conducted with CLC Genomics Workbench (version 11.0.1, QIAGEN, Venlo. NL). The reads of all probes were adapter trimmed (Illumina TruSeq) and quality trimmed (using the default parameters: bases below Q13 were trimmed from the end of the reads, ambiguous nucleotides maximal 2). Mapping was done against the *Mus musculus* (mm10; GRCm38.86) (March 24, 2017) genome sequence. Samples (three biological replicates each) were grouped according to their respective experimental condition. Raw counts were next re-uploaded to the Galaxy web platform. The public server at usegalaxy.org was used to perform multi-group comparisons (Afgan et al., 2016). Differential expression of genes between any two conditions was calculated using the edgeR quasi-likelihood pipeline which uses negative binomial generalized linear models with F-test (Liu et al., 2015; Robinson et al., 2010). Low expressing genes were filtered with a count-per-million (CPM) value cut-off that was calculated based on the average library size of our RNA-Seq experiment (Chen et al., 2016). The resulting p values were corrected for multiple testing by the false discovery rate (FDR) (Benjamini, 1995). A p value of <0.05 was considered significant. RNA-Seq data are deposited with NCBI's Gene Expression Omnibus (GEO) and are accessible through GEO Series accession number GSE170750 (https://www.ncbi.nlm.nih.gov/geo/query/acc.cgi?acc=GSE170750).

ATAC-Seq

Cells were harvested and frozen in culture media containing FBS and 5% DMSO. Cryopreserved cells were sent to Active Motif to perform the ATAC-Seq assay. The cells were then thawed in a 37°C water bath, pelleted, washed with cold PBS, and tagmented as previously described (Buenrostro et al., 2013), with some modifications (Corces et al., 2017). Briefly, cell pellets were resuspended in lysis buffer, pelleted, and tagmented using the enzyme and buffer provided in the Nextera Library Prep Kit (Illumina). Tagmented DNA was then purified using the MinElute PCR purification kit (Qiagen), amplified with 10 cycles of PCR, and purified using Agencourt AMPure SPRI beads (Beckman Coulter). Resulting material was quantified using the KAPA Library Quantification Kit for Illumina platforms (KAPA Biosystems), and sequenced with PE42 sequencing on the NextSeq 500 sequencer (Illumina).

Reads were aligned using the BWA algorithm (mem mode; default settings). Duplicate reads were removed, only reads mapping as matched pairs and only uniquely mapped reads (mapping quality ≥1) were used for further analysis. Alignments were extended *in silico* at their 3'-ends to a length of 200 bp and assigned to 32-nt bins along the genome. The resulting histograms (genomic "signal maps") were stored in bigWig files. Peaks were identified using the MACS 2.1.0 algorithm at a cut off of p-value 1e-7, without control file, and with the –nomodel option. Peaks that were on the ENCODE blacklist of known false ATAC-Seq peaks were removed. Signal maps and peak locations were used as input data to Active Motifs proprietary analysis program, which creates Excel tables containing detailed information on sample comparison, peak metrics, peak locations, and gene annotations. For differential analysis, reads were counted in all merged peak regions (using Subread), and the replicates for each condition

were compared using DESeq2. ATAC-Seq data are deposited with NCBI's GEO and are accessible through GEO Series accession number GSE171075 (https://www.ncbi.nlm.nih.gov/geo/query/acc.cgi?acc=GSE171075).

Downstream analyses and visualization of omics data

Volcano plots were created using ggplot2 (Wickham, 2016) and ggrepel (Slowikowski, 2020). Heatmaps were created using Morpheus (https://software.broadinstitute.org/morpheus). Pearson correlation matrices were calculated in R and plotted as heatmaps using gplots (Gregory R. Warnes, 2020). Pathway analyses for different gene ontology (GO) terms and subsequent functional classification and annotation clustering were performed using the Database for Annotation, Visualization and Integrated Discovery (DAVID) (Huang da et al., 2009). Evolutionary conserved regions (ECR) for selected genes were shown by taking a screenshot from the ECR browser (Ovcharenko et al., 2004). Bar graphs were plotted in Gradphpad Prism version 8.4.3 on Windows (GraphPad Software, La Jolla California USA, www.graphpad.com). ATAC-Seq peaks were visualized using IGV (Robinson et al., 2011; Thorvaldsdottir et al., 2013).

TF Motif Analyses

ATAC-Seq regions that indicated differentially accessible chromatin regions between naive and 2h CpG stimulated samples (DESeq2, $|FC|>2$, $p<0.05$) were used for motif analysis. The regions were adjusted to the same size (500bp). The MEME-Centrimo differential motif analysis pipeline (Bailey and Machanick, 2012) was run on the fasta files representing each chromatin region (significantly increased vs decreased chromatin access after CpG stimulation) to identify overrepresented motifs, using default parameters and the HOCOMOCO v11 motif database. The search for the AP-1 motif among selected sequences was performed with MEME-FIMO.

Figure legends

Fig. 1 Expression of transcription factors in pDCs. A Expression of TFs in pDCs in at least one of the following conditions: naïve, CpG 2h, 6h or 12h (n=3 per condition). **B** Categorization of the expressed TFs according to Hu *et al.* (Hu et al., 2019). **C** Number of expressed vs non-expressed genes per TF family of a TF class is plotted.

Fig. 2 RNA-Seq reveals significant TF expression changes after pDC activation. A Pearson correlation plot for samples used in RNA-Seq. pDCs ($CD3^-CD19^-CD11c^+CD11b^{low}B220^+SiglecH^+CD317^+$) were sorted from BM-derived Flt3-L cultures of C57BL/6N mice and cells were left either naïve or stimulated with CpG for 2h, 6h or 12h. **B** Volcano plots showing global expression of genes in sorted pDCs at steady state and after 2h, 6h, and 12h of CpG stimulation. TF genes with a $|FC|>2$ and a p-value of <0.05 corrected for the false discovery rate (FDR) were considered significantly differentially expressed and are marked in colour (red and blue). **C** Heatmap

showing normalized expression values (cpm, count per million) of differentially expressed TF genes from (**B**) in pDCs at steady state and after 2h, 6h, and 12h of CpG stimulation. Hierarchical clustering on rows with average linkage and the One minus Pearson correlation metric was performed.

Fig. 3 Gene Ontology analysis of CpG-dependent TFs. 661 CpG-dependent TFs (|FC|>2, p<0.05) were analysed by DAVID functional annotation to produce gene clusters (>2 genes/cluster) corresponding to biological process (BP), molecular function (MF), and cellular component (CC) GO annotation terms. Those significantly associated with the TF gene list are plotted with the numbers of genes for each term along with the fold enrichment for each term. A few terms were excluded as being redundant or having wider meaning (**Table S1**). Abbreviations are as follows: casc = cascade; cyt = cytokine; horm = hormone; med = mediated; reg = regulation; rERs = response to endoplasmic reticulum stress; resp = response; sig = signaling.

Fig. 4 pDC activation increases and decreases chromatin accessibility of thousands of regions. **A** Pearson correlation plot for samples used in ATAC-Seq. pDCs ($CD3^-CD19^-CD11c^+CD11b^{low}B220^+SiglecH^+CD317^+$) were sorted from BM-derived Flt3-L cultures of C57BL/6N mice and cells were left either naïve or stimulated with CpG for 2h (n=2). **B** Genomic location distribution of open chromatin sites in naïve and CpG stimulated pDCs according to ATAC-Seq. Two biological replicates were used per condition, and results are shown for pooled samples per condition. **C** Number of differentially accessible peaks detected using DESeq2, comparing naïve to 2h CpG stimulated pDCs, |FC|>2 and p<0.05. **D** Heatmap of normalized ATAC-Seq peak intensities (log_2FC relative to the mean for each peak). Limited to peaks (16,607) that are condition-dependent with |FC|>2 and p<0.05 for at least one pairwise comparison of interest. **E** Differential motif analysis for cluster I and II from (**D**) using MEME Centrimo and the HOCOMOCO v11 motif database. Significant motifs were categorized into known TF families for visualization and interpretation.

Fig. 5 TFs show CpG-dependent expression and chromatin accessibility. **A** Number of differentially accessible peaks of genomic regions associated with TF genes detected using DESeq2 comparing naïve to 2h CpG stimulated pDCs, |FC|>2 and p<0.05. **B** Heatmap of normalized ATAC-Seq peak intensities (log_2FC relative to the mean for each peak) limited to 540 peaks from (**A**) that are condition-dependent with |FC|>2 and p<0.05 for at least one pairwise comparison of interest. **C** The bar graph depicts normalized expression values obtained from RNA-Seq and statistics calculated with edgeR. **D, E** Top panel presents screen shots from the ECR (evolutionary conserved regions) Browser web site of the respective indicated gene. Exonic regions are shown in blue, intronic regions in pink, UTRs in yellow, and CNS in red. Bottom panels present ATAC-Seq peaks in naïve and CpG stimulated (2h) pDCs for the indicated genes visualized with IGV. The AP-1 motif within the promoter sequence of the *Tcf4* gene is highlighted in (**E**).

Acknowledgements

This work was funded by the German Research Foundation (DFG – SCHE692/6-1) and the Manchot Graduate Schools 'Molecules of Infection III' to SS and the DFG EXC 1003, Grant FF-2014-01 Cells in Motion–Cluster of Excellence, Münster, Germany, and the DFG FOR2107 AL1145/5-2 to JA. Computational support of the Zentrum für Informations- und Medientechnologie, especially the HPC team (High Performance Computing) at the University of Düsseldorf is acknowledged. We thank Johannes Ptok and Heiner Schaal (Institute of Virology, University of Düsseldorf) for critical reading of the manuscript.

References

Afgan, E., Baker, D., van den Beek, M., Blankenberg, D., Bouvier, D., Cech, M., Chilton, J., Clements, D., Coraor, N., Eberhard, C.*, et al.* (2016). The Galaxy platform for accessible, reproducible and collaborative biomedical analyses: 2016 update. Nucleic Acids Res *44*, W3-W10.

Alculumbre, S.G., Saint-Andre, V., Di Domizio, J., Vargas, P., Sirven, P., Bost, P., Maurin, M., Maiuri, P., Wery, M., Roman, M.S.*, et al.* (2018). Diversification of human plasmacytoid predendritic cells in response to a single stimulus. Nat Immunol *19*, 63-75.

Ali, S., Mann-Nuttel, R., Schulze, A., Richter, L., Alferink, J., and Scheu, S. (2019). Sources of Type I Interferons in Infectious Immunity: Plasmacytoid Dendritic Cells Not Always in the Driver's Seat. Front Immunol *10*, 778.

Angel, P., Imagawa, M., Chiu, R., Stein, B., Imbra, R.J., Rahmsdorf, H.J., Jonat, C., Herrlich, P., and Karin, M. (1987). Phorbol ester-inducible genes contain a common cis element recognized by a TPA-modulated trans-acting factor. Cell *49*, 729-739.

Aravind, L., Anantharaman, V., Balaji, S., Babu, M.M., and Iyer, L.M. (2005). The many faces of the helix-turn-helix domain: transcription regulation and beyond. FEMS Microbiol Rev *29*, 231-262.

Asselin-Paturel, C., Boonstra, A., Dalod, M., Durand, I., Yessaad, N., Dezutter-Dambuyant, C., Vicari, A., O'Garra, A., Biron, C., Briere, F., and Trinchieri, G. (2001). Mouse type I IFN-producing cells are immature APCs with plasmacytoid morphology. Nat Immunol *2*, 1144-1150.

Bailey, T.L., and Machanick, P. (2012). Inferring direct DNA binding from ChIP-seq. Nucleic Acids Res *40*, e128.

Ball, D.P., Lewis, A.M., Williams, D., Resetca, D., Wilson, D.J., and Gunning, P.T. (2016). Signal transducer and activator of transcription 3 (STAT3) inhibitor, S3I-201, acts as a potent and non-selective alkylating agent. Oncotarget *7*, 20669-20679.

Bauer, J., Dress, R.J., Schulze, A., Dresing, P., Ali, S., Deenen, R., Alferink, J., and Scheu, S. (2016). Cutting Edge: IFN-beta Expression in the Spleen Is Restricted to a Subpopulation of Plasmacytoid Dendritic Cells Exhibiting a Specific Immune Modulatory Transcriptome Signature. J Immunol *196*, 4447-4451.

Benjamini, Y.H., Yosef (1995). Controlling the false discovery rate: a practical and powerful approach to multiple testing. Journal of the Royal Statistical Society, Series B *57 (1): 289–300*.

Bornstein, C., Winter, D., Barnett-Itzhaki, Z., David, E., Kadri, S., Garber, M., and Amit, I. (2014). A negative feedback loop of transcription factors specifies alternative dendritic cell chromatin States. Mol Cell *56*, 749-762.

639 Buenrostro, J.D., Giresi, P.G., Zaba, L.C., Chang, H.Y., and Greenleaf, W.J. (2013). Transposition of
640 native chromatin for fast and sensitive epigenomic profiling of open chromatin, DNA-binding proteins
641 and nucleosome position. Nat Methods *10*, 1213-1218.
642 Chauvistre, H., and Sere, K. (2020). Epigenetic aspects of DC development and differentiation. Mol
643 Immunol *128*, 116-124.
644 Chen, Y., Lun, A.T., and Smyth, G.K. (2016). From reads to genes to pathways: differential
645 expression analysis of RNA-Seq experiments using Rsubread and the edgeR quasi-likelihood
646 pipeline. F1000Res *5*, 1438.
647 Chopin, M., Lun, A.T., Zhan, Y., Schreuder, J., Coughlan, H., D'Amico, A., Mielke, L.A., Almeida, F.F.,
648 Kueh, A.J., Dickins, R.A.*, et al.* (2019). Transcription Factor PU.1 Promotes Conventional Dendritic
649 Cell Identity and Function via Induction of Transcriptional Regulator DC-SCRIPT. Immunity *50*, 77-90
650 e75.
651 Chopin, M., Preston, S.P., Lun, A.T.L., Tellier, J., Smyth, G.K., Pellegrini, M., Belz, G.T., Corcoran,
652 L.M., Visvader, J.E., Wu, L., and Nutt, S.L. (2016). RUNX2 Mediates Plasmacytoid Dendritic Cell
653 Egress from the Bone Marrow and Controls Viral Immunity. Cell Rep *15*, 866-878.
654 Christensen, S.R., Shupe, J., Nickerson, K., Kashgarian, M., Flavell, R.A., and Shlomchik, M.J.
655 (2006). Toll-like receptor 7 and TLR9 dictate autoantibody specificity and have opposing inflammatory
656 and regulatory roles in a murine model of lupus. Immunity *25*, 417-428.
657 Cisse, B., Caton, M.L., Lehner, M., Maeda, T., Scheu, S., Locksley, R., Holmberg, D., Zweier, C., den
658 Hollander, N.S., Kant, S.G.*, et al.* (2008). Transcription factor E2-2 is an essential and specific
659 regulator of plasmacytoid dendritic cell development. Cell *135*, 37-48.
660 Corces, M.R., Trevino, A.E., Hamilton, E.G., Greenside, P.G., Sinnott-Armstrong, N.A., Vesuna, S.,
661 Satpathy, A.T., Rubin, A.J., Montine, K.S., Wu, B.*, et al.* (2017). An improved ATAC-seq protocol
662 reduces background and enables interrogation of frozen tissues. Nat Methods *14*, 959-962.
663 Curran, T., and Franza, B.R., Jr. (1988). Fos and Jun: the AP-1 connection. Cell *55*, 395-397.
664 Deaton, A.M., and Bird, A. (2011). CpG islands and the regulation of transcription. Genes Dev *25*,
665 1010-1022.
666 Decque, A., Joffre, O., Magalhaes, J.G., Cossec, J.C., Blecher-Gonen, R., Lapaquette, P., Silvin, A.,
667 Manel, N., Joubert, P.E., Seeler, J.S.*, et al.* (2016). Sumoylation coordinates the repression of
668 inflammatory and anti-viral gene-expression programs during innate sensing. Nat Immunol *17*, 140-
669 149.
670 Diebold, S.S., Kaisho, T., Hemmi, H., Akira, S., and Reis e Sousa, C. (2004). Innate antiviral
671 responses by means of TLR7-mediated recognition of single-stranded RNA. Science *303*, 1529-1531.
672 Drouin, J. (2014). Minireview: pioneer transcription factors in cell fate specification. Mol Endocrinol *28*,
673 989-998.
674 Eferl, R., and Wagner, E.F. (2003). AP-1: a double-edged sword in tumorigenesis. Nat Rev Cancer *3*,
675 859-868.
676 Elkon, K.B., and Wiedeman, A. (2012). Type I IFN system in the development and manifestations of
677 SLE. Curr Opin Rheumatol *24*, 499-505.

678 Felker, P., Sere, K., Lin, Q., Becker, C., Hristov, M., Hieronymus, T., and Zenke, M. (2010). TGF-
679 beta1 accelerates dendritic cell differentiation from common dendritic cell progenitors and directs
680 subset specification toward conventional dendritic cells. J Immunol *185*, 5326-5335.
681 Fitzgerald-Bocarsly, P., Dai, J., and Singh, S. (2008). Plasmacytoid dendritic cells and type I IFN: 50
682 years of convergent history. Cytokine Growth Factor Rev *19*, 3-19.
683 Fujioka, S., Niu, J., Schmidt, C., Sclabas, G.M., Peng, B., Uwagawa, T., Li, Z., Evans, D.B.,
684 Abbruzzese, J.L., and Chiao, P.J. (2004). NF-kappaB and AP-1 connection: mechanism of NF-
685 kappaB-dependent regulation of AP-1 activity. Mol Cell Biol *24*, 7806-7819.
686 Fulton, D.L., Sundararajan, S., Badis, G., Hughes, T.R., Wasserman, W.W., Roach, J.C., and Sladek,
687 R. (2009). TFCat: the curated catalog of mouse and human transcription factors. Genome Biol *10*,
688 R29.
689 Gilliet, M., Cao, W., and Liu, Y.J. (2008). Plasmacytoid dendritic cells: sensing nucleic acids in viral
690 infection and autoimmune diseases. Nat Rev Immunol *8*, 594-606.
691 Grajkowska, L.T., Ceribelli, M., Lau, C.M., Warren, M.E., Tiniakou, I., Nakandakari Higa, S., Bunin, A.,
692 Haecker, H., Mirny, L.A., Staudt, L.M., and Reizis, B. (2017). Isoform-Specific Expression and
693 Feedback Regulation of E Protein TCF4 Control Dendritic Cell Lineage Specification. Immunity *46*,
694 65-77.
695 Gregory R. Warnes, B.B., Lodewijk Bonebakker, Robert Gentleman, Wolfgang Huber, Andy Liaw,
696 Thomas Lumley, Martin Maechler, Arni Magnusson, Steffen Moeller, Marc Schwartz and Bill Venables
697 (2020). gplots: Various R Programming Tools for Plotting Data. ScienceOpen.
698 Hayashi, T., Beck, L., Rossetto, C., Gong, X., Takikawa, O., Takabayashi, K., Broide, D.H., Carson,
699 D.A., and Raz, E. (2004). Inhibition of experimental asthma by indoleamine 2,3-dioxygenase. J Clin
700 Invest *114*, 270-279.
701 Hornung, V., Rothenfusser, S., Britsch, S., Krug, A., Jahrsdorfer, B., Giese, T., Endres, S., and
702 Hartmann, G. (2002). Quantitative expression of toll-like receptor 1-10 mRNA in cellular subsets of
703 human peripheral blood mononuclear cells and sensitivity to CpG oligodeoxynucleotides. J Immunol
704 *168*, 4531-4537.
705 Hu, H., Miao, Y.R., Jia, L.H., Yu, Q.Y., Zhang, Q., and Guo, A.Y. (2019). AnimalTFDB 3.0: a
706 comprehensive resource for annotation and prediction of animal transcription factors. Nucleic Acids
707 Res *47*, D33-D38.
708 Huang da, W., Sherman, B.T., and Lempicki, R.A. (2009). Systematic and integrative analysis of large
709 gene lists using DAVID bioinformatics resources. Nat Protoc *4*, 44-57.
710 Ishii, K.J., and Akira, S. (2006). Innate immune recognition of, and regulation by, DNA. Trends
711 Immunol *27*, 525-532.
712 Jeong-Hwan Yoon, E.B., Katsuko Sudo, Jin Soo Han, Seok Hee Park, Susumu Nakae, Tadashi
713 Yamashita, In-Kyu Lee, Ji Hyeon Ju, Isao Matsumoto, Takayuki Sumida, Masahiko Kuroda, Keiji
714 Miyazawa, Mitsuyasu Kato, Mizuko Mamura (2019). SMAD3 Determines Conventional versus
715 Plasmacytoid Dendritic Cell Fates. bioRxiv.

716 Kanamori, M., Konno, H., Osato, N., Kawai, J., Hayashizaki, Y., and Suzuki, H. (2004). A genome-
717 wide and nonredundant mouse transcription factor database. Biochem Biophys Res Commun *322*,
718 787-793.
719 Kim, S., Kaiser, V., Beier, E., Bechheim, M., Guenthner-Biller, M., Ablasser, A., Berger, M., Endres,
720 S., Hartmann, G., and Hornung, V. (2014). Self-priming determines high type I IFN production by
721 plasmacytoid dendritic cells. Eur J Immunol *44*, 807-818.
722 Kulakovskiy, I.V., Vorontsov, I.E., Yevshin, I.S., Sharipov, R.N., Fedorova, A.D., Rumynskiy, E.I.,
723 Medvedeva, Y.A., Magana-Mora, A., Bajic, V.B., Papatsenko, D.A.*, et al.* (2018). HOCOMOCO:
724 towards a complete collection of transcription factor binding models for human and mouse via large-
725 scale ChIP-Seq analysis. Nucleic Acids Res *46*, D252-D259.
726 Le Mercier, I., Poujol, D., Sanlaville, A., Sisirak, V., Gobert, M., Durand, I., Dubois, B., Treilleux, I.,
727 Marvel, J., Vlach, J.*, et al.* (2013). Tumor promotion by intratumoral plasmacytoid dendritic cells is
728 reversed by TLR7 ligand treatment. Cancer Res *73*, 4629-4640.
729 Lee, J.U., Kim, L.K., and Choi, J.M. (2018). Revisiting the Concept of Targeting NFAT to Control T
730 Cell Immunity and Autoimmune Diseases. Front Immunol *9*, 2747.
731 Li, S., Wu, J., Zhu, S., Liu, Y.J., and Chen, J. (2017). Disease-Associated Plasmacytoid Dendritic
732 Cells. Front Immunol *8*, 1268.
733 Libermann, T.A., and Zerbini, L.F. (2006). Targeting transcription factors for cancer gene therapy.
734 Curr Gene Ther *6*, 17-33.
735 Lin, Q., Chauvistre, H., Costa, I.G., Gusmao, E.G., Mitzka, S., Hanzelmann, S., Baying, B., Klisch, T.,
736 Moriggl, R., Hennuy, B.*, et al.* (2015). Epigenetic program and transcription factor circuitry of dendritic
737 cell development. Nucleic Acids Res *43*, 9680-9693.
738 Liu, R., Holik, A.Z., Su, S., Jansz, N., Chen, K., Leong, H.S., Blewitt, M.E., Asselin-Labat, M.L.,
739 Smyth, G.K., and Ritchie, M.E. (2015). Why weight? Modelling sample and observational level
740 variability improves power in RNA-seq analyses. Nucleic Acids Res *43*, e97.
741 Liu, Y.J. (2005). IPC: professional type 1 interferon-producing cells and plasmacytoid dendritic cell
742 precursors. Annu Rev Immunol *23*, 275-306.
743 Lou, Y., Liu, C., Lizee, G., Peng, W., Xu, C., Ye, Y., Rabinovich, B.A., Hailemichael, Y., Gelbard, A.,
744 Zhou, D.*, et al.* (2011). Antitumor activity mediated by CpG: the route of administration is critical. J
745 Immunother *34*, 279-288.
746 Lukas, D., Yogev, N., Kel, J.M., Regen, T., Mufazalov, I.A., Tang, Y., Wanke, F., Reizis, B., Muller,
747 W., Kurschus, F.C.*, et al.* (2017). TGF-beta inhibitor Smad7 regulates dendritic cell-induced
748 autoimmunity. Proc Natl Acad Sci U S A *114*, E1480-E1489.
749 Meijer, C.A., Le Haen, P.A., van Dijk, R.A., Hira, M., Hamming, J.F., van Bockel, J.H., and Lindeman,
750 J.H. (2012). Activator protein-1 (AP-1) signalling in human atherosclerosis: results of a systematic
751 evaluation and intervention study. Clin Sci (Lond) *122*, 421-428.
752 Murphy, T.L., Tussiwand, R., and Murphy, K.M. (2013). Specificity through cooperation: BATF-IRF
753 interactions control immune-regulatory networks. Nat Rev Immunol *13*, 499-509.
754 Muslin, A.J. (2008). MAPK signalling in cardiovascular health and disease: molecular mechanisms
755 and therapeutic targets. Clin Sci (Lond) *115*, 203-218.

O'Keeffe, M., Grumont, R.J., Hochrein, H., Fuchsberger, M., Gugasyan, R., Vremec, D., Shortman, K., and Gerondakis, S. (2005). Distinct roles for the NF-kappaB1 and c-Rel transcription factors in the differentiation and survival of plasmacytoid and conventional dendritic cells activated by TLR-9 signals. Blood *106*, 3457-3464.

Ovcharenko, I., Nobrega, M.A., Loots, G.G., and Stubbs, L. (2004). ECR Browser: a tool for visualizing and accessing data from comparisons of multiple vertebrate genomes. Nucleic Acids Res *32*, W280-286.

Panda, S., Antoch, M.P., Miller, B.H., Su, A.I., Schook, A.B., Straume, M., Schultz, P.G., Kay, S.A., Takahashi, J.S., and Hogenesch, J.B. (2002). Coordinated transcription of key pathways in the mouse by the circadian clock. Cell *109*, 307-320.

Patel, L., Abate, C., and Curran, T. (1990). Altered protein conformation on DNA binding by Fos and Jun. Nature *347*, 572-575.

Reizis, B. (2019). Plasmacytoid Dendritic Cells: Development, Regulation, and Function. Immunity *50*, 37-50.

Rezaei Araghi, R., Bird, G.H., Ryan, J.A., Jenson, J.M., Godes, M., Pritz, J.R., Grant, R.A., Letai, A., Walensky, L.D., and Keating, A.E. (2018). Iterative optimization yields Mcl-1-targeting stapled peptides with selective cytotoxicity to Mcl-1-dependent cancer cells. Proc Natl Acad Sci U S A *115*, E886-E895.

Risse, G., Jooss, K., Neuberg, M., Bruller, H.J., and Muller, R. (1989). Asymmetrical recognition of the palindromic AP1 binding site (TRE) by Fos protein complexes. EMBO J *8*, 3825-3832.

Robinson, J.T., Thorvaldsdottir, H., Winckler, W., Guttman, M., Lander, E.S., Getz, G., and Mesirov, J.P. (2011). Integrative genomics viewer. Nat Biotechnol *29*, 24-26.

Robinson, M.D., McCarthy, D.J., and Smyth, G.K. (2010). edgeR: a Bioconductor package for differential expression analysis of digital gene expression data. Bioinformatics *26*, 139-140.

Saas, P., and Perruche, S. (2012). Functions of TGF-beta-exposed plasmacytoid dendritic cells. Crit Rev Immunol *32*, 529-553.

Salio, M., Palmowski, M.J., Atzberger, A., Hermans, I.F., and Cerundolo, V. (2004). CpG-matured murine plasmacytoid dendritic cells are capable of in vivo priming of functional CD8 T cell responses to endogenous but not exogenous antigens. J Exp Med *199*, 567-579.

Sasaki, I., Hoshino, K., Sugiyama, T., Yamazaki, C., Yano, T., Iizuka, A., Hemmi, H., Tanaka, T., Saito, M., Sugiyama, M.*, et al.* (2012). Spi-B is critical for plasmacytoid dendritic cell function and development. Blood *120*, 4733-4743.

Sawai, C.M., Sisirak, V., Ghosh, H.S., Hou, E.Z., Ceribelli, M., Staudt, L.M., and Reizis, B. (2013). Transcription factor Runx2 controls the development and migration of plasmacytoid dendritic cells. J Exp Med *210*, 2151-2159.

Scheu, S., Dresing, P., and Locksley, R.M. (2008). Visualization of IFNbeta production by plasmacytoid versus conventional dendritic cells under specific stimulation conditions in vivo. Proc Natl Acad Sci U S A *105*, 20416-20421.

Serebreni, L., and Stark, A. (2020). Insights into gene regulation: From regulatory genomic elements to DNA-protein and protein-protein interactions. Curr Opin Cell Biol *70*, 58-66.

796 Shaulian, E., and Karin, M. (2002). AP-1 as a regulator of cell life and death. Nat Cell Biol *4*, E131-
797 136.
798 Silver, A.C., Arjona, A., Walker, W.E., and Fikrig, E. (2012). The circadian clock controls toll-like
799 receptor 9-mediated innate and adaptive immunity. Immunity *36*, 251-261.
800 Slowikowski, K. (2020). ggrepel: Automatically Position Non-Overlapping Text Labels with 'ggplot2'.
801 Sood, V., Sharma, K.B., Gupta, V., Saha, D., Dhapola, P., Sharma, M., Sen, U., Kitajima, S.,
802 Chowdhury, S., Kalia, M., and Vrati, S. (2017). ATF3 negatively regulates cellular antiviral signaling
803 and autophagy in the absence of type I interferons. Sci Rep *7*, 8789.
804 Sopel, N., Graser, A., Mousset, S., and Finotto, S. (2016). The transcription factor BATF modulates
805 cytokine-mediated responses in T cells. Cytokine Growth Factor Rev *30*, 39-45.
806 Storch, K.F., Lipan, O., Leykin, I., Viswanathan, N., Davis, F.C., Wong, W.H., and Weitz, C.J. (2002).
807 Extensive and divergent circadian gene expression in liver and heart. Nature *417*, 78-83.
808 Swiecki, M., and Colonna, M. (2015). The multifaceted biology of plasmacytoid dendritic cells. Nat
809 Rev Immunol *15*, 471-485.
810 Takayanagi, H., Kim, S., Matsuo, K., Suzuki, H., Suzuki, T., Sato, K., Yokochi, T., Oda, H., Nakamura,
811 K., Ida, N.*, et al.* (2002). RANKL maintains bone homeostasis through c-Fos-dependent induction of
812 interferon-beta. Nature *416*, 744-749.
813 Tamura, T., Tailor, P., Yamaoka, K., Kong, H.J., Tsujimura, H., O'Shea, J.J., Singh, H., and Ozato, K.
814 (2005). IFN regulatory factor-4 and -8 govern dendritic cell subset development and their functional
815 diversity. J Immunol *174*, 2573-2581.
816 Thorvaldsdottir, H., Robinson, J.T., and Mesirov, J.P. (2013). Integrative Genomics Viewer (IGV):
817 high-performance genomics data visualization and exploration. Brief Bioinform *14*, 178-192.
818 Tomasello, E., Naciri, K., Chelbi, R., Bessou, G., Fries, A., Gressier, E., Abbas, A., Pollet, E., Pierre,
819 P., Lawrence, T.*, et al.* (2018). Molecular dissection of plasmacytoid dendritic cell activation in vivo
820 during a viral infection. EMBO J *37*.
821 Trinchieri, G., and Santoli, D. (1978). Anti-viral activity induced by culturing lymphocytes with tumor-
822 derived or virus-transformed cells. Enhancement of human natural killer cell activity by interferon and
823 antagonistic inhibition of susceptibility of target cells to lysis. J Exp Med *147*, 1314-1333.
824 Tsujimura, H., Nagamura-Inoue, T., Tamura, T., and Ozato, K. (2002). IFN consensus sequence
825 binding protein/IFN regulatory factor-8 guides bone marrow progenitor cells toward the macrophage
826 lineage. J Immunol *169*, 1261-1269.
827 Uchihashi, S., Fukumoto, H., Onoda, M., Hayakawa, H., Ikushiro, S., and Sakaki, T. (2011).
828 Metabolism of the c-Fos/activator protein-1 inhibitor T-5224 by multiple human UDP-
829 glucuronosyltransferase isoforms. Drug Metab Dispos *39*, 803-813.
830 Vandewalle, C., Van Roy, F., and Berx, G. (2009). The role of the ZEB family of transcription factors
831 in development and disease. Cell Mol Life Sci *66*, 773-787.
832 Vaquerizas, J.M., Kummerfeld, S.K., Teichmann, S.A., and Luscombe, N.M. (2009). A census of
833 human transcription factors: function, expression and evolution. Nat Rev Genet *10*, 252-263.
834 Wagner, E.F., and Eferl, R. (2005). Fos/AP-1 proteins in bone and the immune system. Immunol Rev
835 *208*, 126-140.

836 Weiss, M.A., Ellenberger, T., Wobbe, C.R., Lee, J.P., Harrison, S.C., and Struhl, K. (1990). Folding
837 transition in the DNA-binding domain of GCN4 on specific binding to DNA. Nature *347*, 575-578.
838 Wickham, H. (2016). ggplot2: Elegant Graphics for Data Analysis. Springer-Verlag New York.
839 Wingender, E., Schoeps, T., Haubrock, M., Krull, M., and Donitz, J. (2018). TFClass: expanding the
840 classification of human transcription factors to their mammalian orthologs. Nucleic Acids Res *46*,
841 D343-D347.
842 Wu, J., Li, S., Li, T., Lv, X., Zhang, M., Zang, G., Qi, C., Liu, Y.J., Xu, L., and Chen, J. (2019). pDC
843 Activation by TLR7/8 Ligand CL097 Compared to TLR7 Ligand IMQ or TLR9 Ligand CpG. J Immunol
844 Res *2019*, 1749803.
845 Wu, X., Briseno, C.G., Grajales-Reyes, G.E., Haldar, M., Iwata, A., Kretzer, N.M., Kc, W., Tussiwand,
846 R., Higashi, Y., Murphy, T.L., and Murphy, K.M. (2016). Transcription factor Zeb2 regulates
847 commitment to plasmacytoid dendritic cell and monocyte fate. Proc Natl Acad Sci U S A *113*, 14775-
848 14780.
849 Xie, J., Zhang, S., Hu, Y., Li, D., Cui, J., Xue, J., Zhang, G., Khachigian, L.M., Wong, J., Sun, L., and
850 Wang, M. (2014). Regulatory roles of c-jun in H5N1 influenza virus replication and host inflammation.
851 Biochim Biophys Acta *1842*, 2479-2488.
852 Zhang, H.M., Chen, H., Liu, W., Liu, H., Gong, J., Wang, H., and Guo, A.Y. (2012). AnimalTFDB: a
853 comprehensive animal transcription factor database. Nucleic Acids Res *40*, D144-149.
854 Zhou, Q., Liu, M., Xia, X., Gong, T., Feng, J., Liu, W., Liu, Y., Zhen, B., Wang, Y., Ding, C., and Qin,
855 J. (2017). A mouse tissue transcription factor atlas. Nat Commun *8*, 15089.
856

Figure 1

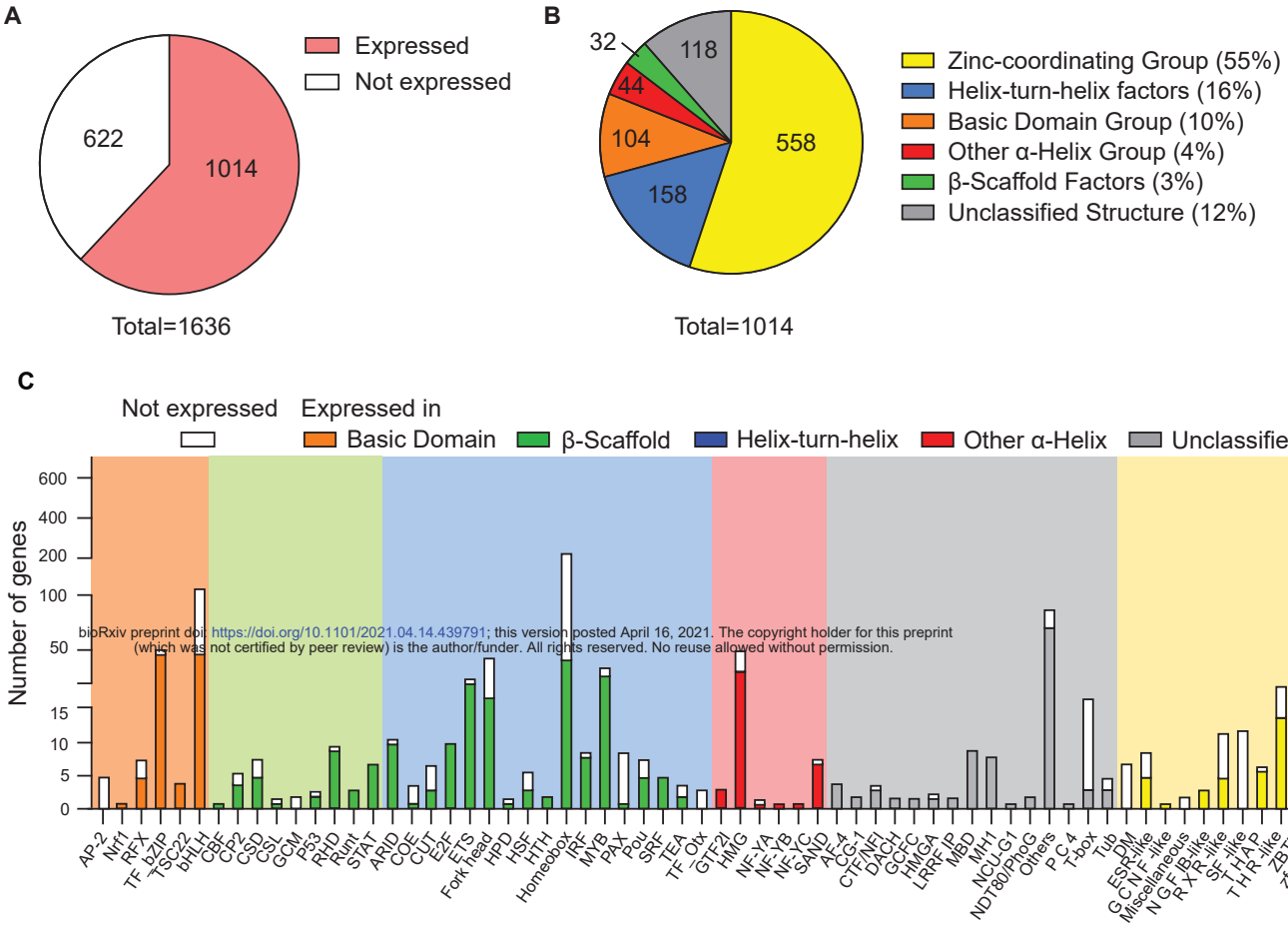

Figure 2

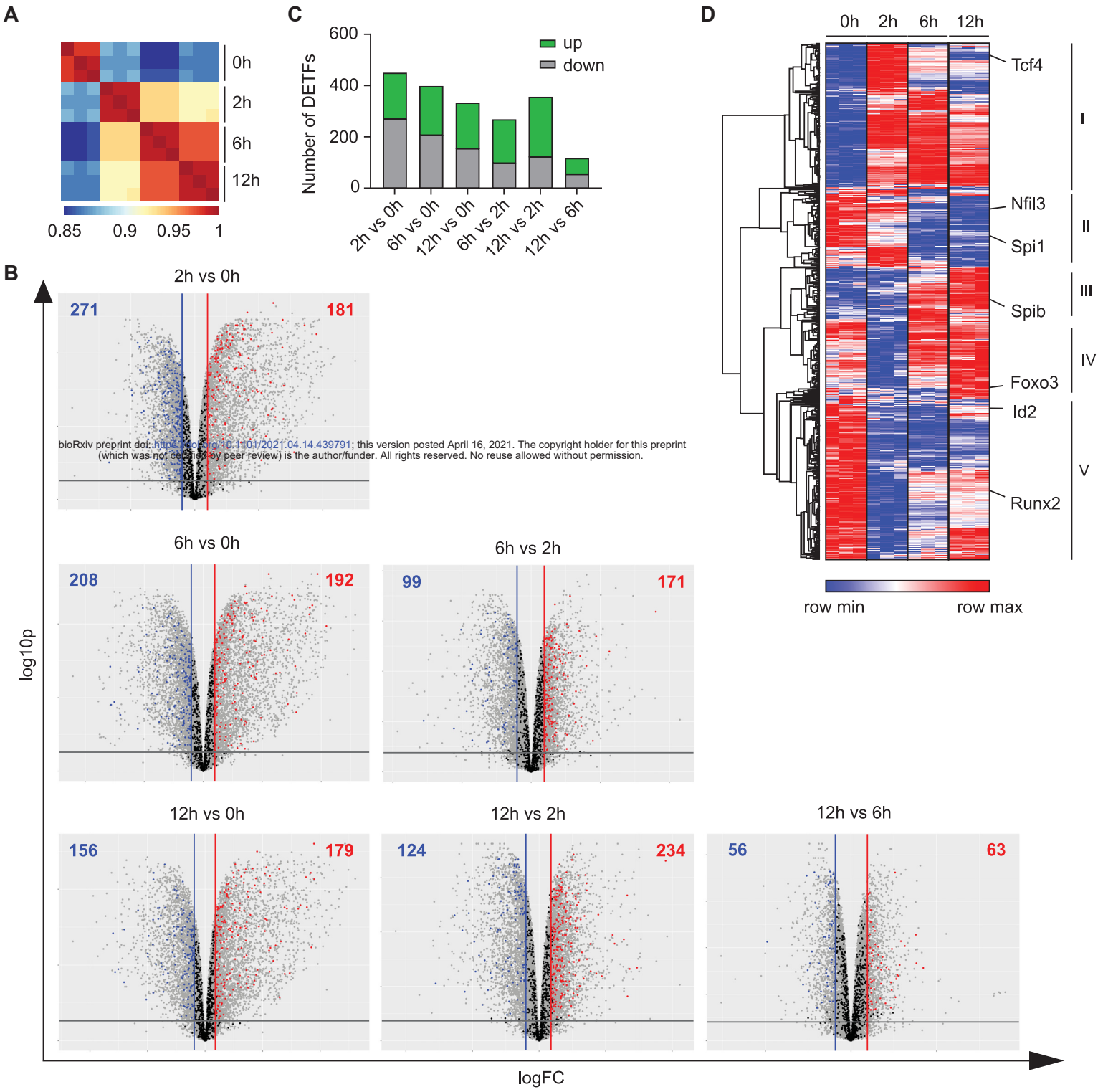

Figure 3

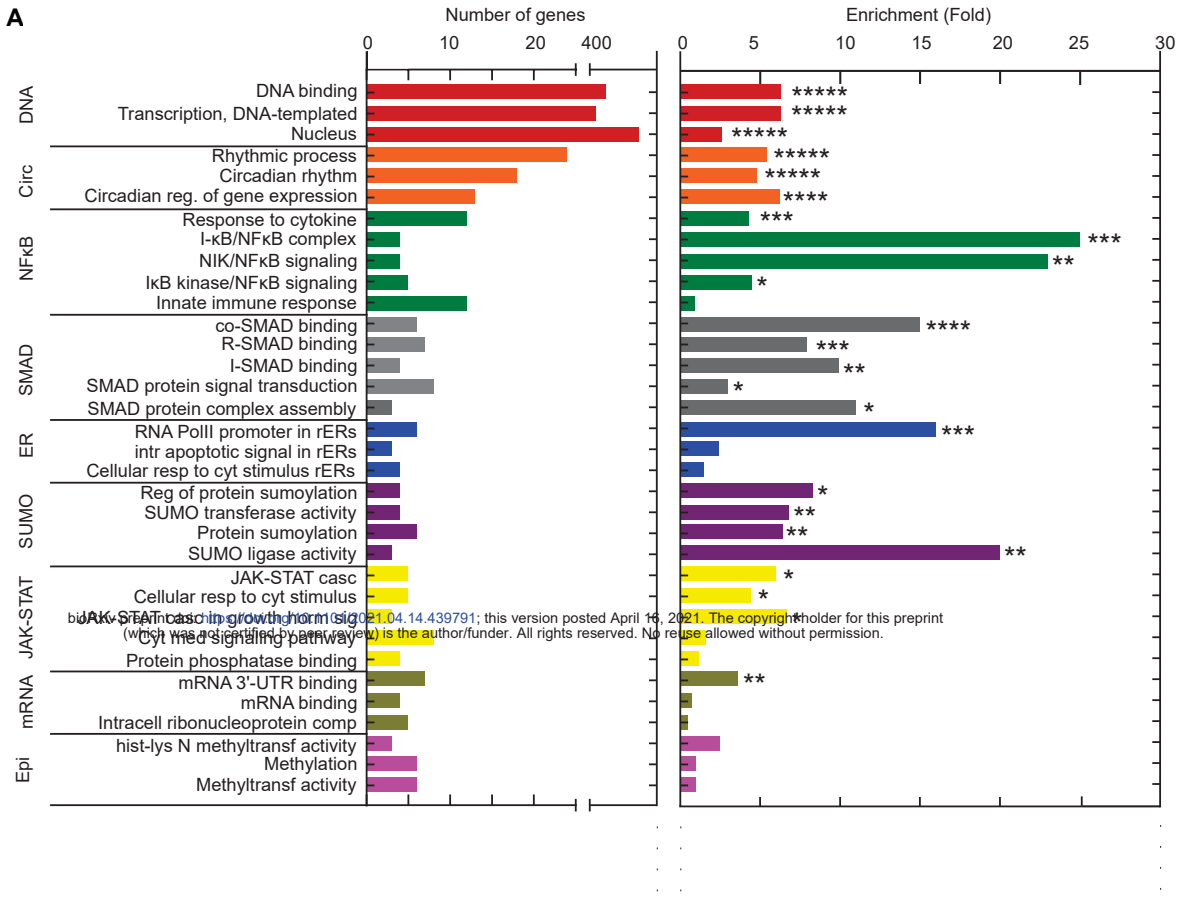

Figure 4

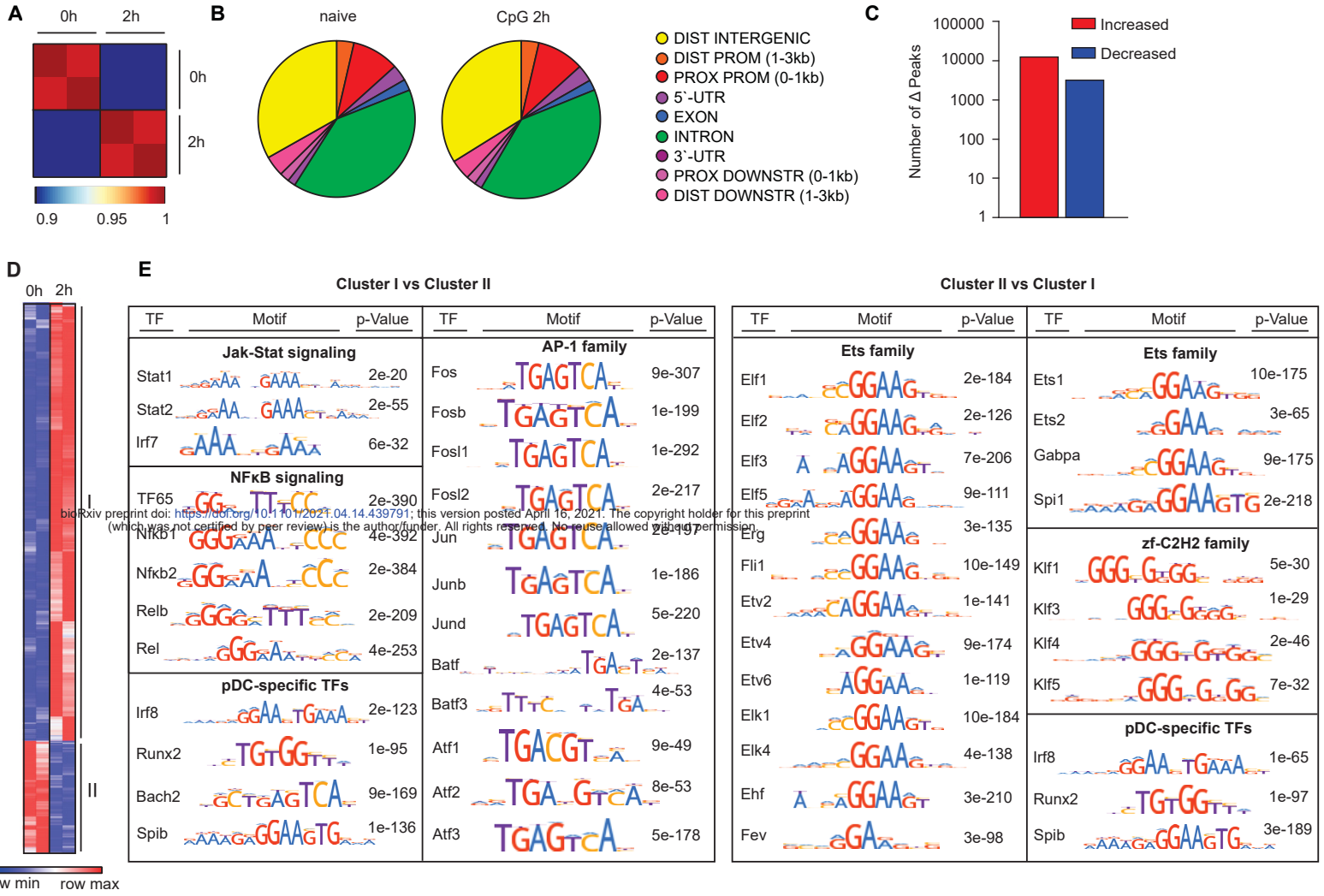

Figure 5

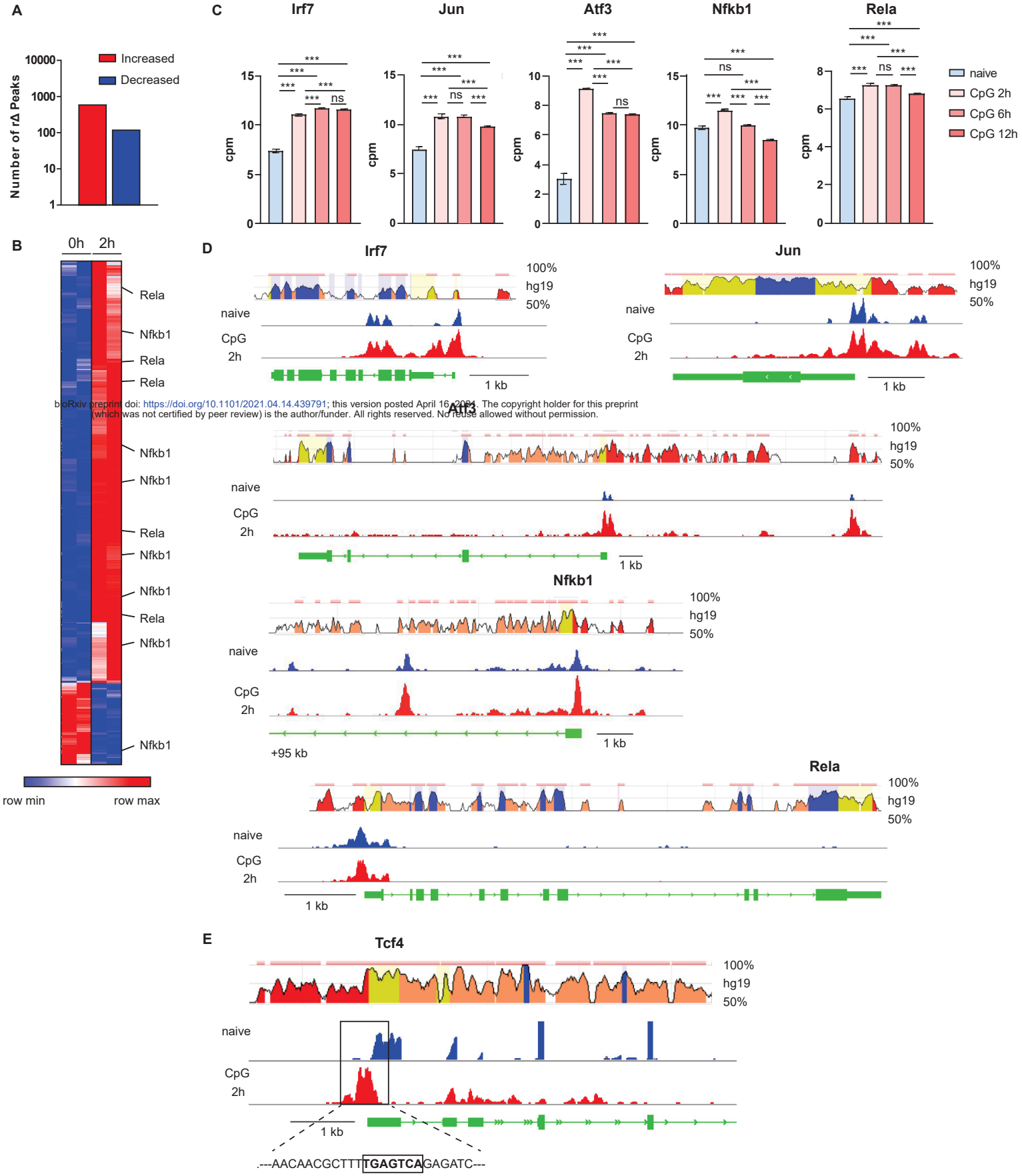

SUPPLEMENTAL TABLE S1
Functional cluster analysis with 661 CpG-dependent TF genes

Annotation Cluster 1 Enrichment Score: 224.49086249688912

Category	Term	Count	%	PValue	Genes	List Total	Pop Hits	Pop Total	Fold Enrich	Bonferroni	Benjamini	FDR
GOTERM_MF_DIRECT	GO:0003677~DNA binding	431	65.70122	1.39E-273	EHF, SPI1, BACH1, BACH2, ELK3, SPIB, SPIC, HOXA9, ZFP281, CREB3L4, SOX15, MYC, CREB3L1, GPE							
644	1847	17446	6.321503	4.18E-271	2.10E-271	1.70E-271						
GOTERM_BP_DIRECT	GO:0006351~transcription, DNA-templated	413	62.95732	1.24E-260	EHF, SPI1,	624	1885	18082	6.34893	2.57E-257	1.29E-257	1.25E-257
GOTERM_CC_DIRECT	GO:0005634~nucleus	495	75.45732	1.96E-141	EHF, SPI1,	628	6019	19662	2.574832	3.58E-139	3.58E-139	3.33E-139

Annotation Cluster 2 Enrichment Score: 11.744756217221672

Category	Term	Count	%	PValue	Genes	List Total	Pop Hits	Pop Total	Fold Enrich	Bonferroni	Benjamini	FDR
GOTERM_BP_DIRECT	GO:0043401~steroid hormone mediated signaling	22	3.353659	1.48E-17	ESRRA, RA	624	53	18082	12.02842	3.07E-14	3.83E-15	3.72E-15
GOTERM_MF_DIRECT	GO:0003707~steroid hormone receptor activity	21	3.20122	3.62E-15	ESRRA, RA	644	56	17446	10.15877	1.11E-12	6.09E-14	4.94E-14
GOTERM_MF_DIRECT	GO:0004879~RNA polymerase II transcription factc	17	2.591463	3.55E-14	THRA, VDR	644	36	17446	12.79253	1.07E-11	5.66E-13	4.60E-13
GOTERM_MF_DIRECT	GO:0008270~zinc ion binding	57	8.689024	0.00552464	RERE, RAR	644	1075	17446	1.436403	0.8123294	0.0309994	0.0251678

Annotation Cluster 3 Enrichment Score: 7.656034402823103

Category	Term	Count	%	PValue	Genes	List Total	Pop Hits	Pop Total	Fold Enrich	Bonferroni	Benjamini	FDR
GOTERM_BP_DIRECT	GO:0048511~rhythmic process	24	3.658537	7.06E-11	HES7, KLF1	624	128	18082	5.433293	1.46E-07	1.33E-08	1.29E-08
GOTERM_BP_DIRECT	GO:0007623~circadian rhythm	18	2.743902	1.63E-07	KLF10, JUN	624	108	18082	4.829594	3.38E-04	1.99E-05	1.93E-05
GOTERM_BP_DIRECT	GO:0032922~circadian regulation of gene expressi	13	1.981707	9.35E-07	ZFHX3, BH	624	61	18082	6.175546	0.0019372	1.02E-04	9.91E-05

Annotation Cluster 4 Enrichment Score: 2.5280383426155817

Category	Term	Count	%	PValue	Genes	List Total	Pop Hits	Pop Total	Fold Enrich	Bonferroni	Benjamini	FDR
GOTERM_BP_DIRECT	GO:0034097~response to cytokine	12	1.829268	1.01E-04	FOSL1, JUN	624	81	18082	4.292972	0.1887868	0.0065348	0.0063487
GOTERM_CC_DIRECT	GO:0033256~I-kappaB/NF-kappaB complex	4	0.609756	3.08E-04	REL, NFKB1	628	5	19662	25.04713	0.0547449	0.0056292	0.0052293
GOTERM_BP_DIRECT	GO:0038061~NIK/NF-kappaB signaling	4	0.609756	3.86E-04	REL, NFKB1	624	5	18082	23.18205	0.5512363	0.0186213	0.0180911
GOTERM_BP_DIRECT	GO:0007249~I-kappaB kinase/NF-kappaB signaling	5	0.762195	0.0233617	IRF1, REL,	624	32	18082	4.527744	1	0.3457532	0.33590789
GOTERM_BP_DIRECT	GO:0045087~innate immune response	12	1.829268	0.81701294	SP110, IRF	624	400	18082	0.869327	1	1	0.97199421

Annotation Cluster 5 Enrichment Score: 2.4533584885560358

Category	Term	Count	%	PValue	Genes	List Total	Pop Hits	Pop Total	Fold Enrich	Bonferroni	Benjamini	FDR
GOTERM_BP_DIRECT	GO:1902895~positive regulation of pri-miRNA tran	8	1.219512	6.05E-06	SMAD1, JU	624	22	18082	10.5373	0.0124634	5.97E-04	5.80E-04
GOTERM_MF_DIRECT	GO:0070410~co-SMAD binding	6	0.914634	2.57E-05	SMAD2, TC	644	11	17446	14.7764	0.0077362	2.16E-04	1.76E-04
GOTERM_MF_DIRECT	GO:0070412~R-SMAD binding	7	1.067073	1.87E-04	SMAD2, ZE	644	24	17446	7.901268	0.0548194	0.0013795	0.00112001
GOTERM_BP_DIRECT	GO:0001657~ureteric bud development	8	1.219512	0.00120144	SMAD2, SM	624	48	18082	4.829594	0.9172627	0.0469695	0.04563209
GOTERM_BP_DIRECT	GO:0007179~transforming growth factor beta rece	9	1.371951	0.00420828	SMAD2, SM	624	75	18082	3.477308	0.9998403	0.1171341	0.11379869
GOTERM_MF_DIRECT	GO:0070411~I-SMAD binding	4	0.609756	0.00658823	SMAD2, SM	644	11	17446	9.850932	0.8641533	0.0352692	0.02863444
GOTERM_BP_DIRECT	GO:0009880~embryonic pattern specification	5	0.762195	0.00856577	SMAD2, SM	624	24	18082	6.036993	1	0.1888113	0.18343496
GOTERM_BP_DIRECT	GO:0060395~SMAD protein signal transduction	8	1.219512	0.01673176	SMAD2, SM	624	77	18082	3.010656	1	0.2988638	0.29035373
GOTERM_BP_DIRECT	GO:0007183~SMAD protein complex assembly	3	0.457317	0.02891013	SMAD2, SM	624	8	18082	10.86659	1	0.3967006	0.38540459
GOTERM_MF_DIRECT	GO:0034713~type I transforming growth factor be	3	0.457317	0.05016191	SMAD2, SM	644	10	17446	8.127019	0.9999998	0.2140712	0.17380041
GOTERM_MF_DIRECT	GO:0046332~SMAD binding	5	0.762195	0.13076376	SMAD2, SM	644	53	17446	2.555666	1	0.4891533	0.39713439
GOTERM_BP_DIRECT	GO:0017015~regulation of transforming growth fa	3	0.457317	0.13799761	SMAD2, SM	624	19	18082	4.575405	1	0.9725546	0.94486121

Annotation Cluster 6 Enrichment Score: 1.8310626466925868

Category	Term	Count	%	PValue	Genes	List Total	Pop Hits	Pop Total	Fold Enrich	Bonferroni	Benjamini	FDR
GOTERM_BP_DIRECT	GO:1990440~positive regulation of transcription fr	6	0.914634	1.86E-05	CEBPB, CR	624	11	18082	15.80594	0.0377754	0.0014803	0.00143817
GOTERM_BP_DIRECT	GO:0070059~intrinsic apoptotic signaling pathway	3	0.457317	0.35347399	CEBPB, DD	624	36	18082	2.414797	1	1	0.97199421
GOTERM_BP_DIRECT	GO:0034976~response to endoplasmic reticulum s	4	0.609756	0.48923142	CEBPB, DD	624	76	18082	1.525135	1	1	0.97199421

Annotation Cluster 7 Enrichment Score: 1.6923550652467598

Category	Term	Count	%	PValue	Genes	List Total	Pop Hits	Pop Total	Fold Enrich	Bonferroni	Benjamini	FDR
GOTERM_BP_DIRECT	GO:0016925~protein sumoylation	6	0.914634	0.0020548	PIAS4, PIAS	624	27	18082	6.439459	0.985934	0.069796	0.06780855
GOTERM_MF_DIRECT	GO:0061665~SUMO ligase activity	3	0.457317	0.00774499	PIAS4, PIAS	644	4	17446	20.31755	0.9044488	0.0404609	0.03284945
GOTERM_BP_DIRECT	GO:0033235~positive regulation of protein sumoyl	4	0.609756	0.01115387	PIAS4, PIAS	624	14	18082	8.279304	1	0.2265766	0.22012486
GOTERM_MF_DIRECT	GO:0019789~SUMO transferase activity	4	0.609756	0.01950048	PIAS4, PIAS	644	16	17446	6.772516	0.9973872	0.0909022	0.07380181
GOTERM_MF_DIRECT	GO:0016874~ligase activity	6	0.914634	0.99761374	PIAS4, PIAS	644	362	17446	0.449007	1	1	0.99761374

Annotation Cluster 8 Enrichment Score: 1.4823485732155635

Category	Term	Count	%	PValue	Genes	List Total	Pop Hits	Pop Total	Fold Enrich	Bonferroni	Benjamini	FDR
GOTERM_MF_DIRECT	GO:0035497~cAMP response element binding	6	0.914634	6.74E-05	JUN, CREB	644	13	17446	12.50311	0.0201379	5.23E-04	4.25E-04
GOTERM_BP_DIRECT	GO:0030968~endoplasmic reticulum unfolded pro	7	1.067073	0.00585734	CREB3L4, C	624	48	18082	4.225895	0.9999949	0.1498322	0.14556576
GOTERM_BP_DIRECT	GO:0006986~response to unfolded protein	5	0.762195	0.09820951	CREB3L4, C	624	51	18082	2.840938	1	0.8145034	0.79131049
GOTERM_CC_DIRECT	GO:0005789~endoplasmic reticulum membrane	4	0.609756	0.99999998	CREB3L4, C	628	710	19662	0.176388	1	1	0.99999998
GOTERM_CC_DIRECT	GO:0005783~endoplasmic reticulum	8	1.219512	1	CREB3L4, C	628	1323	19662	0.189321	1	1	1

Annotation Cluster 9 Enrichment Score: 1.3953787168799636

Category	Term	Count	%	PValue	Genes	List Total	Pop Hits	Pop Total	Fold Enrich	Bonferroni	Benjamini	FDR
GOTERM_BP_DIRECT	GO:0044344~cellular response to fibroblast growth	5	0.762195	0.01878653	NR4A1, EG	624	30	18082	4.829594	1	0.3217	0.31253962
GOTERM_BP_DIRECT	GO:1904628~cellular response to phorbol 13-aceta	3	0.457317	0.02891013	MYC, ZFP3	624	8	18082	10.86659	1	0.3967006	0.38540459
GOTERM_BP_DIRECT	GO:0000165~MAPK cascade	7	1.067073	0.03136762	SMAD1, M	624	69	18082	2.939753	1	0.4189961	0.40706521
GOTERM_BP_DIRECT	GO:0009611~response to wounding	6	0.914634	0.04905994	HHEX, MYC	624	58	18082	2.997679	1	0.5616143	0.54562242
GOTERM_BP_DIRECT	GO:0071364~cellular response to epidermal growt	4	0.609756	0.12618308	MYC, ID1,	624	36	18082	3.219729	1	0.9447928	0.91788988

Annotation Cluster 10 Enrichment Score: 1.3590519762597917

Category	Term	Count	%	PValue	Genes	List Total	Pop Hits	Pop Total	Fold Enrich	Bonferroni	Benjamini	FDR
GOTERM_BP_DIRECT	GO:0051591~response to cAMP	6	0.914634	0.03050679	FOSL1, JUN	624	51	18082	3.409125	1	0.4131377	0.40137367
GOTERM_BP_DIRECT	GO:0071277~cellular response to calcium ion	6	0.914634	0.03526261	JUN, MEF2	624	53	18082	3.280479	1	0.4566508	0.4436477
GOTERM_BP_DIRECT	GO:0032870~cellular response to hormone stimul	5	0.762195	0.0778275	NCOA1, JU	624	47	18082	3.08272	1	0.72639	0.70570614

Annotation Cluster 11 Enrichment Score: 1.2275392798040106

Category	Term	Count	%	PValue	Genes	List Total	Pop Hits	Pop Total	Fold Enrich	Bonferroni	Benjamini	FDR
GOTERM_BP_DIRECT	GO:0009612~response to mechanical stimulus	7	1.067073	0.02108733	FOSL1, JUN	624	63	18082	3.219729	1	0.3366217	0.32703645
GOTERM_BP_DIRECT	GO:0051591~response to cAMP	6	0.914634	0.03050679	FOSL1, JUN	624	51	18082	3.409125	1	0.4131377	0.40137367
GOTERM_BP_DIRECT	GO:0042542~response to hydrogen peroxide	4	0.609756	0.32282261	FOSL1, JUN	624	58	18082	1.998453	1	1	0.97199421

Annotation Cluster 12 Enrichment Score: 1.1533564963509588

Category	Term	Count	%	PValue	Genes	List Total	Pop Hits	Pop Total	Fold Enrich	Bonferroni	Benjamini	FDR
GOTERM_BP_DIRECT	GO:0001843~neural tube closure	9	1.371951	0.01876662	TGIF1, RAF	624	97	18082	2.68864	1	0.3217	0.31253962
GOTERM_BP_DIRECT	GO:0060348~bone development	6	0.914634	0.04321059	SMAD1, RA	624	56	18082	3.104739	1	0.5329306	0.51775547
GOTERM_BP_DIRECT	GO:0031076~embryonic camera-type eye develop	3	0.457317	0.08205379	RARG, RAF	624	14	18082	6.209478	1	0.7427525	0.72160273
GOTERM_BP_DIRECT	GO:0060173~limb development	3	0.457317	0.3660151	RARG, RAF	624	37	18082	2.349532	1	1	0.97199421

Annotation Cluster 13 Enrichment Score: 0.9360546220269985

Category	Term	Count	%	PValue	Genes	List Total	Pop Hits	Pop Total	Fold Enrich	Bonferroni	Benjamini	FDR
GOTERM_BP_DIRECT	GO:0007259~JAK-STAT cascade	5	0.762195	0.00856577	STAT5A, PI	624	24	18082	6.036993	1	0.1888113	0.18343496
GOTERM_BP_DIRECT	GO:0071345~cellular response to cytokine stimulu	5	0.762195	0.02588086	STAT5A, PI	624	33	18082	4.39054	1	0.368523	0.3580293
GOTERM_BP_DIRECT	GO:0060397~JAK-STAT cascade involved in growth	3	0.457317	0.07192523	STAT5A, ST	624	13	18082	6.68713	1	0.6867699	0.66721423
GOTERM_BP_DIRECT	GO:0019221~cytokine-mediated signaling pathway	8	1.219512	0.23911635	STAT5A, CI	624	146	18082	1.587812	1	1	0.97199421
GOTERM_MF_DIRECT	GO:0019903~protein phosphatase binding	4	0.609756	0.6345088	STAT5A, ST	644	88	17446	1.231366	1	1	0.81456954
GOTERM_MF_DIRECT	GO:0004871~signal transducer activity	7	1.067073	0.99999809	STAT5A, ST	644	648	17446	0.29264	1	1	0.99999809

Annotation Cluster 14 Enrichment Score: 0.6460632072222745

Category	Term	Count	%	PValue	Genes	List Total	Pop Hits	Pop Total	Fold Enrich	Bonferroni	Benjamini	FDR
GOTERM_MF_DIRECT	GO:0003730~mRNA 3'-UTR binding	7	1.067073	0.01292527	CARHSP1,	644	53	17446	3.577933	0.9803343	0.063167	0.05128414
GOTERM_MF_DIRECT	GO:0003729~mRNA binding	4	0.609756	0.89902274	CPEB1, ME	644	142	17446	0.7631	1	1	0.89902274
GOTERM_CC_DIRECT	GO:0030529~intracellular ribonucleoprotein comp	5	0.762195	0.9922019	CPEB1, NF	628	320	19662	0.489202	1	1	0.9922019

Annotation Cluster 15 Enrichment Score: 0.18670644339195458

Category	Term	Count	%	PValue	Genes	List Total	Pop Hits	Pop Total	Fold Enrich	Bonferroni	Benjamini	FDR
GOTERM_MF_DIRECT	GO:0018024~histone-lysine N-methyltransferase a	3	0.457317	0.34474797	PRDM9, KM	644	33	17446	2.462733	1	1	0.81456954
GOTERM_BP_DIRECT	GO:0032259~methylation	6	0.914634	0.69625626	PRDM9, KM	624	169	18082	1.028789	1	1	0.97199421
GOTERM_MF_DIRECT	GO:0008168~methyltransferase activity	6	0.914634	0.74628275	PRDM9, KM	644	168	17446	0.967502	1	1	0.81456954
GOTERM_MF_DIRECT	GO:0016740~transferase activity	9	1.371951	1	NCOA1, PR	644	1472	17446	0.165632	1	1	1

Annotation Cluster 16 Enrichment Score: 0.04973056863696993

Category	Term	Count	%	PValue	Genes	List Total	Pop Hits	Pop Total	Fold Enrich	Bonferroni	Benjamini	FDR
GOTERM_BP_DIRECT	GO:0030030~cell projection organization	5	0.762195	0.76842612	PLEK, RFX2	624	151	18082	0.959522	1	1	0.97199421
GOTERM_BP_DIRECT	GO:0042384~cilium assembly	3	0.457317	0.93979174	RFX2, FOXJ	624	129	18082	0.673897	1	1	0.97199421
GOTERM_BP_DIRECT	GO:0060271~cilium morphogenesis	3	0.457317	0.9821426	RFX2, FOXJ	624	170	18082	0.511369	1	1	0.9821426

SUPPLEMENTAL TABLE S2

Centrimo motif enrichment analysis using the HOCOMOCO database and 2174 gene promoter associated regions with increased chromatin accessibility after pDC activation

db_index	motif_id	motif_alt_	consensus	E-value	adj_p-valu	log_adj_p-	bin_locati	bin_width	total_widt	sites_in_bin	total_sites	p_success	p-value	mult_tests
1	TF65_MOUSE.H11MO.0.A		KGGRMTT	4.50E-55	1.30E-57	-131.02	0	166	490	1015	1956	0.33878	5.20E-60	244
1	NFKB2_MOUSE.H11MO.0.C		GGGRAAK'	1.10E-53	3.00E-56	-127.84	0	152	490	937	1924	0.3102	1.20E-58	244
1	NFKB1_MOUSE.H11MO.0.A		GGGAAAK'	2.80E-51	7.80E-54	-122.28	0	176	490	989	1830	0.35918	3.20E-56	244
1	FOS_MOUSE.H11MO.0.A		SDRTGAGT	3.20E-45	9.00E-48	-108.32	0	247	489	699	941	0.50511	3.70E-50	244
1	FOSL1_MOUSE.H11MO.0.A		KRVTGAGT	1.70E-38	4.70E-41	-92.85	0	261	489	859	1177	0.53374	1.90E-43	244
1	FOSL2_MOUSE.H11MO.0.A		KVTGAGTC	5.30E-32	1.50E-34	-77.9	0	162	490	767	1582	0.33061	6.10E-37	244
1	RELB_MOUSE.H11MO.0.C		RGGGRMT	6.00E-32	1.70E-34	-77.77	0	177	489	1010	2020	0.36196	6.90E-37	244
1	REL_MOUSE.H11MO.0.A		DRWRGGC	3.90E-31	1.10E-33	-75.91	0	156	486	952	2106	0.32099	4.50E-36	242
1	FOSB_MOUSE.H11MO.0.A		VTGAGTCA	6.90E-31	1.90E-33	-75.33	0	208	492	1129	2012	0.42276	7.80E-36	245
1	JUND_MOUSE.H11MO.0.A		GRRTGAGT	2.00E-30	5.50E-33	-74.28	0	260	490	1127	1657	0.53061	2.30E-35	244
1	JUN_MOUSE.H11MO.0.A		DVTGAGTC	3.70E-29	1.00E-31	-71.34	0	247	491	1160	1798	0.50305	4.30E-34	245
1	ATF3_MOUSE.H11MO.0.A		VTGAGTCA	1.10E-27	3.10E-30	-67.93	0	244	492	1273	2031	0.49593	1.30E-32	245
1	JUNB_MOUSE.H11MO.0.A		VTGAGTCA	7.20E-25	2.00E-27	-61.47	0	208	492	1050	1903	0.42276	8.20E-30	245
1	BACH2_MOUSE.H11MO.0.A		TGCTGAGT	3.40E-23	9.40E-26	-57.63	0	170	490	855	1810	0.34694	3.80E-28	244
1	SPI1_MOUSE.H11MO.0.A		VRAAAGA(	3.00E-20	8.40E-23	-50.83	0	192	486	907	1753	0.39506	3.50E-25	242
1	IRF8_MOUSE.H11MO.0.A		RAAARRG(	1.20E-14	3.30E-17	-37.96	0	227	481	1025	1772	0.47193	1.40E-19	240
1	RUNX1_MOUSE.H11MO.0.A		BYYTGTGG	1.30E-14	3.60E-17	-37.85	0	197	489	965	1912	0.40286	1.50E-19	244
1	RUNX2_MOUSE.H11MO.0.A		BYCTGTGG	1.70E-14	4.90E-17	-37.56	0	249	489	1258	2071	0.5092	2.00E-19	244
1	EHF_MOUSE.H11MO.0.B		VWACSAG	3.90E-14	1.10E-16	-36.77	0	232	486	940	1599	0.47737	4.50E-19	242
1	IRF1_MOUSE.H11MO.0.A		RRAANWG	1.10E-13	3.10E-16	-35.7	0	187	481	718	1428	0.38877	1.30E-18	240
1	BATF_MOUSE.H11MO.0.A		DSTYYYRA'	4.10E-13	1.10E-15	-34.4	0	189	483	965	1984	0.3913	4.80E-18	241
1	NFE2_MOUSE.H11MO.0.A		ATGACTCA	5.80E-13	1.60E-15	-34.06	0	121	487	386	1048	0.24846	6.60E-18	243
1	SPIB_MOUSE.H11MO.0.A		RAAAGAG(	6.00E-12	1.70E-14	-31.72	0	190	484	591	1151	0.39256	7.00E-17	241
1	CREB1_MOUSE.H11MO.0.A		NRRTGACC	1.20E-11	3.30E-14	-31.04	0	134	490	629	1727	0.27347	1.40E-16	244
1	IRF2_MOUSE.H11MO.0.B		RAAAVHG/	3.20E-11	8.90E-14	-30.05	0	147	481	569	1395	0.30561	3.70E-16	240
1	RUNX3_MOUSE.H11MO.0.A		KKCTGTGG	2.50E-10	6.90E-13	-28	0	229	489	1086	1949	0.4683	2.80E-15	244
1	ELF1_MOUSE.H11MO.0.A		SRACCCGC	7.20E-10	2.00E-12	-26.94	0	231	487	809	1401	0.47433	8.20E-15	243
1	NF2L1_MOUSE.H11MO.0.C		HGTCATN	7.30E-10	2.10E-12	-26.91	0	174	494	922	2128	0.35223	8.30E-15	246
1	IRF4_MOUSE.H11MO.0.A		RAAARRG(	1.50E-09	4.20E-12	-26.2	0	195	483	1002	2058	0.40373	1.70E-14	241
1	ELF3_MOUSE.H11MO.0.B		RAABVAG(	4.30E-09	1.20E-11	-25.15	0	203	487	950	1892	0.41684	4.90E-14	243
1	ETV4_MOUSE.H11MO.0.B		SAGGAAGT	2.40E-08	6.80E-11	-23.42	0	219	493	1133	2171	0.44422	2.70E-13	246
1	PRDM1_MOUSE.H11MO.0.A		RAAAGTG/	2.60E-08	7.40E-11	-23.33	0	127	487	677	2032	0.26078	3.00E-13	243
1	NF2L2_MOUSE.H11MO.0.A		RTGACTCA	7.30E-08	2.00E-10	-22.32	0	119	487	643	2050	0.24435	8.30E-13	243
1	IRF9_MOUSE.H11MO.0.C		GAAAGCG/	7.40E-08	2.10E-10	-22.3	0	197	489	457	875	0.40286	8.50E-13	244
1	GABPA_MOUSE.H11MO.0.A		GGVRCCG(	3.20E-07	8.80E-10	-20.85	0	233	487	893	1580	0.47844	3.60E-12	243
1	ELF2_MOUSE.H11MO.0.C		TDNCAGG/	4.40E-06	1.20E-08	-18.22	0	226	486	815	1483	0.46502	5.10E-11	242
1	PEBB_MOUSE.H11MO.0.C		TYTGTGGT	7.10E-06	2.00E-08	-17.73	0	194	490	960	2062	0.39592	8.10E-11	244
1	STAT2_MOUSE.H11MO.0.A		RRGRAAAH	2.80E-05	7.70E-08	-16.38	0	140	482	611	1696	0.29046	3.20E-10	240
1	ATF1_MOUSE.H11MO.0.B		VTGACGTC	4.50E-05	1.30E-07	-15.89	0	217	491	498	916	0.44196	5.10E-10	245
1	ELK1_MOUSE.H11MO.0.B		RCCGGAAC	1.70E-04	4.80E-07	-14.54	0	238	490	986	1773	0.48571	2.00E-09	244
1	FLI1_MOUSE.H11MO.0.A		GGVRCCG(	1.90E-04	5.30E-07	-14.45	0	179	487	828	1910	0.36756	2.20E-09	243
1	PO2F2_MOUSE.H11MO.0.B		AYATGCAA	2.40E-04	6.60E-07	-14.23	0	198	490	883	1875	0.40408	2.70E-09	244
1	ETV6_MOUSE.H11MO.0.C		RCAGGAAI	2.80E-04	7.90E-07	-14.05	0	234	492	1165	2165	0.47561	3.20E-09	245
1	ETS1_MOUSE.H11MO.0.A		VRRRCMG	4.00E-04	1.10E-06	-13.71	0	231	487	1071	1986	0.47433	4.60E-09	243
1	ATF2_MOUSE.H11MO.0.A		RRTGABGT	4.00E-04	1.10E-06	-13.71	0	118	490	545	1815	0.24082	4.60E-09	244
1	NFIL3_MOUSE.H11MO.0.C		DRTTATGY	5.70E-04	1.60E-06	-13.35	0	200	490	776	1623	0.40816	6.50E-09	244
1	DDIT3_MOUSE.H11MO.0.C		MTGATGH	7.20E-04	2.00E-06	-13.12	0	259	491	1033	1735	0.52749	8.20E-09	245
1	BACH1_MOUSE.H11MO.0.C		TGCTGAGT	7.50E-04	2.10E-06	-13.08	0	167	487	166	336	0.34292	8.60E-09	243
1	ETV2_MOUSE.H11MO.0.A		RRARRCAC	1.40E-03	3.90E-06	-12.46	0	231	485	918	1687	0.47629	1.60E-08	242

1	IRF7_MOUSE.H11MO.0.C	GAAASYGA	1.50E-03	4.20E-06	-12.38	0	129	491	649	2044	0.26273	1.70E-08	245
1	ERG_MOUSE.H11MO.0.A	VVRCMGG	9.20E-03	2.60E-05	-10.57	0	175	487	844	2032	0.35934	1.10E-07	243
1	FEV_MOUSE.H11MO.0.B	GCVGGAA(	1.30E-02	3.70E-05	-10.2	0	207	491	1036	2174	0.42159	1.50E-07	245
1	CEBPG_MOUSE.H11MO.0.B	RKMTGAT(	1.50E-02	4.30E-05	-10.05	0	77	489	226	1036	0.15746	1.80E-07	244
1	GFI1B_MOUSE.H11MO.0.A	KCWGTGR'	8.10E-02	2.30E-04	-8.4	0	195	491	946	2110	0.39715	9.20E-07	245
1	ATF4_MOUSE.H11MO.0.A	RNMTGAT	9.00E-02	2.50E-04	-8.29	0	77	489	127	535	0.15746	1.00E-06	244
1	BATF3_MOUSE.H11MO.0.A	BRSTTTCAI	1.20E-01	3.30E-04	-8	0	134	484	651	2006	0.27686	1.40E-06	241
1	NFAC3_MOUSE.H11MO.0.B	TGGAAAAI	1.60E-01	4.40E-04	-7.73	0	222	492	1003	1992	0.45122	1.80E-06	245
1	ELK4_MOUSE.H11MO.0.B	SRRCCGGA	4.80E-01	1.30E-03	-6.61	0	232	488	1105	2111	0.47541	5.60E-06	243
1	IRF3_MOUSE.H11MO.0.A	RAAARGG/	7.20E-01	2.00E-03	-6.21	0	145	481	713	2062	0.30146	8.40E-06	240
1	NFAC2_MOUSE.H11MO.0.C	TGGAAAA\	7.90E-01	2.20E-03	-6.11	0	56	492	302	2084	0.11382	9.10E-06	245
1	RORG_MOUSE.H11MO.0.B	RRAASTRG	8.30E-01	2.30E-03	-6.06	0	131	489	628	2020	0.26789	9.60E-06	244
1	KLF1_MOUSE.H11MO.0.A	DGGGYGK(	8.70E-01	2.40E-03	-6.02	0	213	487	788	1605	0.43737	1.00E-05	243
1	MITF_MOUSE.H11MO.0.A	YCWYGTG/	1.10E+00	3.20E-03	-5.75	0	169	491	793	2039	0.3442	1.30E-05	245
1	SIX4_MOUSE.H11MO.0.C	WGWAAC(	1.30E+00	3.60E-03	-5.63	0	203	487	1003	2173	0.41684	1.50E-05	243
1	MAFK_MOUSE.H11MO.0.A	DWWWYT	1.50E+00	4.30E-03	-5.44	0	217	481	387	733	0.45114	1.80E-05	240
1	TBX21_MOUSE.H11MO.0.A	RRAGGTG\	1.60E+00	4.50E-03	-5.4	0	179	489	890	2174	0.36605	1.80E-05	244
1	STAT1_MOUSE.H11MO.0.A	RRRAAAHV	1.90E+00	5.40E-03	-5.21	0	167	479	808	2060	0.34864	2.30E-05	239
1	NR1D2_MOUSE.H11MO.0.A	RRRDAWG	2.10E+00	5.90E-03	-5.13	0	156	482	783	2144	0.32365	2.50E-05	240
1	CREM_MOUSE.H11MO.0.C	CRVTGACG	3.10E+00	8.70E-03	-4.75	0	182	490	548	1288	0.37143	3.60E-05	244
1	KLF4_MOUSE.H11MO.0.A	KRRRVWG	3.80E+00	1.10E-02	-4.56	0	216	486	1018	2088	0.44444	4.40E-05	242
1	CEBPA_MOUSE.H11MO.0.A	DRTTGTGC	3.80E+00	1.10E-02	-4.54	0	298	490	992	1509	0.60816	4.40E-05	244
1	MAF_MOUSE.H11MO.0.A	RWWBTGC	4.20E+00	1.20E-02	-4.45	0	216	484	986	2012	0.44628	4.90E-05	241
1	SUH_MOUSE.H11MO.0.A	BYSTGGGA	4.90E+00	1.40E-02	-4.3	0	96	490	498	2168	0.19592	5.60E-05	244
1	E2F2_MOUSE.H11MO.0.B	GGCGCGA/	5.80E+00	1.60E-02	-4.13	0	169	491	359	883	0.3442	6.60E-05	245
1	CEBPB_MOUSE.H11MO.0.A	DRTTGYGC	6.10E+00	1.70E-02	-4.07	0	266	490	801	1346	0.54286	7.10E-05	244

CentriMo (Local Motif Enrichment Analysis): Version 5.3.3 compiled on Feb 21 2021 at 14:52:25
The format of this file is described at https://meme-suite.org/meme/doc/centrimo-output-format.html.
centrimo --oc . --verbosity 1 --dfile description --score 5.0 --ethresh 10.0 --bfile new_sequences.fasta.bg new_sequences.fasta db/MOUSE/HOCOMOCOv11_core_MOUSE_mono_meme_format.meme

7.2 Acknowledgements

First of all I would like to thank Prof. Dr. rer. nat. Stefanie Scheu for supervision, guidance and help during my PhD thesis. For giving me the opportunity to work in her lab, for supporting the study scientifically and financially and for giving me the possibility to attend national and international meetings to present my work – which I have enjoyed a lot!

Furthermore, I would like to thank Prof. Dr. rer. nat. Michael Feldbrügge for being my second supervisor and careful reading of this thesis.

Importantly, Dr. Shafaqat Ali and Sonja Schavier have helped me continuously to learn new laboratory techniques and to handle large experiments many times. Also Dr. Daniel Degrandi has trained me and helped me with the confocal microscopy. Thank you for your support!

Lastly, I want to thank my parents and my husband for their support throughout the past years to achieve my aims and dreams.

7.3 Eidesstattliche Erklärung

Hiermit erkläre ich an Eides statt, dass ich die vorgelegte Dissertation selbstständig verfasst und keine anderen als die angegebenen Quellen und Hilfsmittel verwendet habe. Die Arbeit wurde weder in der vorgelegten noch in einer ähnlichen Form bei einer anderen Institution eingereicht.

Düsseldorf, den 07. Juli 2021

(Ritu Mann-Nüttel)